FROM SPECTRUM TO SPACE: THE INTEGRATION OF FREQUENCY-

SPECIFIC INTENSITY CUES TO PRODUCE AUDITORY SPATIAL

RECEPTIVE FIELDS IN THE BARN OWL

INFERIOR COLLICULUS

by

DAVID RAYMOND EUSTON

"From Spectrum to Space: The Integration of Frequency-Specific Intensity Cues

to Produce Auditory Spatial Receptive Fields in the Barn Owl Inferior Colliculus,"

a dissertation prepared by David R. Euston in partial fulfillment of the

requirements for the Doctor of Philosophy degree in the Department of

Psychology. This dissertation has been approved and accepted by:

_____

Dr. Terry Takahashi, Co-chair of the Examining Committee

_____

Dr. Richard Marrocco, Co-chair of the Examining Committee

_____

Date

Committee in charge: Dr. Terry Takahashi, Co-chair
                         Dr. Richard Marrocco, Co-chair
                         Dr. Michael Posner
                         Dr. Shawn Lockery

Accepted by:

_____

Vice Provost and Dean of the Graduate School

An Abstract of the Dissertation of

David Raymond Euston   for the degree of   Doctor of Philosophy

in the Department of Psychology   to be taken   August 2000

Title: FROM SPECTRUM TO SPACE: THE INTEGRATION OF

FREQUENCY-SPECIFIC INTENSITY CUES TO PRODUCE AUDITORY

SPATIAL RECEPTIVE FIELDS IN THE BARN OWL INFERIOR

COLLICULUS

Approved: _____
                      Dr. Terry T. Takahashi, Co-chair

                    _____
                      Dr. Richard T. Marrocco, Co-chair

        Neurons in the barn owl's inferior colliculus (IC) derive their spatial

receptive fields (RF) from two auditory cues: interaural time difference (ITD) and

interaural level difference (ILD). ITD serves to restrict a RF in azimuth but the

precise role of ILD was, up to this point, unclear. Filtering by the ears and head

insures that each spatial location is associated with a unique combination of

frequency-specific ILD values (i.e., an ILD spectrum). We isolated the effect of

ILD spectra using virtual sound sources in which ITD was held fixed for all spatial locations while ILD spectra were allowed to vary normally. A cell's response to these stimuli reflects the contribution of ILD to spatial tuning, referred to as an "ILD-alone RF".   In a sample of 34 cells, individual ILD-alone RFs were distributed and amorphous, but consistently showed that the ILD spectrum is facilatory at the cell's best location and inhibitory above and/or below.

Prior results have suggested that an IC cell's spatial specificity is generated by summing inputs which are narrowly tuned to frequency and selective for both ILD and ITD. Based on this premise, we present a developmental model which, when trained solely on a cell's true spatial RF, reproduces both the cell's true RF and its ILD-alone RF. According to the model, the connectivity between a space-tuned IC cell and its frequency-specific inputs develops subject to two constraints: the cell must be excited by ILD spectra from the cell's best location and inhibited by spectra from locations above and below but along the vertical strip defined by the best ITD.

To assess how frequency-specific inputs are integrated to form restricted spatial RFs, we measured the responses of 47 space-tuned IC cells to pure tones at varying ILDs and frequencies. ILD tuning varied with frequency. Further, pure-tone responses, summed according to the head-related filters, accounted for 56 percent of the variance in broadband ILD-alone RFs. Modelling suggests that, with broadband sounds, cells behave as though they are linearly

summing their inputs, but when testing with pure tones, non-linearities arise.

This dissertation includes unpublished co-authored materials.

CURRICULUM VITA

NAME OF AUTHOR: David Raymond Euston

PLACE OF BIRTH: Santa Rosa, California

DATE OF BIRTH: January 16, 1964

GRADUATE AND UNDERGRADUATE SCHOOLS ATTENDED:

      University of Oregon
      New Mexico State University
      University of California at Davis
      University of California at Santa Cruz

DEGREES AWARDED:

      Doctor of Philosophy in Psychology, 2000, University of Oregon
      Master of Arts in Experimental Psychology, 1993, New Mexico State
         University
      Bachelor of Arts and Sciences in Psychology and Physics, 1989,
         University of California at Davis

AREAS OF SPECIAL INTEREST:

      Cognitive Neuroscience

PROFESSIONAL EXPERIENCE:

      Research Assistant, Department of Psychology, University of Oregon,
         Eugene, 1993-1997

      Co-instructor, Department of Psychology, University of Oregon, Eugene,
         1996

Lab Instructor, Department of Psychology, University of Oregon, Eugene, 1995

Teaching Assistant, Department of Psychology, New Mexico State University, Las Cruces, 1991-92

AWARDS AND HONORS:

National Institutes of Health Neuroscience Traineeship, 1997-1999

ACKNOWLEDGEMENTS

I would like to thank my primary advisor, Terry Takahashi, who allowed me the freedom to pursue my own ideas but also maintained an active interest in my work. Thanks also to my dissertation committee—Rich Marrocco, Michael Posner, and Shawn Lockery—for their criticisms, encouragement, and guidance.

I have benefited greatly from interactions with others both within the lab and in the greater owl research community, among them: Kip Keller, Avinash Bala, Michael Spezio, Klaus Hartung, Jamie Mazer, and Ben Arthur. I am especially indebted to Kip Keller for his assistance with head-related transfer functions.

I am grateful to my parents, Florence Harrison, John Harrison, Stan Euston, and Ann Euston, for their love and encouragement. The care and concern of my two sisters and brother-in-law—Kim Euston, Dawn Gomersall and Tim Gomersall—has been, and will always be, important to me. Many friends buoyed me along the way and helped keep me sane, including: Alan Benson, Mark Evans, Brent Field, Amy Hayes, Lori Markson, Ellen Peters, Heather Scott, Douglas Siu, Michael and Teresa Spezio, and Ian Thornton.

Finally, I would like to recognize those owls who, regrettably, were sacrificed to make this research possible.

TABLE OF CONTENTS

LIST OF FIGURES

<u>Chapter I</u>

Figure   Page

<u>Chapter II</u>

<u>Chapter III</u>

LIST OF TABLES

CHAPTER I

INTRODUCTION

Being visually-oriented creatures by nature, it is easy for us to underestimate the importance of spatial hearing. Spatial hearing in humans, one might suppose, serves no higher purpose than to indicate the general direction of interesting or hazardous events outside the current focus of visual awareness. As such, its function might be the same as that of peripheral vision, albeit with a more extended range. In fact, auditory spatial acuity in humans is quite precise-- better than 2 degrees in the region directly in front of a person (Blauert, 1997, p. 38). The auditory system is thus capable of augmenting the visual system to provide more robust apprehension of the spatial layout of the environment. In some circumstances, the auditory system provides information which the visual system cannot, such as the location of a bird hidden in a tree. Perhaps more importantly, auditory localization is one of the key mechanism for parsing our auditory environment into separate information channels (i.e., "streams") (Bregman, 1990). This last point is obvious to anyone who has interacted with a person who wears hearing aids, which impair spatial hearing. Such people find it extremely difficult to focus on a single speaker among many. Spatial hearing thus plays a central role in communication, a function of great importance to humans.

In other organisms, such as the owl, spatial hearing is critical to survival. Because the barn owl often hunts when visibility is poor, it must be able to rely on its hearing to catch prey. Observations show that owls can catch mice even in complete darkness (Payne, 1971). To make this possible, the owl has evolved anatomical specializations, such as asymmetrically placed ears, that enhance its spatial hearing. Another specialization is the facial ruff, a disk of feathers that surrounds the owl's face. The ruff has directionally-selective filtering properties that improve the quality of frequency-specific cues available for sound localization (Knudsen et al., 1994).

This dissertation is concerned with the neural mechanisms of sound localization, with special emphasis on how the brain interprets frequency-specific intensity cues (i.e., spectral cues). I use as a model system the inferior colliculus of the owl, a brain area in which cells have restricted auditory spatial receptive fields (i.e., they respond only when a sound is in a limited region of space). Hence, the research can be focussed upon uncovering how cells use intensity cues to derive spatial receptive fields.

Background

Cues for Auditory Localization

For most animals, the cues available for auditory localization fall into two categories: time and intensity. A sound arising from a source located off the midline arrives at slightly different times in the two ears, giving rise to an

interaural time difference (ITD) that is a robust cue for azimuth. Intensity cues can be either binaural or monaural. In humans, the shadowing of the head means that a sound will be louder in the ear nearer the source, at least for frequencies above ~1000 Hz. These differences in intensity are often referred to as interaural level differences (ILDs). In owls, ILDs are augmented by asymmetries in the external ears. The pinna also induces frequency-specific attenuation and amplification that varies with sound source location. When referring to the filtering manifest at a single ear, these intensity changes are referred to collectively as the "monaural spectrum."

To elaborate, the external ears and face induce frequency-specific alterations in both time and intensity that vary with location. The directionally dependent filtering is referred to as the head-related transfer function, or HRTF. Because of HRTF filtering, all cues, not just monaural ones, are in principle frequency-dependent (i.e., they are spectral cues).

Humans appear to use all three cues, ITD, ILD and monaural spectra, to localize sounds. To localize sounds in azimuth, we rely on ITD for low frequencies (below ~1400 Hz) and overall ILD for higher frequencies. This is referred to as the "duplex theory" of sound localization, first put forth by Lord Rayleigh (1907). Localization in the vertical plane, on the other hand, appears to rely primarily on monaural spectral cues. Humans with one ear plugged can localize sounds in elevation quite accurately (Oldfield and Parker, 1986). Further, experiments have shown that the auditory system can be fooled if the

monaural spectrum from one location is imposed upon a sound source at a different location. Under these conditions, subjects sometimes judge the sound as coming from the location specified by the monaural spectral cues (Blauert, 1969/70). (see Middlebrooks and Green, 1991, for a more complete review of auditory localization in humans).

Sound localization in owls is based primarily on ITD and ILD spectral cues. HRTFs recorded from a barn owl are presented in the first figure of Chapter II. The HRTFs reveal that ITD changes with azimuth and is fairly consistent across frequencies. The distribution of ILD values, on the other hand, changes radically as a function of frequency. At low frequencies, ILD varies with azimuth, paralleling ITD. At high frequencies, a strong elevational gradient develops though ILD changes non-monotonically along any given direction. Because of the highly frequency-dependent distribution of ILD, every location in space will have an associated unique set of frequency-specific ILD values (i.e., an "ILD spectrum"). In this dissertation, I will argue that it is an IC cell's selectivity for ILD spectrum that contributes to its spatial tuning.

HRTFs have been recorded from many mammals, including humans (e.g., Shaw, 1974; Mehrgardt and Mellert, 1977; Middlebrooks et al., 1989), ferrets (Carlile, 1990a, 1990b), cats (Calford and Pettigrew, 1984; Musicant et al, 1990; Rice et al., 1992), guinea pigs (Carlile and Pettigrew, 1987; Hartung and Sterbing, 1997) and monkeys (Spezio et al., 2000). Each of these measurements reveals strongly frequency-dependent monaural intensity values

which could serve as an elevational cue. In many cases, the monaural spectrum could also be used to determine the azimuth of a sound source, though the degree to which this cue is actually used in this capacity is unclear (for a review, see Middlebrooks and Green, 1991).

One of the striking features of the HRTFs in many species is the occurrence of "notches" in the monaural spectrum (i.e., strong attenuation in a narrow frequency band). It has been suggested that the frequency of these notches may be used as a directional cue (human: Batteau, 1967; cat: Rice et al., 1992). Indeed, psychophysical experiments with humans suggest these notches are used for determining elevation (Hebrank and Wright, 1974; Bloom, 1977). Notches are also seen in monaural spectra measured from the owl, but they do not appear to be used (Egnor, 2000).

Research on the Role of Intensity Cues for Sound Localization in Owls

The study of the IC as the neural locus of the owl's localization ability got its start when Knudsen, Konishi and Pettigrew (1977) showed that cells in the IC have tightly restricted auditory receptive fields. Soon thereafter, it was demonstrated that these cells are arranged as a map of external space (i.e., adjacent locations in the external world correspond to adjacent cells in the IC) (Knudsen and Konishi, 1978a). Early on it was shown that cells in the IC are ITD tuned and that a cell's preferred ITD correlates with the azimuth of its preferred location, thus establishing that ITD encodes azimuth (Moiseff and Konishi, 1981).

The role of ILD, on the other hand, took longer to discover and is still not completely known. Knudsen and Konishi (1979) showed that plugging the right ear caused an owl to orient leftward and downward relative to a sound's true location, while plugging the left ear had the opposite effect. Similar experiments showed that plugging an ear had parallel effects on the locations of receptive fields in the IC (Knudsen and Konishi, 1980). Because an earplug completely disrupts ILD but leaves the monaural spectrum in one ear intact, these experiments supported the idea that ILD, rather than monaural spectrum, is the primary intensity cue used by owls and that one of its functions is to indicate elevation. Moiseff and Konishi (1983) showed that IC cells are tuned to ILD. This is a necessary condition if ILD is, in fact, a localization cue; however, this study did not address whether a cell's ILD tuning actually correlates with its preferred location, thus leaving the role of ILD unproven. In 1989, Olsen, Knudsen and Esterly recorded from the optic tectum, which receives a direct projection from the IC, and demonstrated that a cell's preferred ILD did in fact correlate with its preferred elevation, but only within a limited range between -30 and +20 degrees elevation relative to the horizontal plane. These lines of evidence all suggested a dichotomy in which ITD determines a cell's azimuthal selectivity and ILD determines its elevational selectivity. Moiseff (1989) showed that sounds presented over headphones could be used to elicit head turns in elevation and azimuth by separately controlling ILD and ITD respectively,

although he pointed out that the ILD and ITD axes that the owl uses are not completely orthogonal.

The idea that ITD and ILD encode roughly orthogonal dimensions was nicely complimented by the finding that these two cues are processed in anatomically separate pathways (please refer to Figure 1). The cochlea projects via the eighth nerve to two cochlear nuclei which are specialized for encoding time and intensity. Cells in nucleus magnocellularis show precise time-locking to the stimulus but low dynamic ranges. Cells in the nucleus angularis show the opposite pattern (Sullivan and Konishi, 1984; Konishi et al., 1985). The nucleus magnocellularis projects to the nucleus laminaris where ITD is extracted by cells with coincidence detection properties (Carr and Konishi, 1990). The nucleus angularis projects to the nucleus ventralis lemnisci lateralis, pars posterior (VLVp) where level differences are compared via bilateral, mutually inhibitory connections between the left and right halves of the nucleus (Takahashi and Keller, 1992a). The ITD and ILD streams converge in the lateral shell (LS) of the IC, as shown in Figure 1, though the time pathway is relayed through the contralateral IC core (Takahashi and Konishi, 1988a; Adolphs, 1993). Takahashi, Moiseff and Konishi (1984) established that the two pathways are functionally independent: inactivation of the ITD pathway did not alter an IC cell's tuning to ILD and vice versa. With this anatomical data, the story was clear and intuitive: two cues, two pathways, two orthogonal dimensions of space (i.e., azimuth and elevation).

What these experiments did not address fully is how ILD *spectra* contribute to a cell's spatial tuning. For example, the study by Olsen et al. (1989), which found that ILD tuning correlates with preferred elevation, was performed with broadband flat-spectrum ILDs (i.e., the same ILD at each frequency). The same is true of the other headphone studies mentioned above. Flat-spectrum ILDs can be viewed as a crude approximation to the true ILDs experienced by the owl and, as such, provide a limited view of the role played by ILD. The complexity of ILD cues, revealed by HRTF measurements, make it likely that the role of ILD is more complicated that these initial studies suggest.

Two previous studies shed light on how ILD spectra are interpreted by IC cells. In the first, Brainard et al. (1992) measured receptive fields of cells in the owls optic tectum using pure tones instead of the usual broadband sounds. The observed receptive fields were large and typically included responses in several discrete regions besides the true preferred location. Importantly, the pure-tone receptive fields measured at different frequencies overlapped at the cell's preferred location. Though not stated explicitly by the authors, these findings suggest that a cell's tuning to ILD and ITD *at each frequency* matches the ILD and ITD values occurring at the center of the receptive field. The authors stress instead the role of cross-frequency interactions in canceling the ambiguities inherent with a single frequency channel. This study was an important first step towards understanding how cells process ILD spectra but it had two limitations.

First, the results showed the effects of *both* ILD and ITD, because it is
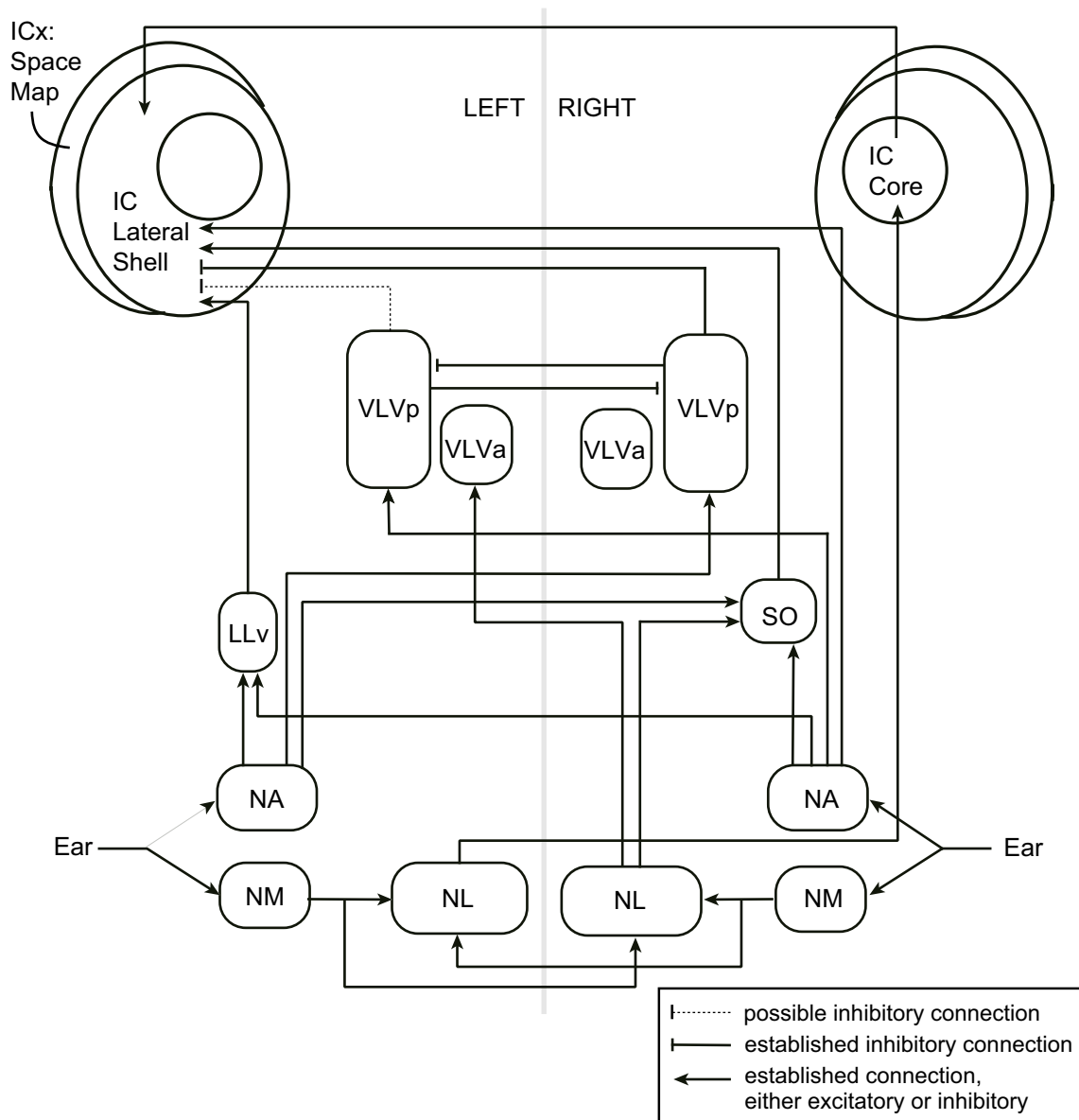
Figure 1. Known anatomical connections from the cochlea to the inferior colliculus of the owl. Only half of the connections are shown; all connections can be assumed bilaterally symmetric. Sources: Takahashi and Konishi, 1988a; Takahashi and Konishi, 1988b; Adolphs, 1993; Takahashi and Keller, 1992a; Takahashi et al., 1995. NM, nucleus magnocellularis; NA, nucleus angularis; NL, nucleus laminaris; SO, nucleus of the superior olive; LLv, nucleus lemnisci lateralis, pars ventralis; VLVp, nucleus ventralis lemnisci lateralis, pars posterior; VLVa, nucleus ventralis lemnisci lateralis, pars anterior.

impossible to dissociate the two cues using free-field sources. Second, the conclusions were based on a limited number of frequencies for any given cell: usually two and sometimes three.

More recently, Gold and Knudsen (2000) have addressed the issue of spectral tuning more directly. Working in the optic tectum, they compared the ILD tuning in different frequency bands with the ILD values occurring at the cell's best location. They claimed to have found a correspondence between these two values; however, the variance in their data is comparable to the size of the effect. The results must therefore be interpreted with caution. Even so, their effect is very likely real—in this dissertation, I will present evidence that provides provisional support for Gold's conclusion.

Overview

As with many new discoveries, the findings presented here were enabled by a new technology. Our lab has developed the ability to create virtual sound sources for owls using stimuli presented over headphones (Keller et al., 1998). To do this, we insert microphones in the ear canal and record the directional filtering of the ears over a range of locations (i.e., we measure the HRTFs). To simulate a free field sound source, we simply apply to a sound the directional filter appropriate to a desired location. Using this technique, we are able to re-create, with high accuracy, the waveform that would have been present at the eardrum had the sound originated from an external source. This technique has

originally developed and validated using human subjects (Wightman and Kistler, 1989a, 1989b). Whereas stimuli delivered over headphones normally sound like they are localized within the head, sounds filtered by the HRTFs sound as though they are originating from "out there" in the external world (Wightman and Kistler, 1989a, 1989b; Hartmann and Wittenberg, 1996; Kulkarni and Colburn, 1998). This technique has also been used successfully to study auditory localization in the cat (Poon and Brugge, 1993; Brugge et al., 1994; Delgutte et al., 1995, 1999; Rice et al., 1995; Nelken et al., 1997; Reale and Brugge, 2000).

The goal of the research presented here was to uncover how frequency-specific ILD cues contribute to an IC cell's spatial tuning. There are two parts to this question, the first phenomenological and the second mechanistic. To describe the phenomenon one must address how ILD spectrum contributes to an IC cell's firing. More specifically, for a particular location, is the cell inhibited, excited or unaffected by ILD spectra? Answering this question required the use of virtual sound sources. Under normal free-field conditions, both ILD and ITD vary together as a function of space. With virtual sounds, however, these two cues can be varied independently. As a result, it was possible to measure the contribution of ILD to the cell's response at each point in space. I call the resulting response surface the "ILD-alone" receptive field because it was measured with only ILD varying. The results of this experiment are the primary focus of Chapter II.

I was also interested in the mechanisms whereby ILD spectra are converted into spatial information. My approach to this question was to decompose the cell's response into its component parts. I used pure tones to probe the ILD tuning of a cell on a frequency-by-frequency basis. I then asked, given a pattern of frequency-specific ILD tuning curves, can one predict how the cell would behave with broadband sounds? Answering this question is the primary task of Chapter III. Here again, the virtual sound source technique proved invaluable. The synthesis of pure-tone responses leads naturally to a prediction of the ILD-alone response, not the cell's true receptive field. This provided for a direct comparison between pure-tone and broadband data that yielded important insights into the underlying computations performed by the cell.

This dissertation consists of two, self-contained papers (Chapters II and III), co-authored with my advisor, Terry Takahashi. Both are intended for eventual publication in a peer-reviewed journal.

CHAPTER II

THE CONTRIBUTION OF LEVEL DIFFERENCE CUES TO SPATIAL

RECEPTIVE FIELDS IN THE BARN OWL INFERIOR COLLICULUS

Introduction

The barn owl's inferior colliculus (IC) is known to contain a topographically

organized map of sound source location (Knudsen and Konishi, 1978a). Cells in

this map have tightly restricted spatial receptive fields based entirely on auditory

cues, the two most important of which are interaural time difference (ITD) and

interaural level difference (ILD) (Knudsen and Konishi, 1980; Moiseff and

Konishi, 1981; Moiseff and Konishi, 1983). These cues are shaped by

directionally dependent filtering of the external ears and face so that each spatial

location is associated with a unique combination of frequency-dependent ILDs

and ITDs (Brainard et al., 1992; Keller et al., 1998). As shown in Figure 1, ITD

varies monotonically with azimuth at all frequencies. The spatial distribution of

ILD, on the other hand, is much more frequency dependent: At low frequencies,

ILD varies with azimuth, paralleling ITD, while at high frequencies ILD varies in a

complex, non-monotonic fashion with both elevation and azimuth.

Both ILD and ITD are spectral cues: a space-selective cell must match its

tuning to the correct values of ITD and ILD at each frequency. With ITD,

Figure 1. Directional dependence of interaural time difference (ITD) and interaural level difference (ILD) in the barn owl. Values shown were obtained from probe tubes microphones inserted deep into the ear canal. Each diamond represents the entire frontal hemifield from the owl's perspective. Coordinates are double-polar (Knudsen, 1982).

ITD

ILD

3500 Hz

5000 Hz

6500 Hz

8500 Hz
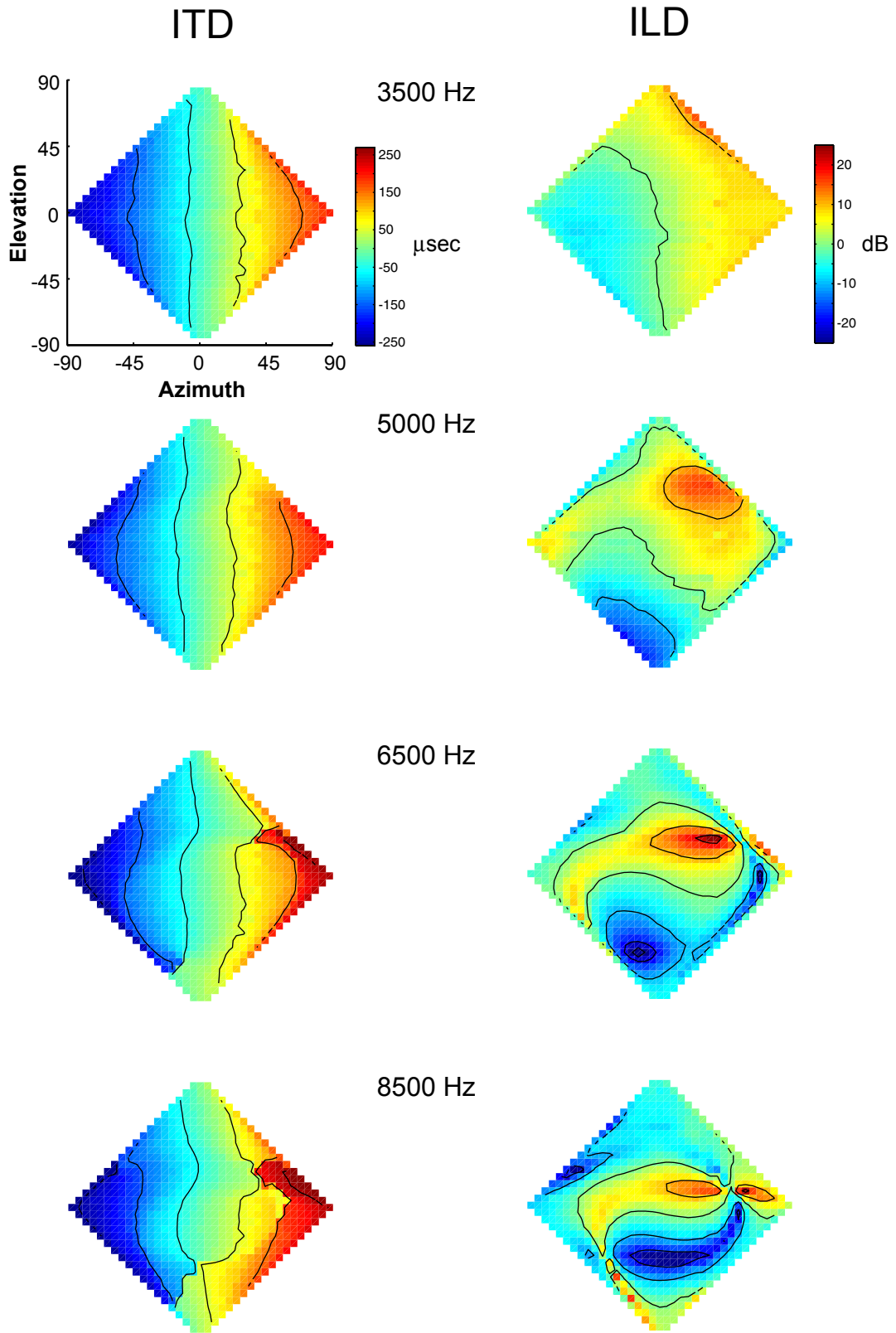
frequency-specific matching is trivial because ITD cues are relatively consistent across frequency. ITD's role in determining a cell's receptive field is also straightforward: it provides restriction in azimuth (Moiseff and Konishi, 1981). With ILD, on the other hand, frequency-specific matching is of central importance. Information at one frequency is needed to cancel the ambiguities that arise at another (Brainard et al., 1992). However, the specific role of frequency-specific ILD values in generating a receptive field is unclear. In this study, we present a technique for studying how ILD spectra contribute to spatial tuning.

The complex correspondence between ILD spectra and spatial location would seem to require that a cell develop its ILD selectivity via experience. Indeed, there is abundant evidence that this is the case. The mechanisms of plasticity seems to be geared towards maintaining a correspondence between visual and auditory maps in the optic tectum, which derives its auditory spatial tuning from the IC (Knudsen, 1999). Owls raised under conditions that disrupt the normal correspondence of visual and auditory cues (e.g., with prisms over their eyes) still develop cells in the optic tectum with overlapping visual and auditory receptive fields (Knudsen and Brainard, 1991). These adaptive adjustments in tuning properties are associated with shifts in the anatomical position of the auditory space map within the IC (Brainard and Knudsen, 1993). This plasticity appears to apply for tuning to both ITD and ILD cues (Mogdans and Knudsen, 1992). More recent evidence suggests that this acquired tuning to

ITD and ILD can even vary on a frequency-by-frequency basis (Gold and Knudsen, 2000). This developmental evidence plays an integral role in our attempts to explain specific patterns of ILD selectivity in space-tuned cells in the adult owl.

To provide a more specific analysis of how ILD selectivity develops, we make three assumptions, each supported by empirical evidence. First, space-tuned cells initially receive inputs from a range of frequency- and ILD-selective cells located in the lateral shell (LS) of the central nucleus of the IC (Adolphs, 1993; Mazer, 1995). Second, the strength of the connection between each of those inputs and the space-tuned cell is established via a Hebbian learning rule, in which the connection strength is proportional to the degree of coactivation between the input and the output cell. Pharmacological manipulations have demonstrated that NMDA receptors, known to have Hebbian-like properties, play an important role in adaptation to abnormal rearing conditions (Feldman et al., 1996). Finally, the preferred location of a space-tuned cell is determined by a training signal, probably of visual origin. Though it has not yet been demonstrated, the existence of such a visual training signal seems incontrovertible (Knudsen, 1999).

These assumptions lead to a simple explanation of how frequency-specific ILD tuning might arise. A sound-emitting object located at what will eventually be a cell's preferred location would elicit activity concurrently in the output cell (via the training signal) and in all those input cells activated by sounds at this location.

In combination with the Hebbian learning rule, this would lead the space-tuned cell to strengthen its connections with those input cells whose frequency-specific ILD tuning matched the ILD spectra associated with its preferred location.

This constitutes what is perhaps the simplest scenario capable of accounting for ILD selectivity in space-tuned cells. It predicts that a cell should be driven maximally by the ILD spectra associated with its best location. Further, because ILD contains both horizontal (at low frequencies) and vertical information (at higher frequencies), we would expect ILD to confer both azimuthal and elevational restriction. However, at least two other factors may play an important role in determining a cell's final tuning properties. The first is inhibition. Recent evidence shows that inhibition plays a key role in adaptive adjustments to ITD shifts (Zheng and Knudsen, 1999) and it seems reasonable to assume that plasticity of inhibitory connections may partly determine ILD selectivity as well. If true, then ILD selectivity may develop not only to provide maximum excitation at the cell's best location but also to provide maximum inhibition at other locations. In satisfying these dual constraints, the cell may no longer be maximally excited at its best location. The second factor that may influence ILD selectivity is ITD. As previously mentioned, ILD cues at low frequency are redundant with ITD. Because ITD is a robust cue for azimuth, it is possible that cells don't establish the low-frequency ILD tuning which would support azimuthal restriction. ILD would thus play a secondary role, providing selectivity only where ITD information was insufficient.

To examine these issues, we developed a technique to visualize the role of ILD in generating a cell's spatial receptive field. Normally, spatial receptive fields are measured with free-field sound sources. Because ITD and ILD vary together as a function of location, it is impossible to separate their effects. To dissociate these cues, we used virtual sound sources, which afforded complete control over both ITD and ILD spectra. Using this technique, we were able to keep ITD constant while measuring the response to ILD spectra from different locations. In so doing, we were able to measure the spatial receptive field the cell would have had were it tuned solely to ILD, obtaining what we call an "ILD-alone" receptive field. The ILD-alone receptive field allows us to address whether ILD by itself can support a two dimensional receptive field. It also allows us to see whether, in fact, a cell is tuned optimally to the ILD spectra occurring at the center of its receptive field.

In the second half of this paper, we present a developmental model that shows how experience-dependent plasticity might lead to the ILD-selectivity seen in the mature owl's IC cells. The model learns to mimic the true spatial receptive fields measured from cells in our study. Furthermore, when tested with ILD-alone stimuli, which the model did not see during training, the model still matches the cell's performance. The model provides a plausible account of how space-tuned IC cells build their receptive fields and explains why ILD-alone receptive fields have the shapes they do.

Methods

Stimuli

Techniques for the measurement and use of HRTFs were identical to those reported by Keller, et al. (1998). HRTFs were recorded at 684 locations in the frontal hemisphere, spaced every 5 degrees using bipolar coordinates (Knudsen, 1982). In this coordinate system, azimuth specifies the angular separation between a given location and the medial plane, while elevation specifies the separation between a location and the horizontal plane passing through the owl's head at eye level.

During recording sessions, stimuli were presented via earphones (model ER-1, Etymotic Research, Elk Grove Village, IL). To simulate a localized external sound source, a signal was convolved with two binaural filters, one that imposed the spectral profile appropriate for the specified location and the other that compensated for the response characteristics of the earphones. Each bird was tested using its own HRTFs. All sounds, whether broadband noise or pure tones, were 100 ms long and had five ms onset and offset ramps. Stimuli were separated by a 100 ms inter-stimulus interval. ABL levels in all tests were set to approximately 15-20 dB above the average threshold of IC cells.

To measure ILD-alone receptive fields, a set of filters was created which preserved each location's amplitude spectra but equated the delay in left and right ears. The fast Fourier transform was used to extract the amplitude and

phase spectrum of the time-domain filters. The phase spectrum from each ear was then replaced with a linear phase spectrum corresponding to a fixed delay. The amplitude and phase spectra were then transformed back into the time domain using an algorithm that minimized the difference between the filter's spectrum and the desired spectrum. (invfreqz() function in the Matlab Signal Processing Toolbox, version 5.2, the Mathworks, Inc., Natick, MA). The result was a set of filters with zero interaural phase difference (i.e., ITD) across frequencies but with the normal ILD spectrum. During stimulus presentation, the ITD was set to the cells best ITD using a separate filter. ABL equalization was accomplished by scaling each set of time-domain HRTF filters so that the average of the left and right peak amplitudes was identical for every spatial location.

Neurophysiology

Techniques for neural recording are reported elsewhere (e.g., Takahashi and Keller, 1992b), except as noted below. All procedures were approved by the Institutional Animal Care and Use Committee of the University of Oregon.

The locations of recording sites were verified histologically, using an electrode coated with DiI (Molecular Probes, Eugene, OR) to provide a reference mark. All recording sites were established to be within the lateral shell of the ICc or the ICx. Functional criteria were used to select space-specific neurons; the

spatial receptive fields of all included cells had half-maximum extent less than 35 degrees in azimuth and 50 degrees in elevation.

For every cell encountered three tests were run. ITD tuning was measured using a broadband noise having a flat ILD spectrum. ITDs typically covered the range -240 to +240 microseconds in 10 microsecond steps. Each stimulus was presented 10-20 times in randomized order. There were two space tests. For the normal space test, a series of spatially localized broadband noises was simulated at equally spaced locations every 10 degrees in azimuth and elevation for a total of 360 locations. For the purposes of subsequent analysis and display, responses at the other 324 locations were interpolated using a linearly weighted average of the responses at the four adjacent locations. Stimuli were randomized and repeated 6-10 times. An ILD-alone space test was identical to the standard space test except that ITD and ABL were equalized, as described above.

Model

The model consisted of a single output unit, corresponding to an ICx cell, and an array of 651 input units, corresponding to IC LS cells. The input cells were narrowly tuned to ILD and frequency and arranged according to preferred ILD and frequency. The inputs covered all ILDs between –30 and +30 dB, in 3 dB steps and all frequencies between 3000 and 9000 in 200 Hz steps. The subscripts i and j are used to denote a particular input unit's preferred ILD and

frequency, respectively. The output of the model was a squared, weighted sum of the inputs:

$$O(L) = \left(\sum_i \sum_j w_{ij} \cdot I_{ij}(L) \right)^2,$$

Where both output, O, and input, I_{ij}, are specific to a particular location in space, L, and w_{ij} represents the weight between a particular input and the output unit.

Each input unit was simultaneously tuned to ILD, ITD, and frequency. Tuning curves were chosen to approximate actual tuning curves of LS cells, measured in our lab (unpublished data). ILD and frequency tuning were approximated by gaussian curves,

$$g(x, \mu, \sigma) = e^{\frac{-1}{2}\left(\frac{x-\mu}{\sigma}\right)^2},$$

where x represents the ILD or frequency of the stimulus, μ is the cells preferred ILD or frequency and σ is an empirically derived constant, which describes the tuning width. Values of σ were 7.07 dB and 200 Hz for ILD and frequency, respectively. ITD tuning was approximated by a half-wave rectified cosine function:

$$h(x, \mu, f) = \text{rectify}(\cos(2\pi f \cdot (x - \mu))),$$

where x represents the stimulus ITD, μ the preferred ITD, and f the frequency at which that ITD occurred. The preferred ITD was set on a frequency-by-frequency basis so that the ITD tuning of all LS units matched the frequency-specific ITD values present at the desired best location of the ICx unit. Note that the response of a model LS cell was periodic with respect to ITD, an effect that is

seen in true LS cells. The response of an input unit to a particular combination of ITD, ILD, and frequency was taken as the product of its individual responses to each cue. The net response to a broadband sound with a particular ILD and ITD spectrum was the sum of the separate responses to each frequency band:

$$E_{ij}(L) = \sum_f g(ILD(f,L),\mu_{\mathrm{ILD}},\sigma_{\mathrm{ILD}}) \cdot h(ITD(f,L),\mu_{\mathrm{ITD}},f) \cdot g(f,\mu_f,\sigma_f),$$

where E represents the response of the cell with ABL equal at all locations, μ_{ILD}, μ_{ITD} and μ_f are preferred ILD, ITD, and frequency of the cell and σ_{ILD} and σ_f specify the tuning width to ILD and frequency. LS cells in fact respond stronger to louder sounds, so the effects of ABL were also accounted for. The net response of an input unit was thus:

$$I_{ij}(L) = \mathrm{atten}(E_{ij}(L),\Delta A(L,\mu_f)),$$

where ΔA represents the location-specific reduction or increase in amplitude seen at that unit's preferred frequency. The function atten() is the output activity before attenuation times a sigmoidal curve:

$$atten(r,\Delta A) = r \cdot \frac{1}{(1 + e^{-a(\Delta A - b)})}.$$

The constants a, and b were chosen to match pure-tone ABL response (i.e., rate-intensity) curves measured from IC cells (a=0.14, and b=-15).

During training, sounds were presented to the model from all 684 locations for which we had HRTF measurements. For each location, the activity of each LS unit was calculated based on the acoustic cue values at that location and the tuning curve properties described above. Simultaneously, the output unit activity

was set according to a training signal. The training signal was derived from the true receptive field of the cell we wished to mimic. The cell's responses were scaled between zero and one and a small positive value, called the "offset" value, was subtracted from the response at every location. The offset, which typically ranged between 0 and 0.4, served to make activity levels that were near zero become slightly negative.

For each location, the weights were adjusted incrementally according to the product of input (i.e., LS unit activity) and output values (i.e., ICx unit activity):

$$\Delta \overline{w} = \text{Input} \cdot \text{Output},$$

where $\Delta \overline{w}$ is the change in all weights due to the sound at a particular location. The net strength of a given weight, w_{ij}, was the sum of all such incremental weight changes.

$$w_{ij} = \sum_{L} \Delta w_{ij} = \sum_{L} I_{ij}(L) \cdot (R(L) - k).$$

Here, $I_{ij}(L)$ is the activity in a single LS unit for a sound at location L, and R(L) is the activity of the real cell at that same location. The subscripts i and j denote the preferred ILD and frequency of an input unit. The term k is the constant offset value mentioned above. Training consisted of a single presentation of the sound from each of the 684 locations. Repeated presentations of the stimulus set would merely have scaled the weights, equivalent to multiplying by a constant. For each cell, an interative search routine was used to determine the offset value that gave the maximum correlation between the responses of the real cell and those of the model to *true* space stimuli.

In order to test the model's ability to generate receptive fields at any given location, a series of simulations was conducted using artificial receptive fields, specified by a two-dimensional gaussian distribution:

$$RF(x, y) = e^{-\frac{1}{2}\left(\frac{x-\mu_x}{\sigma_x}\right)^2} \cdot e^{-\frac{1}{2}\left(\frac{y-\mu_y}{\sigma_y}\right)^2},$$

where RF(x,y) is the response of the cell at each azimuth, x, and elevation, y. The value of both σ_x and σ_y was eight, while the values μ_x and μ_y were the desired azimuth and elevation of the receptive field. The model was trained on azimuths between -60 and +60 in 10-degree increments and on elevations between -50 and +50 degrees, also in 10-degree increments. We excluded locations where the sum of azimuth and elevation as greater than or equal to 80 degrees.

Data Analysis

In order to assess whether the response in the lowest regions of the ILD-alone receptive field was below spontaneous rate, we ran T-tests to answer two questions: 1.) Is the spontaneous rate significantly different from zero, and 2.) Is the minimum response significantly different from spontaneous? Here we describe how the mean, standard deviation, and degrees of freedom were determined in order to compute the studentized T statistic. The test of whether spontaneous rate differed significantly from zero was based on spontaneous activity collected during a continuous recording period before and after each test.

The rate was expressed as spikes per 100 ms epoch (the duration of each test stimuli). To determine whether the spontaneous rate was significantly different from zero, we first had to estimate the variance in the spontaneous rate. We wanted a variance term comparable to the variance we would use in testing whether the minimum response differed significantly from spontaneous rate. Therefore, the variance estimate was obtained from the ILD-alone test results. For every location, the variance over all repetitions was computed. We then averaged the variance estimates for all locations whose response was less than 20 % of the maximum response. The degrees of freedom was the same as that used in testing whether the minimum response was less than the spontaneous rate: five times the number of repetitions of the stimulus set (explained below). To determine whether the minimum response to ILD-alone stimuli was less than spontaneous rate, the minimum response was estimated by averaging the mean response for the five locations with the smallest response rates. The variance was estimated by pooling the variance term used in the previous test (for spontaneous rate) with the averaged standard deviation over all five minimum response locations. The degrees of freedom was set to the total number of stimuli repetitions used in estimating the minimum response, which was the number of repetitions times five (for the number of locations).

Assessments of the model's ability to replicate the receptive field on which it was trained were based on a comparison of the best location of the model with

the best location of the real cell. Best location was determined via a weighted

sum of all responses greater than or equal to 60 % of the maximum firing rate.

To compare the model's ILD-alone receptive field with that of a real neuron,

both the neural response and the model's response were scaled so that all

values fell between zero and one. The degree of similarity was quantified via the

square of the Pearson product-moment correlation value, taken over all 684

locations for which we had measured HRTF data. For the purposes of

calculating this correlation, the missing data from the real cell were interpolated

based on the firing at the nearest measured locations.

<div align="center">Results</div>

<div align="center">ILD's Contribution to Spatial Tuning</div>

Our goal in this experiment was to visualize the spatial selectivity conferred

by ILD, independent of ITD. To dissociate ILD and ITD, we used virtual sound

sources, presented over headphones. Using microphones inserted in the owl's

ears, we first measured the filtering characteristics of the owl's ears and face,

often referred to as "head-related transfer functions" (HRTFs). Using these

measurements, we created a set of filters that allowed us to duplicate the

waveform that would have been received by the eardrum from an external sound

source. Stimuli created in this way can be used to measure efficiently the

response to sounds from different locations without physically moving a speaker

(Keller et al., 1998). To isolate ILD, we altered these filters, preserving the

normal spatial variation in frequency-specific ILDs (i.e., ILD spectra) but setting

ITD to the cell's preferred value. We thus created a stimulus set in which the

frequency-specific ILD values associated with a particular location were identical

to those encountered with real external stimuli but the ITD values were the same

at every location. We also set the average sound pressure level in the two ears

constant across all spatial locations. With external sound sources, the average

binaural level (ABL) drops off as one moves away from the region of space

directly in front of the bird. Hence, responses at these locations are normally

reduced. By equalizing ABL values across space, we revealed ILD-sensitive

responses at peripheral locations that might otherwise have been missed for lack

of sufficient intensity. Via these manipulations of ITD and ABL, we were able to

visualize the spatial receptive field that would result were a cell sensitive solely to

ILD (i.e., an ILD-alone receptive field).

Our results are based on the responses of 34 space-specific neurons

recorded in two subdivisions of the owl's IC: the lateral shell of the IC core and

the external nucleus of the IC (ICx). For each cell, we measured its "true" spatial

receptive field (i.e., with both ITD and ILD varying as they do with free-field sound

sources) and its receptive field with ITD held fixed, referred to as an ILD-alone

receptive field. In both cases, we simulated virtual sound sources from 360

locations in the frontal hemifield. As shown for five cells in Figure 2 (column 1,

"Real Neuron") the true spatial receptive fields measured in this way were similar

in shape and size to those observed using free field stimuli (Knudsen and

Figure 2. True and ILD-alone receptive fields from six cells ("Real Neuron") and the results of modeling these receptive fields ("Model"). Each row shows the responses a single cell along with the results of the model trained on that cell's data. The first column and second columns show the receptive fields produced by simulated free-field sound sources ("True Receptive Fields"). The second two columns show responses to ILD-alone stimuli. All responses are scaled between zero and one and activity values are indicated by the scale bar in the lower right. The white loop is the half-height contour for the true spatial receptive field.

True Receptive Field

ILD-Alone Receptive Field

Real Neuron   Model   Real Neuron   Model

$R^2 = 0.67$

897 R 27

$R^2 = 0.90$

897 L 21

$R^2 = 0.71$

897 R 24

$R^2 = 0.72$

897 L 27

$R^2 = 0.29$

891 L 21

1

0
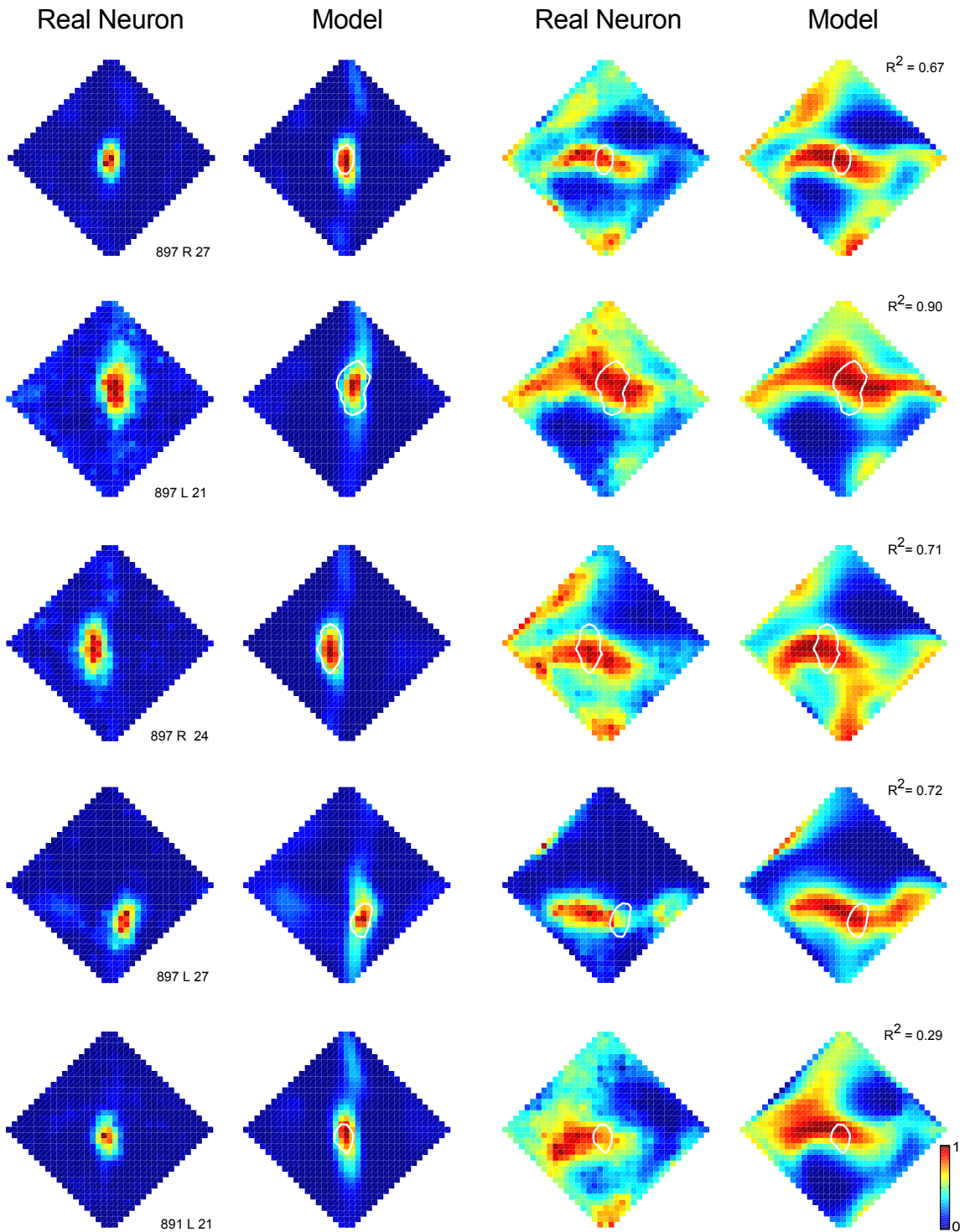
Konishi, 1978c), confirming the efficacy of the virtual space technique (see also Keller et al., 1998).

Whereas normal spatial receptive fields are tightly restricted in both elevation and azimuth, ILD-alone receptive fields were extended in both horizontal and vertical dimensions and typically showed islands of response separate from the main excitatory region (Figure 2, row 3). However, they consistently showed a prominent horizontal band of activity that intersected the spatial receptive field. This band was usually flanked above and/or below by regions of minimum response. For cells whose receptive fields were at high elevations, an inhibitory band was usually only apparent below the receptive field, while the opposite was true for cells whose receptive field was located significantly below the zero-elevation plane. In most cells, these minimum-response regions were apparently inhibited: of the 28 cells with statistically significant spontaneous rates, 24 had trough responses significantly below spontaneous rate ($p<0.05$). This inhibition is even more remarkable in light of the fact that ITD was set to the cell's preferred value at all locations. Non-optimal ILD spectra are thus sufficient to completely inhibit a cell, even when that cell is driven at its best ITD.

The extended shapes of the ILD-alone receptive fields (e.g., Figure 1, row 1, column 3) are due, in part, to ABL equalization. With free-field sound sources, ABL can be as much as 40 dB lower at peripheral locations relative to central locations (Keller et al., 1998). Equalizing ABL thus results in stronger responses

to upper, lower and lateral locations. True spatial receptive fields measured with ABL set everywhere equal also showed increased activity at peripheral locations, especially at elevations above 60 degrees (N=20, not shown).

The finding that the horizontal excitatory band seen in ILD-alone receptive fields corresponds with the elevation of the true receptive field is not surprising. Along a narrow vertical strip passing through the cell's preferred location, ITD values are the same in both true and ILD-alone tests. The stimuli along this strip are therefore almost identical, except that ILD-alone stimuli are ABL equalized while 'true' stimuli are not. Accordingly, the responses to ILD-alone stimuli are similar to the true receptive field along this vertical strip; the cell is excited at its best location and fails to be excited, or is in fact inhibited, for locations above and below.

What is novel in the present study is the ability to observe a cell's response to ILD spectra from locations off the best-ITD strip, where either ITD or ABL would normally cause the cell not to respond. The uncovered responses show clearly that ILD has the potential to influence the spatial selectivity of a cell in both elevation and azimuth and that this influence is highly complex; however, as will be discussed later, the influence of ILD is most important when ITD values are optimal (i.e., along the best-ITD strip). One possibility that our results clearly rule out was that ILD, by itself, might have provided the means for tightly restricting a receptive field in both azimuth and elevation. At low frequencies, ILD varies with azimuth and a properly tuned cell might have exploited this to

provide azimuthal restriction. Instead, cells appear to rely primarily on ITD for this purpose.

Modeling Space-Tuned Cells

The goal of our model to capture the process whereby simple acoustic cues are transformed into spatial receptive fields, with particular emphasis on the role of ILD. A cell in the model develops spatial selectivity via experience, a constraint which, we feel, increases the credibility of the model. A consideration of developmental mechanisms also provides important insights into the functioning of the mature system. In addition, the model was designed to use the same stimuli used in neurophysiological tests so that our results would be directly comparable with those of real cells. We first show that the model can replicate true receptive fields. We then show that it can predict the shape of ILD-alone receptive fields.

In designing the model, we attempted to remain true to known anatomical and neurophysiological properties of the IC. Cells in the IC lateral shell (LS) respond selectively to simple auditory cues, including frequency, ITD and ILD. These cells provide the sole ascending input to the ICx, where cells are tuned to space (Wagner et al., 1987; Feldman and Knudsen, 1997). The fact that ICx cells have much wider frequency tuning curves than LS cells suggests that the LS to ICx projection is highly convergent (i.e., many-to-one) (Knudsen and Konishi, 1978c). The LS to ICx projection thus appears to be the locus of across-

frequency integration and hence, the transformation from simple acoustic

parameters into space. Accordingly our model was built of an array of narrowly

frequency-tuned LS 'cells' that project via weighted links to a single ICx 'cell,'

which will ultimately develop a spatial receptive field (See Figure 3).
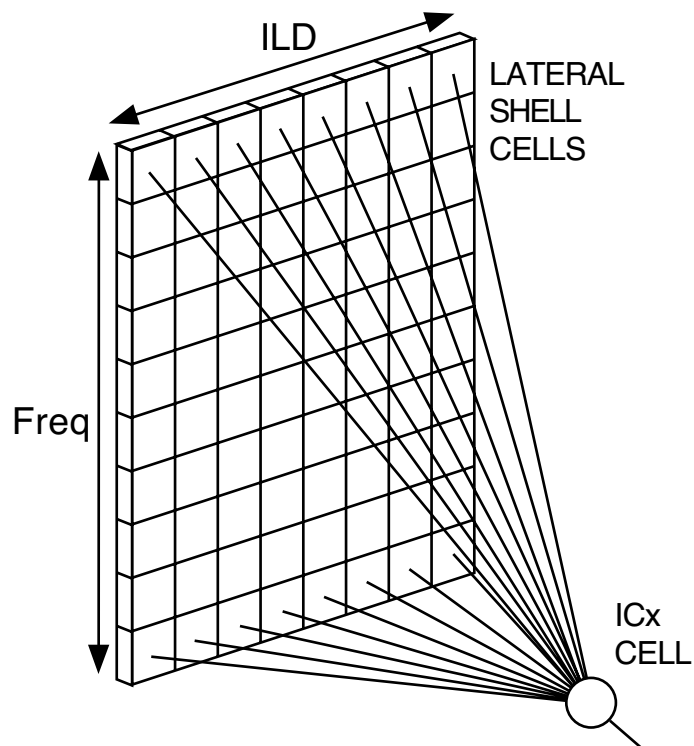
Figure 3. Structure of the ICx model. Each square in the input layer represents a lateral shell cell tuned to a particular value of ILD and frequency. These cells all send activity to the ICx cell, which sums these inputs to determine its output level. For simplicity, only a subset of the input units and connections are shown.

The input layer simulates activity patterns occurring in the LS during

experience with normal external sound sources. All inputs are narrowly selective

for ITD, ILD, and frequency, and the input layer consists of an array of cells

covering a range of best ILDs and frequencies. ITD tuning curves were modeled as a half-wave rectified sine function. As will be discussed later, this periodicity captures an intrinsic ambiguity present in real LS cells due to a process known as "phase ambiguity". The best ITD of each cell was chosen to correspond with the best location (i.e., center of the receptive field) of the cell whose behavior we were attempting to mimic. Thus, at each frequency, one ITD peak matched the frequency-specific ITD value found at the center of the cell's receptive field. The spacing of the other ITD peaks varied with the best frequency of the cell so that these other peaks failed to reinforce one another once frequency channels were combined (Takahashi and Konishi, 1986; Wagner et al., 1987). In addition, unit activity was monotonically related to the ABL (i.e., units responded more strongly to louder sounds). The parameters for tuning curve characteristics were chosen to approximate curves from LS and ICx cells previously measured in our lab (unpublished data). The acoustic data needed to simulate external sound sources were taken from the aforementioned HRTFs.

Activity in the output unit (i.e., ICx cell) is equal to the weighted sum of activity levels in the input layer. The output is squared before comparing with the data. This non-linear transform was added after exploratory analyses showed that it improved the fit of the model to the data. During training, the output unit was driven by an external teaching signal, which was high whenever a sound source was in the desired best location and fell off rapidly away from the best location. In theory, such a signal might be provided by the visual system

(Knudsen and Knudsen, 1989). In practice, we used the measured auditory receptive field of the cell that we wished to mimic as the training input.

Weights were adjusted using a form of Hebbian learning, inspired by the known NMDA-receptor mediated plasticity in the IC (Feldman et al., 1986; Feldman and Knudsen, 1998). During training, the model was presented with sounds from 683 evenly-spaced locations in the frontal hemifield while the output was driven by the aforementioned training signal. For each location, the weight between a given input unit and the output unit was incrementally adjusted by an amount proportional to the product of input and output activity. In the end, the strength and sign of a weight were proportional to the correlation between input and output activity taken over all locations. Unlike many instantiations of the Hebbian learning rule, we allowed negative correlations to yield negative weights. While the idea that a single weight can be either positive or negative based on training is neurally implausible, this mechanism provides a functional approximation to simultaneously training both excitatory and inhibitory synapses, where the inhibitory inputs are presumably routed via an inhibitory interneuron. To allow inhibitory weights to develop, we assumed that whenever an output cell was not actively responding, it was partially inhibited. If an output unit was inhibited while an input unit was active, the corresponding weight was driven negative. The degree of inhibition was influenced by a constant value, an 'offset', which was subtracted from the output activity. This offset caused all non-preferred locations, which usually elicit zero spikes in real space-tuned cells, to

take on negative values. There is no a priori basis for setting the level of

inhibition, so the offset was treated as a free parameter and adjusted, for each

cell, to maximize the correlation between the cell's and the model's normal

spatial receptive field during training.

The model was trained using the true receptive fields of the 34 cells in our

sample. In all cases, the model was able to generate narrowly restricted spatial

receptive fields that closely approximated the true receptive fields on which they

were trained (compare Figure 2, column 1 vs. column 2). The model also

mirrored the extent of a receptive field, being smaller for more tightly tuned cells.

The ability of the model to correctly duplicate the correct azimuth is not

surprising, given that the ITD tuning of all input cells was purposely set to

correspond with the correct location. The ability to replicate elevation is a better

test of the model because it depends on the tuning of the cell to frequency-

specific ILD values. Figure 4a compares the elevation of the true receptive field

with the elevation of the receptive field on which the model was trained. As can

be seen, the model closely approximates the elevation of the spatial receptive

field on which it was trained. Using a criterion probability of .01, the fitted

regression line was not significantly different from the perfect fit line

(elevation$_{model}$ = 1.08*elevation$_{data}$- 1.09, $p(\text{slope} \neq 1) = .04$, $p(\text{intercept} \neq 0) = .02$).

We examined the model's ability to learn receptive fields at different

locations by training the model on a second set of artificial true receptive fields

which we placed at equally-spaced intervals in the frontal plane, covering those

locations usually seen in recordings of receptive fields in the IC. Figure 4b

shows the errors between the model and the desired receptive field for all tested

locations. In general, the errors between desired and achieved location were

small, especially in a central region between –40 and +40 degrees azimuth and

–30 and +30 elevation. Outside of this area, errors were somewhat larger,

especially for locations in the lower right. The average absolute elevational error

for all tested locations was 3.4 degrees. We conclude that the model provides a

good match to the true receptive fields observed with real cells over most

locations for which receptive fields are seen in the owl's space map.

Clearly, some locations are easier to learn than others. These differences

are due in part to the quality of the underlying ILD cues available at each

location. However, the largest errors are attributable to the effects of low ABL in

the periphery. Successful learning at peripheral locations depended on the

model's ability to inhibit activity evoked from central locations. Hence, the ability

of the model to learn these locations was highly sensitive to the intensity of the

training stimuli and the degree of inhibition within the model. The performance at

peripheral locations could be improved by increasing the intensity of the training

sounds, but not without sacrificing performance at central locations. In the end,

we choose an intensity level that balanced the errors in the periphery with those

in the central region and provided good fits to the ILD-alone data, as described

below.
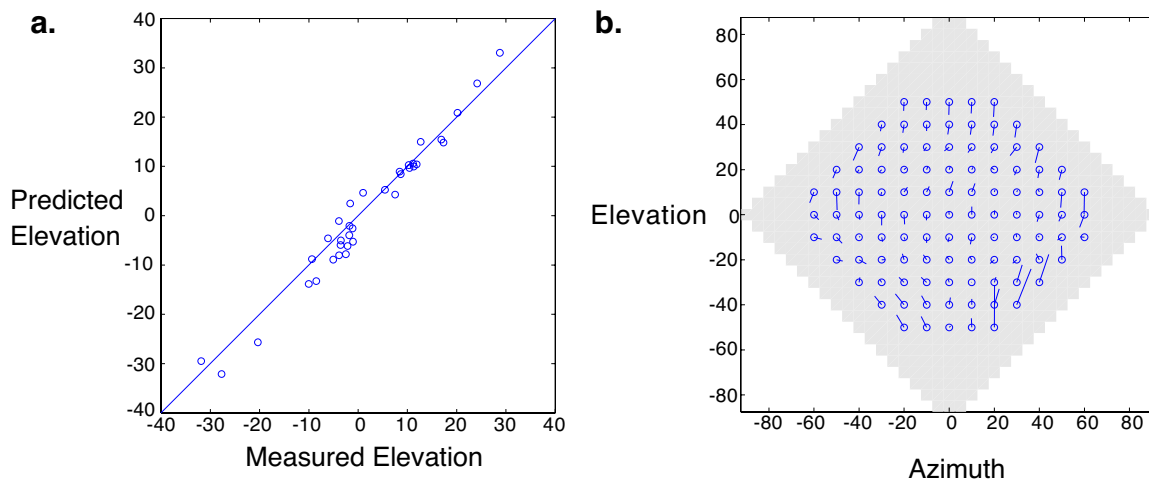
Figure 4. Accuracy of the model in reproducing the location of a training signal. (a) Best elevation of a model cell as a function of the best elevation of the receptive field used during training, where training stimuli are those within our sample of 34 cells. (b) Best location of the model after training with idealized receptive fields evenly spaced in central space. The circles show the location of the receptive field used in training, the line indicates the direction and magnitude of the error between the receptive field center and that of the training signal.

The importance of inhibition to the model can be assessed by examining the offset value, which is a free parameter whose value is chosen to maximize the similarity between the model's output and the neural response. As mentioned before, the offset parameter indirectly determines the balance of excitatory and inhibitory weights in the trained model. If it is zero, then all weights will be positive. If the offset is any positive number, both excitatory and inhibitory weights will develop. Furthermore, the strength of the inhibitory connections will increase with increasingly positive offsets. When the model was trained using the true receptive fields of our cells, the offset values were all positive, ranging from .07 to .33 with an average of .16. The magnitude of these values of course depends on the specific range of activity values used in the model. The

important fact is that offset values were consistently positive, suggesting that the ICx may rely on inhibitory as well as excitatory inputs to determine spatial selectivity.

Model Validation: The ILD-alone Receptive Field

The ability of the model to replicate the true spatial receptive fields on which it was trained shows that the model is *sufficient* to account for the receptive fields of real cells. However, it does not address the *necessity* of the proposed mechanism. Towards this end, we tested the ability of our model to replicate the ILD-alone receptive fields measured from our cells. This provides an independent validation of the model because the model was trained solely on the true receptive fields; the ILD-alone receptive fields thus represent a novel stimulus set. The ILD-alone receptive field is a particularly useful data set in this regard in that cells respond in a graded fashion to many of the locations tested. Thus, in contrast to the true space receptive fields, which are almost binary in nature, ILD-alone receptive fields provide many gradations of response for the model to match.

The ILD-alone stimuli presented to the model were identical to those used during physiological recording. For each cell, the model was first trained via experience with normal auditory cues and the measured true spatial receptive field. We then fixed the weights and presented the ILD-alone stimuli. The output of the model for several representative cells is shown in Figure 2, column 4. As

can be seen, the model generally captured the gross features of the ILD-alone receptive field quite well, including a horizontal band of excitation passing through the true receptive field. As with real cells, this excitatory band is often flanked by inhibitory zones.

The most serious discrepancy between the model's ILD-alone receptive field and the measured ILD-alone receptive field was a misalignment of the location of the horizontal excitatory band. In many cases, this error can be attributed to difficulties in learning the location of the true receptive field. As mentioned above, some locations are harder to learn than others, owing to intrinsic differences in the quality of ILD cues at different locations. If the model was not able to match the true receptive field, it also tended to have noticeable misalignment in the ILD-alone receptive field. However, even in the more serious cases of misalignment, such as the one shown in the bottom row of Figure 2, the general shape of the ILD-alone receptive field was preserved, albeit shifted up or down relative to the measured ILD-alone receptive field.

The model was also consistently less selective than the real cell. This can be seen clearly in Row 4; the model responds robustly at many locations where the neuron responds only weakly. It is precisely because of this effect that the squaring non-linearity was introduced on the output of the model. The squaring tends to enhance regions of strong response relative to less responsive regions. Obviously, the squaring non-linearity doesn't completely compensate for whatever non-linear integration processes are happening in real ICx cells.
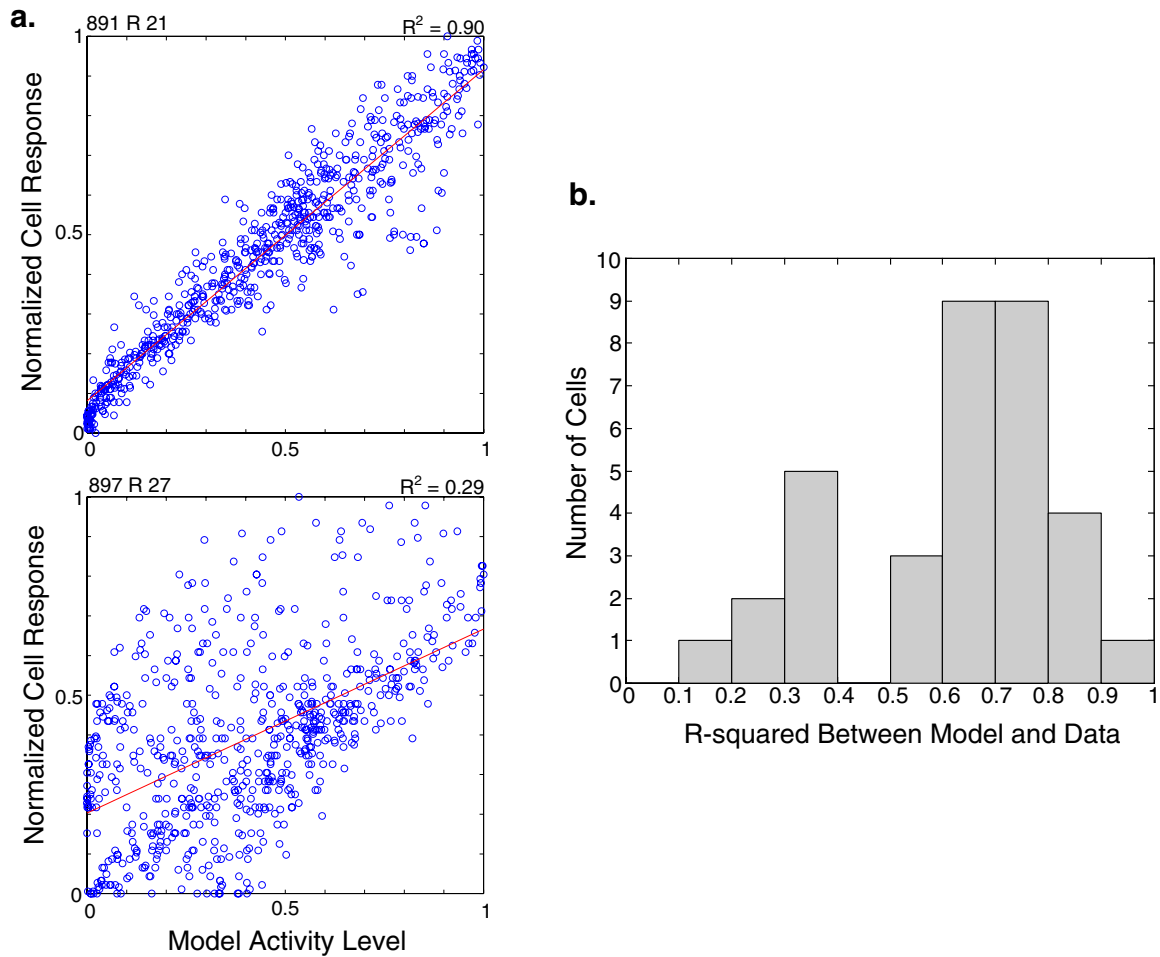
Figure 5. Assessment of the fit between model ILD-alone receptive fields and those measured from real cells. a.) Plot of the activity in the model vs. the activity in the real cell for each of the 684 locations on which the model was tested (neural responses were interpolated where data were not available). The line shows the best-fit regression line through the data. The R-squared value of this fit is shown in the upper right of each graph. b.) Distribution of R-squared values indicating the strength of correlation between the model and the neuronal activity for all cells in our sample.

    We quantified our results by comparing the activity of the model against the

activity of the cell on a location-by-location basis, as shown in Figure 5. A linear

regression of model response against the real neurons response was strongly

significant for all cells. To compare the relative quality of fit, we focused on the

R-squared value, which indicates the degree of variance in the cell's response

accounted for by the model. The value of R-squared ranged from .14 and .91,

with a mean of .60 (Figure 5b). We have included an example of one of the

weaker-fitting cells in our data (Figure 2, Row 5.) The residual errors, indicated

by the spread of the data around the regression line in Figure 5, are presumably

due both to measurement error in the neurophysiological data and to

discrepancies between the model and the actual neural mechanisms, a point to

which we will return in the discussion. In conclusion, we take the good fit to the

data in most cells and the fact that the overall pattern of results was similar even

in the worst cells as support for our model.

<u>Discussion</u>

Our experiment shows how virtual sound sources can be used to dissociate

the influences of ILD and ITD cues in the formation of auditory spatial receptive

fields. By setting ITD constant across locations we were able to reveal the

influence of ILD spectra on spatial receptive fields in the owl's IC. The resultant

ILD-alone receptive fields show that ILD spectra is facilitatory at the cell's best

location and inhibitory above and/or below. Furthermore, they show that cells

would respond to many more locations where ITD cues not restricting the

receptive field in azimuth.

We have also presented a simple model of how receptive fields in the ICx are formed over the course of development. The model is based on known physiology and tuning properties of the IC and incorporates a Hebbian learning rule inspired by plasticity within the IC. We have shown that this simple model is capable of reproducing the measured spatial receptive fields of IC cells. Further, we demonstrate that it is sufficient to support accurately placed receptive fields over large regions of the frontal hemifield. Finally, we have shown that this model, trained solely on a cell's true spatial receptive field, is capable of reproducing the amorphous shape of the ILD-alone receptive field measured from that same cell. This last step provides an independent validation of the model.

What mechanisms underlie the development of spatial receptive fields in the model? During training, ITD and ABL play an important role in shaping the tuning of the ICx unit to ILD spectra. Recall that the weights are determined solely via the correlation between input and output units, where the inputs are LS activity and the outputs are spatially tuned responses. The variation of ILD spectra with location is complex and its contribution to the final weights is difficult to interpret. ITD and ABL cues, on the other hand, are more consistent across frequency and their effects more easily discernable. Because input-layer cells are ITD tuned, the only possible stimulus locations that might drive the input units are those locations where the ITD cue values match the input units' intrinsic tuning. When ITD is not optimal, the product of the input and output unit activity,

which determines the change in weight strength, will be zero. Hence, the only locations which can influence the weights are those where ITD matches the input units' intrinsic tuning. This occurs primarily along a narrow vertical strip cutting through the cell's true receptive field (see Figure 6 b). As we will discuss shortly, ITD is also excitatory in one or two other regions, known as "side-peaks", and these will influence the weights. ABL effects are less extreme, but still important. Sounds from peripheral locations will be quieter (i.e., will have lower ABL) and will hence evoke less firing in the LS units. Consequently, peripheral locations will exert a weaker influence over the final weights.

Consider the effects of sounds at various locations on the development of weights. A sound from a location that will ultimately be the cell's best location will elicit activity in those units in the LS layer whose ILD and frequency tuning match the ILD spectrum corresponding to that location. At the same time, the training signal associated with this location will cause the output unit to have a strong positive activation, leading to a strengthening of the weight from all active units in the LS layer. Consequently, the fully trained model will be strongly excited by sounds originating from its best location.

A sound located above or below the cell's nascent receptive field, but along the vertical strip defined by the cell's preferred ITD, will also evoke a pattern of activity over the LS units; however, these patterns will be paired with a negative activity value in the output unit because, by supposition, all non-preferred locations elicit negative activity. As illustrated in Figure 6c, the product of activity

in the input and output units will be negative and the weights from input cells selective to spectra at these locations will be driven negative. After training, the model will thus be strongly inhibited by the ILD spectra corresponding to locations above or below the receptive field, but along the best-ITD strip. Note that low ABL levels will reduce the input strength when training stimuli originate from extremely high or low elevations. Consequently, these locations will not develop as strong an inhibitory influence on the cell (see Figure 6c).

Of particular interest is the effect of this learning mechanism on ITD side-peaks. The ITD tuning of LS cells with narrow frequency tuning is periodic, owing to a process that arises when comparing the time of arrival of a periodic signal at the two ears. The auditory system cannot discriminate ITDs that differ from the true ITD by an integer number of cycles (e.g., a 360-degree phase shift). This potential mismatch, often referred to as 'phase ambiguity,' is what leads to the observed ITD side-peaks. Cross-frequency interactions are known to reduce the response at side-peaks (Takahashi and Konishi, 1986). The correct ITD peak, referred to as the main peak, will be at the same ITD for every frequency. The location of the side-peaks, on the other hand, will differ at each frequency because the spacing of the side-peaks is inversely proportional to the cell's best frequency. Hence, when frequency channels are combined, as happens in the ICx, the ITD main peak will be reinforced while the side-peaks will not (Takahashi and Konishi, 1986). There are also demonstrated inhibitory processes, which suppress the ITD side peaks (Fujita and Konishi, 1991; Mori, 1997; Mazer 1998);

however all of the side-peak suppression mechanisms postulated thus far focus on the role of ITD.

Our model makes the novel prediction that ILD spectra should also play a role in side-peak suppression. This occurs because ITD side-peaks elicit positive activity in the input units coupled with negative activity in the output unit. Consequently, the model develops inhibitory weights to ILD spectra arising from side-peak locations. Side-peaks are usually at peripheral locations were ABL is low. Hence, the influence of these locations on the final weights will be weak. Perhaps because the inhibitory effects are weak, they are not readily apparent in our ILD-alone receptive fields; however, this prediction is consistent with our observation that ITD side-peaks are smaller when testing with true spatial stimuli than with ITD stimuli in which ILD spectrum is held constant, even when ABL effects are accounted for.

To summarize, the effects of ITD and ABL insure that the trained ICx unit receives strong excitatory inputs when presented with the ILD-spectrum at the center of its receptive field and strong inhibitory inputs when presented with the ILD spectra at locations directly above and below the receptive field (see also Figure 6e).

Both the data and the model point to the importance of ILD-based inhibition as a mechanism for shaping spatial receptive fields. In our measured ILD-alone receptive fields, the evidence for inhibition is that responses to locations above and below the receptive field are often lower than the cell's spontaneous rate. Of

Figure 6. How spatial receptive fields form in the model. a.) Pattern of activity fed to the output unit during training. b.) Mean activity over the input units during training as a function of location. This response surface reflects the ITD selectivity of input units. c.) Patterns of correlated firing that occur during training and that ultimately determine the weight strengths. d.) The ILD-alone receptive field for the model cell trained on the true receptive field shown in a. e.) The weight matrix for the trained model cell. This shows which frequency-specific ILD values the cell will respond to and whether those responses will be excitatory or inhibitory. Each square represents a single input unit with best ILD and frequency given by the axes. In b and d, the geometric shapes indicate corresponding points in space. In e, the geometric shapes indicate the frequency-specific ILD values (white lines) from the location specified by that shape in b and d. The model develops inhibitory weights for those frequency-specific ILD values that occur at the locations specified by the triangle and square. Conversely, the model is tuned to be strongly excited by the ILD spectrum arising at the location indicated by the circle.

a.

Training Signal

b.

Mean Input Strength

c.

Correlation between
Input and Training Signal

strong positive
zero
weak negative
strong negative

d.

ILD-alone RF

e.

Weight Matrix
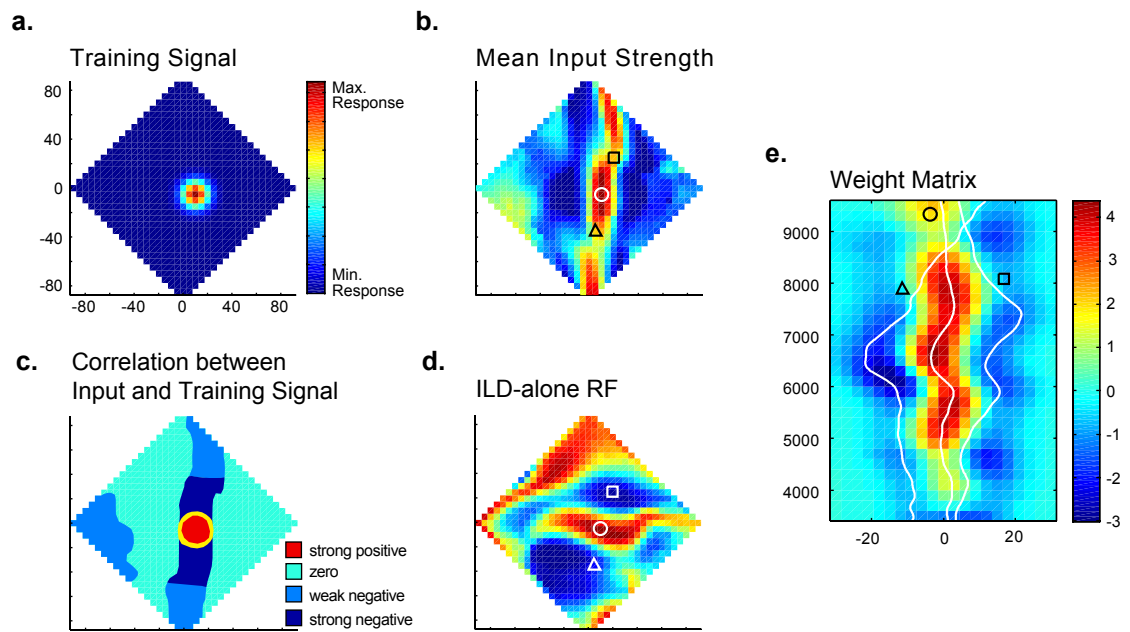
course, we cannot rule out the possibility that non-optimal ILD values simply remove a tonic excitatory influence, perhaps by exerting an inhibitory influence at an earlier processing stage. Discriminating these two possibilities will involve further experiments with pharmaceutical manipulations. The model also suggests that inhibition is important in the formation of tightly restricted receptive fields, as evinced by the finding that the model matches true receptive fields better when allowed some degree of inhibition. In the model, the locus of inhibition is the LS to ICx projection.

Our findings are consistent with other studies implicating inhibition as a contributing factor to spatial selectivity. Knudsen and Konishi (1978b) found that many space-tuned cells were inhibited by sounds placed outside their receptive field (i.e., they had an inhibitory surround). Brainard et al. (1992) showed that when receptive fields were measured with pure tones, cells exhibited firing to sounds at many locations outside of the true receptive field; however, these regions of extra activity were reduced when a second tone was played simultaneously. This suggests that inhibition is a critical mechanism in the resolution of spatial ambiguities.

Inhibition may explain why ICx cells fire only when both ITD and ILD cues are near optimal values, reminiscent of a logical AND-gate (Moiseff and Konishi, 1983; Olsen et al., 1989). It seems quite likely that this AND-like behavior is supported by inhibitory mechanisms: if either ITD or ILD spectra departs from optimal values, the cell is inhibited. Others have shown that ITD can suppress a

space-tuned cell's firing below spontaneous rate (Fujita and Konishi, 1991). Our study shows that ILD spectrum can have the same effect.

The mechanisms whereby inhibitory synapses are shaped by experience are largely unknown. Our assumption is that pairing of presynaptic activity with post-synaptic inhibition leads to a strengthening of an inhibitory synapse. Admittedly, our model is speculative in this regard; however, recent experiments with barn owls suggest that both excitatory and inhibitory mechanisms play a role in developmental plasticity. Owls raised with prisms over their eyes develop auditory receptive fields aligned with their shifted visual world (Knudsen and Brainard, 1991). Recently, Zheng and Knudsen (1999) have shown that inhibitory, GABA-ergic mechanisms play a role in this process by *suppressing* the response to non-adaptive receptive field locations.

The errors we observe in the model's ability to predict the measured ILD-alone receptive field may be partly attributable to measurement error. Noise in the measured ILD-alone receptive field puts an upper limit on the maximum degree of correlation between model and data. Errors in the measurement of the true spatial receptive field may have an even greater effect. The ability of the model to accurately match the ILD-alone receptive field depends on accurate information about the location of the true receptive field, because that is the only information the model receives during training.

Errors may also be attributable to the fact that some locations are intrinsically more difficult to learn than others, owing to the differences in the

quality of the underlying ILD cues (e.g., the steepness of the ILD gradient). The

errors may be magnified when testing with ILD-alone stimuli. In other words, a

small misalignment between the model and the data in the true receptive field

case may lead to a large error in the model's ability to predict the ILD-alone

receptive field. Most of the errors we observed appear to be related to

misalignments between the model's true receptive field and that of the real cell,

due either to measurement error or the inability of the model to completely

reproduce the true receptive field.

Our goal in building the model was to capture the essential features of the

owl's IC with a minimal number of assumptions and the simplest possible

architecture. Inclusion of more details would likely lead to better performance.

For example, it has been shown that lateral interactions within a map during

development can improve discriminability when the adjacent elements to be

mapped are quite similar (Kohonen, 1997). In our model, lateral inhibitory

connections between adjacent cells within the space map might have improved

its discriminative abilities in areas where the ILD cues were more difficult to learn.

We have also assumed that ICx cells receive connections only from those LS

cells whose ITD tuning corresponds with the cell's true receptive field location.

However, it is quite likely that cells with other preferred ITDs may play an

important role, especially in the suppression of ITD side-peaks. Another possible

structural difference between our model and the real system is that we have

omitted intermediate processing layers. Mazer (1995) has suggested that spatial

tuning in the ICx arises via a processing cascade where activity is passed through several intermediate cells before it reaches the ICx. While our model performs well with a single layer of cells, it would probably perform even better with an intermediate layer or two[1].

Another simplification of our model was our choice of linear summation plus squaring to describe processing in the post-synaptic cell. While the success of our model suggests that there is a strong linear component to the frequency convergence process, the integration of signals by a cell membrane is likely to be at least partly non-linear. The commonly reported finding that ICx cells respond poorly to pure tones (Knudsen and Konishi, 1978c) suggests that their combination of afferent activity is more akin to an AND-gate. In other words, an ICx cell is much more responsive when appropriate inputs come over many different frequencies channels simultaneously. Our squaring function captures this effect in a crude way. The squaring increases the contrast between strong and weak responses and the strong responses are often associated with inputs along many frequency channels. However, a more precise implementation of the convergence process, whatever it might be, might significantly improve the predictive ability of the model.

In conclusion, the process of transforming spectral information into spatial

---

[1] In a linear system, such as ours, increasing the number of layers will not lead to performance improvements; however, even slight non-linearities can render intermediate layers quite useful.

locations is complex, owing to the complex spatial distribution of cues and to the

necessity of performing matches simultaneously at many different frequencies.

However, a very simple mechanism appears to captures the gross features of

this process: a cell is tuned to those ILD spectral values which match the cells

preferred location and is inhibited by ILD spectra from locations above and below

the receptive field but along the best-ITD line. Our model shows how

developmental mechanisms would naturally lead to such a configuration. The

end result is that ILD restricts a receptive field perpendicular to the vertical band

defined by the cell's preferred ITD. ILD may also play a secondary role in the

suppression of ITD side-peaks.

<u>Bridge</u>

In the preceding chapter, we introduced a novel technique for dissociating

the effects of interaural time difference (ITD) and interaural level difference (ILD),

allowing us to uncover the role of frequency-specific ILDs in the generation of a

space-tuned cell's receptive field. We also presented a model that generated

spatial receptive fields much like those of real cells. We tested the model's ability

to generate the ILD-alone receptive fields, also measured from real cells, and the

results were encouraging.

Essentially, the following chapter examines the functioning of this model in

more detail. The model is based on the premise that an ICx cell derives its

spatial selectivity by integrating inputs from the IC lateral shell. Of this general

arrangement there seems little doubt. Less clear is *how* the ICx cell integrates its

inputs. Does it simply sum them or is does it use a more exotic integration

process such as logical ANDing? In this next chapter we test the specific

hypothesis that activity in an ICx cell is determined via a linear sum of its lateral

shell inputs.

CHAPTER III

THE ROLE OF FREQUENCY-SPECIFIC ILD TUNING IN THE COMPUTATION

OF SPATIAL LOCATION IN THE BARN OWL INFERIOR COLLICULUS

Introduction

In many species, including humans, the ability to localize sounds relies heavily on spectral cues. For each location, the external ears and face induce frequency-specific changes in both the intensity and arrival time of a sound. The ears and other features of the head thus function as a directionally dependent filter whose transfer characteristics are often referred to as the "head-related transfer function" (HRTF). The brain determines location by inferring what filtering a sound has received and using the known correspondence between HRTFs and locations to map the sound source into space. The information available at any single frequency is often ambiguous, and hence, accurate localization requires utilization of the entire spectrum (Takahashi and Konishi, 1986; Brainard, et al., 1992; Carlile and King, 1994). In other words, the animal must simultaneously match cues at multiple frequencies in order to determine a unique spatial location. While the basic principles involved in this complex process are well appreciated, the specific neural mechanisms that underlie it are not well understood.

We have investigated how spectral cues are transformed into spatial

information in the inferior colliculus (IC) of the barn owl. It has been shown that cells in the external nucleus of the inferior colliculus (ICx) have tightly restricted auditory spatial receptive fields (Knudsen et al., 1977). These cells are arranged topographically according to their best location, forming a map of external space (Knudsen and Konishi, 1978a). Our investigation focuses on how the restricted receptive fields of ICx cells are computed from spectral cues.

The evidence to date suggests that, rather than using monaural spectra, owls localize sounds based primarily on the intensity difference between the two ears, often referred to as the interaural level difference (ILD). First, introducing an earplug into one ear, which leaves monaural cues in the non-occluded ear intact, leads to systematic errors in sound localization and corresponding shifts in receptive field locations of IC cells (Knudsen and Konishi, 1979; Knudsen and Konishi, 1980). Second, changes in the ILD of a broadband noise presented over headphones induce vertical head movements (Moiseff, 1989). Third, neurophysiological studies have shown that space-tuned cells in the owl's optic tectum, which receives its auditory input directly from the IC, are tuned to ILD. More importantly, the ILD tuning of these cells varies with the cell's preferred elevation within a limited region of frontal space (Olsen et al., 1989). This contrasts with the situation in humans and other mammals were monaural spectral cues are equally important as ILD cues (Middlebrooks, 1997).

Measurements of the owl's HRTFs show that the relationship between ILD and spatial location is complex and frequency-dependent (Brainard et al., 1992;

Keller et al., 1998). Below roughly 4000 Hz, ILD varies monotonically with azimuth. At higher frequencies, ILD varies irregularly with both elevation and azimuth, though an elevational gradient is prominent in the region directly in front of the owl. At any particular frequency, ILD cues are ambiguous (i.e., a given ILD value usually occurs in more than one region of space), but ILD cues considered simultaneously at several different frequencies specify a unique location.

In addition to ILD, the other important cue for localization in owls is the interaural time difference (ITD). ITD is computed in a dedicated brain pathway that combines with intensity cues in the lateral shell (LS) of the IC, which provides the primary input to the ICx (Wagner et al., 1987; Feldman and Knudsen, 1997). ITDs arise via the differential path length from a sound source to the laterally separated ears. It provides a robust cue for azimuthal position (Moiseff and Konishi, 1981). In contrast to ILD, the ITD at a particular location varies only slightly with frequency. Thus, while ITD is in principle a spectral cue, it is often treated as a though it were a single, frequency-independent value.

How might the brain transform frequency-specific ILD values (i.e., ILD spectra) into spatial locations? It is known that cells in the LS are narrowly tuned to both frequency and ITD (Moiseff and Konishi, 1981; Takahashi and Konishi, 1986). In addition, these cells are selective for ILD, having sigmoidal or peaked ILD tuning curves (Moiseff and Konishi, 1983; Adolphs, 1993; Mazer, 1995). It is also known that ICx cells have broad frequency tuning curves, suggesting that they integrate inputs from many different LS cells (Knudsen and Konishi, 1978c).

An ICx cell presumably derives its spatial specificity through a selective combination of appropriately tuned LS cell inputs. Given that a pure tone stimulates only those LS cells selective for a single frequency, our premise is that pure tones can be used to probe the underlying tuning properties and input strengths of the LS cells that drive an ICx cell.

Relatively little is known about how space-tuned cells integrate intensity cues across frequency to generate spatial receptive fields. ILD tuning in the IC has been studied primarily with flat-spectrum broadband noises, which do not allow the mechanisms of spectral integration to be addressed (Moiseff and Konishi, 1981, 1983; Adolphs, 1993; Mazer, 1995). Brainard, Esterly, and Knudsen (1992) showed that the receptive field of an optic tectum cell measured with a pure tone was ambiguous, but that the true receptive field corresponded to the overlap of several single-frequency receptive fields. Space-tuned cells are thus able to combine information across frequencies to resolve ambiguity. This disambiguation process presumably relies on a cell's ability to discriminate frequency-specific ILD values. Indeed, measurements of the ILD tuning of optic tectum cells using narrow-band noise confirm that ILD tuning does vary with frequency (Esterly and Knudsen, 1989; Gold and Knudsen, 2000).

As a starting point, we assumed that an ICx cell derives its spatial selectivity via a linear summation of appropriately tuned excitatory and inhibitory LS inputs. If this is the case, then a cell's receptive field measured with broadband sounds should be completely predictable from the sum of its responses to pure tones. In

order to test this hypothesis, we measured the pure-tone ILD tuning of space-tuned IC cells over a range of frequencies. We also measured the owl's HRTFs. Combining a cell's frequency-specific ILD tuning curves with the acoustically measured ILD values at each location allowed us to generate a prediction of the cell's broadband spatial receptive field. Because a cell's spatial receptive field is determined by both ITD and ILD, this prediction process actually has two parts. First, we predict the contribution of ILD to spatial tuning. Second, we combine this with the measured ITD tuning of the cell to predict the true receptive field. The successes and failures of this predictive model provide important insights into the nature of the spectral integration process performed by ICx cells.

Because all our pure-tone ILD tuning curves were measured at the same ITD, the sum of their inputs can only reveal how a cell would respond were it tuned solely to ILD and not to ITD (i.e., it reflects the ILD contribution to spatial tuning). We call the spatial receptive field generated in this way the pure-tone predicted "ILD-alone" receptive field. The ILD-alone receptive field can also be measured directly using virtual sound sources, presented over headphones. Virtual sound sources are generated by using the measured HRTFs to re-create, at the eardrum, the waveform that would have been received by an external sound source at a particular location. Because the sounds are generated using digital signal processing techniques, the filters can be manipulated to generate a set of spatial stimuli in which the ILD spectrum is identical to that experienced under normal conditions but the ITD is set everywhere to the cell's preferred ITD.

The receptive field measured with these stimuli is referred to as the broadband ILD-alone receptive field. The ability to measure the ILD-alone receptive field directly allows us to verify the pure-tone predicted ILD-alone receptive field directly without making assumptions about the role of ITD.

The aforementioned analysis is agnostic with respect to the specific pattern of frequency specific inputs a cell might receive. It merely seeks to test whether the sum of the pure-tone responses is sufficient to predict a cell's broadband ILD-alone and true receptive fields. A specific hypothesis about the ILD tuning of an ICx cell is that it will match, at each frequency, the ILD value occurring at the cell's preferred location. A test of this hypothesis has recently been performed for space-tuned cells in the optic tectum (Gold and Knudsen, 2000). The authors suggest that a cell's ILD tuning does, in fact, correspond with the HRTF-derived ILDs from its preferred location; however, the variance in their measurements was large relative to the range of ILDs examined in their study. Thus, the hypothesis needs to be re-examined in more detail.

In summary, our goals in this study were threefold. First, to characterize the pure-tone ILD tuning curves of ICx cells, with the hope of shedding light on the nature of the LS inputs to ICx cells. Second, to see whether the pure-tone tuning curves can be used to predict the broadband ILD-alone and true receptive fields. This sheds light on the degree to which the LS to ICx processing step is linear. Third, to compare the best ILD tuning at each frequency with those values that occur at a cell's best location.

Methods

Stimuli

Details of the measurement and use of HRTFs are given elsewhere (Keller et al., 1998) but are explained here briefly. Head related transfer functions were recorded for each of the three owls used in this experiment. Owls were sedated with valium (0.025 ml/h, 5 mg/ml diazepam C-IV) and anesthetized with ketamine (0.05 ml/h, 5 mg/ml) delivered roughly once every four hours. Measurements were made in an echo-attenuating chamber (1.8 x 1.8 x 1.8 m) lined with acoustic foam. A small, moveable speaker served as the sound source. The owl's head was held in roughly the same orientation as that of a normal standing owl, with the flat portion of the inner, upper beak at 45 degrees downward. Miniature Knowles microphones (EM4046), fitted with 3.2 cm long probe tubes were then inserted into the ears so that the end of the tube was within 2 mm of the eardrum. During HRTF recording, the speaker was moved to a particular location and the transfer function of the speaker-ear-microphone system was measured at 30 kHz using broadband noise presented over the speaker. The transfer function of the speaker and microphone were also recorded and subsequently removed using digital signal processing techniques. This process yielded a finite impulse response filter for each ear. All filters were 255 points long. All frequency-domain analyses were based on a 1024-point FFT of the raw HRTF values. For details of signal processing techniques used in creating the

filters, please refer to Keller et al. (1998).

HRTFs were recorded with the speaker at 684 different locations covering the entire frontal hemifield, spaced every 5 degrees in azimuth and elevation using "double-polar" coordinates (Knudsen, 1982). In double-polar coordinates, azimuth specifies the angular separation between a given location and the medial plane, while elevation specifies the separation between a location and the horizontal plane passing through the center of the owl's head. The location zero degrees azimuth, zero degrees elevation was taken to be directly in front of the owl.

During recording sessions, stimuli were presented via earphones (model ER-1, Etymotic Research, Elk Grove Village, IL). To simulate a localized external sound source, a signal was convolved with two binaural filters, one that imposed the spectral profile appropriate for the specified location, and the other that compensated for the response characteristics of the earphones. Each bird was tested using its own HRTFs. All non-spatial stimuli (e.g., those used in ITD and frequency tests) were convolved with the same earphone inverse filters used in spatial tests.

To measure ILD-alone receptive fields, a set of filters was created that preserved each location's amplitude spectra but equated the ITD in left and right ears. The fast Fourier transform was used to extract the amplitude and phase spectrum of the time-domain filters. The phase spectrum from each ear was then replaced with a linear phase spectrum corresponding to a fixed delay. The

amplitude and phase spectra were then transformed back into the time domain

using an algorithm that minimized the difference between the filter's spectrum

and the desired spectrum. (invfreqz() function in the Matlab Signal Processing

Toolbox, version 5.2, The Mathworks, Inc., Natick, MA). The result was a set of

filters with zero interaural phase difference (i.e., ITD) across frequencies but with

the normal ILD spectrum. During stimulus presentation, the ITD was set to the

cell's preferred ITD using a separate filter. ILD-alone stimuli were also

manipulated so that the average sound pressure level, referred to as the average

binaural level (ABL), was equal at all locations, accomplished by scaling each

left-right pair of HRTF time-domain filters so that the average of the left and right

peak amplitudes was identical for every spatial location.

We also created a set of "ABL-equalized" spatial stimuli. Here, ITD and ILD

were allowed for vary normally but filters were scaled, as described above, so

that each location had equal ABL.

All stimuli, with the exception of binaural interaction plots (described below)

were presented with an inter-stimulus interval of 100 ms, which is faster than the

600-700 ms used in previous studies. We have conducted several validations

tests in which various tests were run at differing inter-stimulus interval values

from zero to 600 ms. We have found that inter-stimulus interval has little effect

on the overall shape of ITD, space, and frequency tuning curves, though it does

reduce the overall magnitude of response. ILD tuning curves performed at a

single frequency are affected by inter-stimulus interval, but ILD tuning curves

performed with randomly varying frequencies (as in our ILD-frequency test, described below) are minimally affected. The faster inter-stimulus interval was necessary in order to obtain responses to all stimulus sets before losing a cell.

Neurophysiology

Our data are based on single-cell recordings from the IC of three owls. Techniques for neural recording were similar to those used previously in our lab and reported elsewhere (e.g., Takahashi & Keller, 1992b) with the exception that the present results were obtained using bilaterally implanted recording wells. The wells, made of stainless steel, have a 7 mm inner diameter. Wells were implanted bilaterally over the owls telencephalon under isoflourine anesthesia (0.75 %, oxygen flow rate 1.0 liters/min.). A headplate with a small post extending upward was also attached to the head at this time. Both the headplate and recording wells were held in place with dental cement. Between recording sessions, the wells were filled with an antibiotic ointment and covered by small dalryn caps. Using these wells allowed for an extended number of recording sessions with each bird: 9-12 sessions of roughly 14 hours each. All procedures were approved by the institutional animal care and use committee of the University of Oregon.

During recording sessions, owls were sedated with valium (0.025 ml/h, 5 mg/ml diazepam C-IV) and anesthetized with ketamine (0.05 ml/h, 5 mg/ml) delivered roughly once every four hours. Single cells in the IC were isolated

using blunt-tip tungsten microelectrodes with a platinum coating (Fredrick Haer Co., 12 M Ohms). Action potentials were recorded using the Datawave Technologies' Discovery data acquisition package (Datawave Technologies, Longmont, CO) which stores the time of occurrence of each spike as well as a 32-point representation of the waveform. The waveforms were sorted off-line according to shape using a commercial software product (Autocut, Datawave Technologies), allowing us to verify that all data came from the same cell over the course of several tests and, in a few cases, allowing us to extract data from more than one cell at a single recording site.

The locations of recording sites were verified histologically, using an electrode coated with DiI (Molecular Probes, Eugene, OR) to provide a reference mark. The electrode was prepared by applying several coats of a saturated solution of DiI dissolved in ethyl alcohol, using a pipette as an applicator. Only a single DiI penetration was made for each side of the brain. The location of all other penetrations were determined relative to the reference mark. With one possible exception, all recording sites were established anatomically to be within the lateral shell of the IC or ICx (see Figure 1). The single outlier appears to be in the optic tectum; however, the responses from this site were no different in character than our other data and so the cell was not excluded.

While anatomical data showed that we were in the correct region of the brain, we relied primarily upon functional criteria to select space-specific neurons.

Figure 1. Anatomical location of all cells included in our analysis. A, Side view of an owls skull with a cut-away revealing the optic tectum, cerebellum and brainstem. The white line shows the approximate slice plane which extends horizontally through the rest of the brain. Note that the slice plane is perpendicular to the electrode penetration lines. The electrode was lowered from the top of the brain downward. B, Location of all penetrations superimposed on a horizontal section through the owl's inferior colliculus. Penetration locations were transformed into a common reference frame by aligning slices from each bird. Each white circle represents a single electrode penetration. In addition to the optic tectum and ICx, both the core and lateral shell (LS) of the IC are labeled. The lateral shell extends in the anterior and posterior directions, forming a band between the core and the ICx. Note that in many cases, several cells were recorded along a single penetration. The scale bar at the bottom left corresponds to one mm.
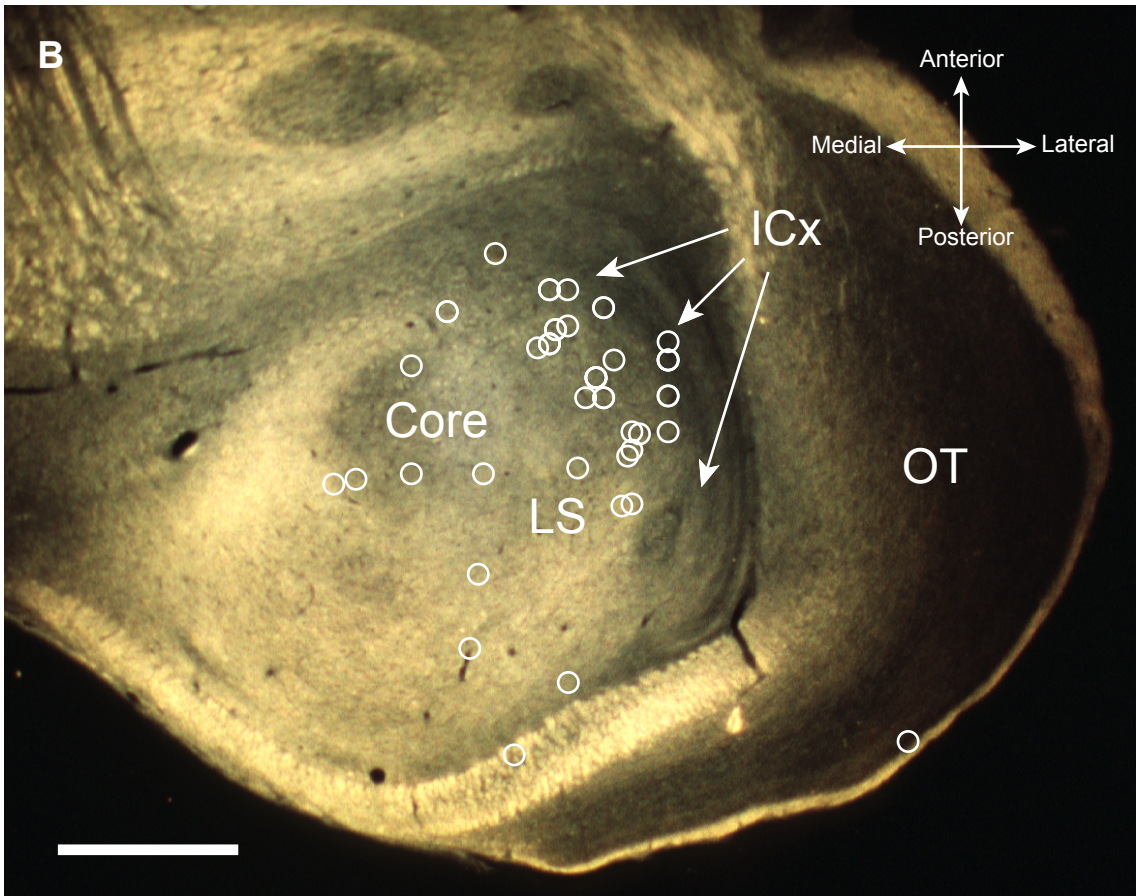
For each cell encountered, we measured its spatial receptive field by playing sounds from 360 evenly spaced locations in the frontal hemifield using virtual sound sources. The degree to which a neuron was space-specific was determined using a weighted moment-arm calculation on its receptive field. For each measured receptive field, all locations that elicited spike rates below spontaneous rate were set to zero and the surface was then scaled between zero and one. We then determined the location that elicited maximum firing (i.e., the peak location). The spatialization index was defined as the sum of the responses at each location times the distance of that location from the peak. This quantity was inversely correlated with a cell's degree of spatial specificity. We included in our sample only cells whose spatialization index was less than 15. We found that this index accorded well with more traditional metrics for selecting ICx cells including degree of ITD side-peak suppression (see Takahashi and Konishi, 1986) and width of the frequency tuning curve.

For every cell encountered a series of tests was run. We first measured the cell's true spatial receptive field, as mentioned above. The stimuli were divided into blocks, where each block contained a single occurrence of each stimulus location. Stimuli within a block were randomized and the blocks were repeated 5-10 times (i.e., 5-10 repetitions of each stimulus). We then measured the cell's ITD tuning curve using a broadband sound. ITDs typically covered the range -240 to +240 microseconds in 10 microsecond steps. Each stimulus was presented 10-20 times, also randomized by blocks. The ITD that elicited the

maximum response (i.e., the cell's best ITD) was used in all subsequent tests

that required a fixed ITD. In the third test, we measured the cell's response to

pure tones presented at all combinations of evenly spaced ILD and frequency

values. Preliminary screening was used to determine the range of frequency

values to use. ILD, on the other hand, was set to cover the normal range of ILDs

occurring in the HRTFs: -30 to +30 dB, though in a few cells it ranged only out to

+/- 25 dB. Note that positive ILD values mean the right ear was louder than the

left. Spacing of ILD and frequency values was typically 4 dB and 200 Hz,

respectively. We typically measured the response of the cell to 5-15 stimulus

blocks. The response to this entire set of stimuli is referred to henceforth as the

"ILD-frequency response surface". In the majority of cells, we also measured the

ILD-alone receptive field, using the same technique used to measure the true

spatial receptive field but with the ILD-alone stimuli described above. An ABL-

equalized space test was run on some cells. In this test, ITD and ILD varied

normally, but ABL was set to the same value for every location.

In a limited number of cases, we also measured a cell's response to all

possible combinations of left and right intensity. The resulting response surface

is referred to as a "binaural interaction plot," or BIP. This test was always

preformed using a pure tone with a fixed frequency. The inter-stimulus interval

used for BIP tests was usually 150 ms.

Tones and noises were presented at 15-20 dB above the average tone or

noise threshold of IC cells. Average tone and noise thresholds were determined

via measurements from a group of IC cells, some included in the present sample

and others not. If a cell failed to respond well to our stimuli, the sound pressure

level was typically increased by five dB.

Though all receptive fields were measured at only 360 locations, for the

purposes of display, we used linear interpolation to generate missing values so

that we had data for every location from which we had recorded an HRTF. This

resulted in 684 data points for each receptive field surface. For the purposes of

analyses, only the valid 360 locations were used.

Analyses

ILD-alone Receptive Fields

To generate predicted ILD-alone receptive fields from the ILD-frequency

response surfaces, we used a linear sum of the pure-tone responses, selected

according to the HRTF-based ILD values. We first limited our HRTFs to those

frequencies covered by the ILD-frequency surface. We next interpolated our

ILD-frequency surface so that the frequency axis values matched those of the

HRTFs and the ILD axis had spacing of 0.5 dB. ILD values were computed from

the HRTFs and rounded to 0.5 dB spacing so that they matched the ILD values

in the interpolated ILD-frequency surface. HRTF-based ILD values that were

beyond the usual -30 to +30 dB range represented in the ILD-frequency surface

were set to the most extreme ILD value with the same sign. For each location,

we now had an HRTF-derived ILD spectrum that also corresponded to a string of

values on the ILD-frequency response surface (i.e., those squares traversed by the ILD-spectrum line). The predicted response at a particular location was simply the average of this string of values.

As we describe below, we often observed that broadband ILD-alone receptive fields were more restricted than the corresponding pure-tone predicted ILD-alone receptive fields. To quantify this effect we first scaled both measured and predicted responses from each cell so they fell between zero and one and then fit the data to a curve of the form:

$y = x^n$

where y is the measured response, x is the predicted response and n is an empirically derived exponent. Curve fitting was accomplished via a simple exhaustive search for the exponent that produced the minimum mean squared error.

In addition to the mean squared error obtained from our curve fitting, we also wanted a parameter-free estimate of the variance in our predicted ILD-alone receptive fields. To accomplish this, the measured and predicted ILD-alone receptive fields were first scaled between zero and one. We then divided the predicted ILD-alone receptive field responses into 10 bins evenly spaced between zero and one. For each of these bins we took the corresponding measured ILD-alone values and found their mean and variance. The "random variance" estimate was taken to be the average variance across all bins, weighted according to the number of data points in each bin.

<u>Predicting True Spatial Receptive Fields</u>

We sought to predict a cell's true spatial receptive field based only on its broadband ITD tuning curve and its pure-tone ILD-frequency response surface. This process involved several steps, which we outline first before providing details. We first converted ILD-frequency response surfaces into ILD-alone receptive fields. We also converted ITD tuning curves into "ITD-alone" receptive fields, defined as the receptive field a cell would have were it tuned solely to ITD. We then multiplied the ITD-alone and ILD-alone receptive fields together. Finally, the product of these two single-cue receptive fields was adjusted for the effects of ABL, because the single-cue receptive fields are generated under the assumption that ABL is everywhere equal while in a normal space test ABL tapers off dramatically at peripheral locations.

Because ITD tuning is relatively insensitive to ILD (Takahashi et al., 1984), the ITD response at every location in space was easily estimated knowing only the cell's ITD tuning curve to flat-spectrum broadband sounds. Of course, ITD, like ILD, is a frequency-specific cue; however, unlike ILD, ITD changes only slightly with frequency. Hence, we estimated the ITD at each location by a single number: the frequency-weighted average of all ITD values at that location. A cell that responded most strongly to, say, 6000 Hz would thus have its broadband ITD tuning curve mapped into space using an ITD map dominated by the ITD cue values at 6000 Hz. The frequency tuning curves used in this analysis were

derived from the ILD-frequency responses surfaces: we took the maximum

response at each frequency, independent of ILD. Once we had the ITD at each

location, we took the broadband ITD tuning curve and mapped this into space,

thus generating the ITD-alone receptive field.

The next step in generating a spatial receptive field was to multiply the ITD-

and ILD-alone receptive fields. Before multiplying, each receptive field was first

linearly scaled so that the minimum value over all space was zero and the

maximum one. Multiplication yielded a prediction of what the cell's receptive field

would have looked like had ABL been equal at all locations (i.e., its ABL-

equalized receptive field).

To adjust for the effects of ABL on the predicted spatial receptive field, we

used an empirically derived function. In a subset of 20 cells, we measured both

the true spatial receptive field, in which ABL values varied in the normal fashion,

and an ABL-equalized spatial receptive field, in which ABL values were set the

same for every location. Both sets of test results were scaled between zero and

one. We then computed the ABL at each location in both tests, using a

frequency-weighted mean, resulting in a map of how much quieter the true-space

stimuli were than the ABL-equalized stimuli. We thus had three quantities for

each location: the true-space firing rate, R_{true}, the ABL-equalized firing rate, R_{eq},

and the attenuation of the true-space stimulus relative to the ABL-equalized

stimulus, ΔA. We fit this data with a scaled sigmoid function of the form:

$$R_{true} = \frac{R_{eq}}{1 + e^{b \cdot (a - \Delta A)}}.$$

The constants a and b were derived through a simple exhaustive search of parameter space to find the values that minimized the mean squared error between the data and the function. The resulting values were: a=0.3 and b=-9. This function was then used to adjust for the effects of ABL in the product of the ILD-alone and ITD-alone receptive fields. The effect of this operation was to reduce firing at peripheral locations where normal spatial stimuli are highly attenuated.

To quantify the ability of the model to match the cell's response, we compared the azimuth and elevation of the measured and predicted true receptive fields. In both cases, we first determined the set of locations encircled by the half-height contour line. In cases where more than one peak was present, we used only the contour surrounding the largest peak. The position of the receptive field center was then computed based on a response-weighted mean of these locations.

<u>ILD Curves</u>

ILD tuning curves were obtained from the ILD-frequency response surfaces by taking the responses to all ILDs measured at a single frequency. These pure-tone ILD curves were used to determine the average ILD tuning curve shape for curves with different peak ILDs. To compute the averages, we first interpolated ILD tuning curves so that their axis had one dB spacing and scaled them so that all responses fell between zero and one. ILD curves were grouped according to

ILD that elicited maximum response (i.e., the peak) into 9 bins whose corner values were: -30 -25 -15 -9 -3 3 9 15 25 30. Note that this grouping ignores the frequency at which a curve was measured. Within a single bin, ILD curves were shifted by single decibel steps so that all peaks were aligned. The aligned curves were then averaged.

For every ILD curve, we needed to determine the preferred ILD and the variance in this estimate. The preferred ILD was determined using a gaussian-weighing function. The gaussian curve was given by:

$$y = e^{\frac{-1}{2}\left(\frac{(x-a)}{b}\right)^2},$$

where x is ILD and y is the response to that ILD. The constant a is the location of the ILD peak. The constant b, set to the value 10, was chosen so that the gaussian curve provided a good visual match to the average pure-tone ILD tuning curves measured from ICx cells. For each tuning curve we wished to assess, we created a set of gaussian curves whose peak ILDs ranged from -30 to +30 in one dB steps. To find the preferred ILD for a given tuning curve, we took the dot-product of that curve with each of our gaussian curves. The preferred ILD was taken to be the peak ILD of the gaussian curve whose dot product with the tuning curve was greatest.

We also estimated the variance in the preferred ILD. Essentially, we wished to transform the quantified errors in measurement into an estimate of the variance in the ILD tuning curve peak. For each curve, we took the variance in the neural firing rate at each point as an estimate of the true neural noise. We

then ran 2000 simulations of separate measurements of the ILD tuning curve introducing random noise with the aforementioned variance. We then used the gaussian estimation technique to determine the preferred ILD of each simulated curve, creating a distribution of values. The variance of this distribution was taken to be the variance in the preferred ILD of the original ILD curve.

Among the questions we wished to address was how well the preferred ILD at each frequency matched the HRTF-based ILD values measured at a cell's preferred location. To address this question, we needed to screen our ILD curves so that our analysis was based only on cells with strong firing rates and low preferred ILD variances. We excluded from analysis curves whose maximum firing rate was less than 20 % of the maximum firing of the ILD-frequency response surface from which that ILD curve was derived. Because some cells had very high responses to extreme ILDs, we determined the maximum firing rate of an ILD-frequency surface based only on those responses between -20 and +20 dB. We also excluded an ILD curve if the variance in the estimate of the preferred ILD was greater than three dB.

Modeling

The object of the model was to generate the best possible linear system capable of recreating the observed ILD-alone surfaces. We chose a single-layer neural network architecture consisting of an array of input units and a single output unit. This architecture is modeled loosely after the IC, where inputs

correspond to the LS and the output to an ICx cell. The network was presented with HRTF-derived input patterns and trained to reproduce the observed ILD-alone receptive field of a single cell. We thus trained the network separately for each cell in our sample.

The input array consisted of cells with narrow ILD and frequency tuning covering every combination of best ILD and best frequency within a set range of values. We included one input unit for every ILD-frequency combination in the ILD-frequency response surface. This was done so that our results would be directly comparable to those obtained via a simple sum of pure-tone responses. Units were added to cover frequencies between 2000 Hz and 11000 Hz, maintaining even spacing. A typical instantiation of the model thus had input units covering 16 ILD values and 40 frequencies for a total of 640 units. The single output unit derived its activity from a weighted sum of the input unit activities.

Input unit activity was determined from the HRTF-derived ILD spectra. The ILD tuning curves of input cells were triangular, with responses ranging from zero at the preferred ILD of the adjacent cell to one at the cell's own preferred ILD. Frequency tuning curves were rectangular but were so narrow that the cell responded to only a single frequency in our discretely sampled spectra. For each location, the activity in each unit was determined from its tuning curves and the frequency-specific ILD values present at that location. Implicit in the model is the assumption that each input unit also had ITD tuning matched to the preferred

ITD of the output unit. Output unit activity (i.e., the training signal) was taken

directly from the ILD-alone receptive field, scaled between zero and one.

Training was accomplished using a modified version of the back-

propagation algorithm (Rumelhart and McClelland, 1986). We used an

adaptively adjusted learning rate and momentum to speed the learning process

(see the Matlab Neural Network Toolbox, The Mathworks, Inc., Natick, MA).

Patterns were presented repeatedly in blocks and the weights adjusted after

every block. To prevent over-training the network, gaussian-distributed noise

was added to the training patterns. The standard deviation of the noise added to

each input unit was 0.4 times the specified activity of that unit. This level of noise

was selected because it led to "smooth" input weights; that is, units with similar

tuning characteristics had similar weights. This redundancy in the weight matrix

shows that the system is not relying on single weights to encode specific patterns

as it does when over-trained.

Results

ILD Tuning Characteristics of Space-tuned IC Cells

We measured the responses of 46 space-tuned IC cells to all combinations

of equally-spaced ILD and frequency values, creating an "ILD-frequency

response surface". The set of all responses measured at a single frequency

defines an ILD tuning curve.   Of particular interest in our study was the

frequency-dependence of ILD tuning within a single cell. However, we start by

describing the general characteristics of the observed ILD tuning curves.

The ILD tuning curves for all cells, independent of frequency, are shown in Figure 2. For all curves shown, ILD responses were measured in the range –30 to +30 dB, where, for this analysis only, positive values mean the intensity was greater in the ipsilateral ear. The "best ILD" was taken to be the ILD that elicited maximum response (i.e., the peak of the ILD tuning curve). Best ILD values covered the entire range between +30 and –30 dB though a large proportion of the peaks fell between –10 and +10 dB. The distribution of best ILD values was symmetric; in other words, the number of ipsi-louder and contra-louder best ILD values was roughly equal.

ILD tuning curves were, in general, peaked but the shape of the curve depended upon the location of the peak. Figure 2B shows the averaged ILD tuning curves for different peak ILD values. The shape of broadband ILD tuning curves in the LS have been described according to three loose categories: peaked, sigmoidal and open-peaked, where "open-peaked" refers to a curve with a well defined maximum but where one of the flanks fails to return to base rates even at extreme ILDs (Mazer, 1995). Our measurements indicate that the pure-tone ILD tuning curves of space-tuned IC cells may also be described according to these three categories. However, whether a curve is open, open-peaked, or sigmoid appears to depend on the cell's best ILD. Cells tuned to ILDs near zero tend to be symmetrically peaked, cells tuned to more extreme ILD values tended to be

Figure 2. ILD tuning curves. In both A and B, positive ILD means ipsilateral ear louder. A, This plot shows all ILD tuning curves from all cells, regardless of frequency. Curves are sorted according to the ILD value at their peak. Each curve has been interpolated to one dB spacing so that all curves could be displayed on a common plot. B, Average ILD tuning curves. ILD curves from A were grouped according the peak ILD values shown in the legend. Each group of curves was aligned and averaged, yielding the curves shown here.

A

B
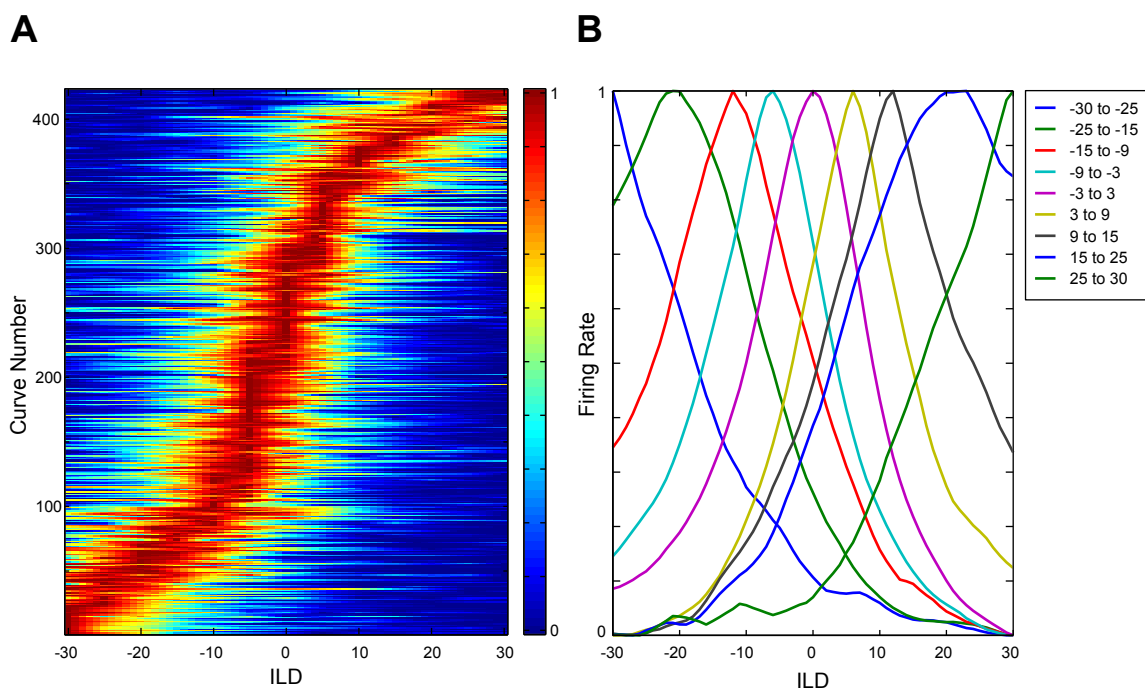
open-peaked, and cells whose peak was near +/- 30 dB tended to be sigmoidal.

Of course, we cannot exclude the possibility that the flanks of all curves would

have returned to base rates had the curves been extended to sufficiently

extreme, and non-physiological, ILD values. However, the reduction in the

steepness of the slope near +/- 30 dB argues against this possibility. In a handful

of cells, ILD tuning curves at one frequency were extended to +/- 50 dB and cells

were found to be, in fact, open-peaked (data not shown).

Figure 3 shows the distribution of best ILD, determined by the position of the

peak, as a function of the frequency at which the curve was measured.   Here,

and in the rest of the paper, positive ILD values correspond to *right ear louder*. In

general, the range of ILD values increased with increasing frequency. In

particular, tuning to ILD values more extreme than +/- 25 dB were seldom

observed below eight kHz. A similar pattern was seen in the acoustic ILD values

measured at each cell's best location, consistent with the idea that a cell's ILD

tuning matches the ILD cue values at its best location (see Figure 3B).

We observed that ILD tuning curves for a single cell often changed with

frequency. The ILD-frequency response surfaces are shown in the first column

of Figure 4.   In some cases, frequency-dependent ILD changes can be dramatic.

For example, in the third row, ILD tuning changed from -20 dB at 8000 Hz to +10

dB at 7200 Hz. However, the changes were smaller in most cells. The changes

in ILD tuning were highly sensitive to frequency. As shown in rows four and five,

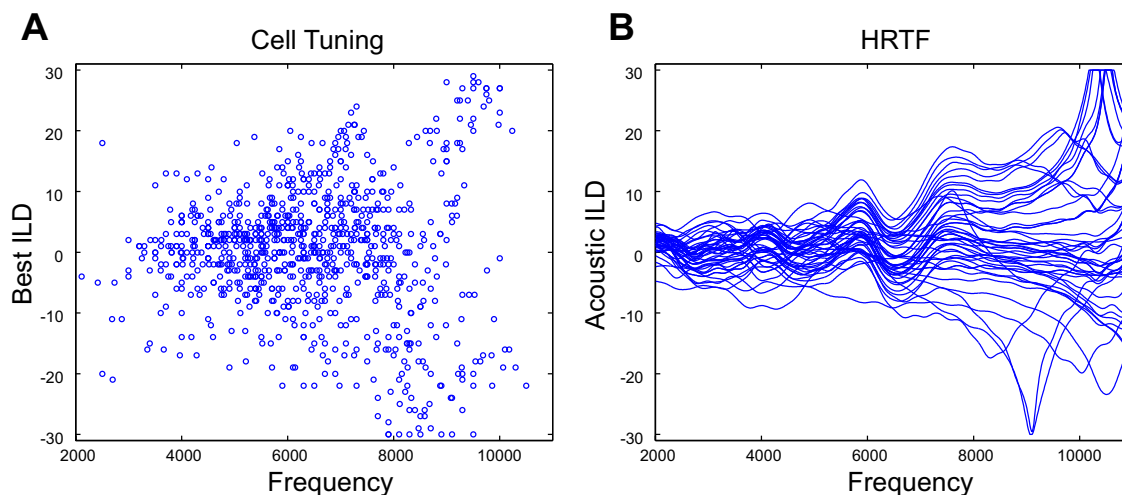even ILD tuning curves spaced apart by a mere 200-300 Hz showed clearly

Figure 3. Distribution of the peak of the ILD tuning curve and acoustic ILD values as a function of frequency. A, The location of each ILD peak ("Best ILD") as a function of the frequency at which the ILD tuning curve was measured. Data have been collapsed across all cells. B, Each trace represents the HRTF-derived acoustic ILD values associated the best location of a single cell, plotted as a function of frequency. Traces are shown for all 46 cells in our sample. Acoustic ILD values more extreme than +/-30 have been truncated.

different preferred ILDs.

In cells with significant spontaneous activity, inhibitory zones were prominent in the ILD-frequency response surfaces. As exemplified in the first three rows, it was common to see inhibition on both sides of the ridge defined by the preferred ILD at each frequency.

Relationship Between Pure-Tone ILDs and ILD-Alone Receptive Fields

In order to compare pure-tone responses with those measured using broadband sounds, we used the HRTFs to transform pure-tone ILD-frequency response surfaces into a predicted ILD-alone spatial receptive field. For a given

location, we first used the HRTFs to determine the acoustic ILD value occurring at each frequency. We then took each frequency in turn and asked: how strongly would the cell have responded to this ILD at this frequency? The net response to the ILD spectrum from a particular location was taken to be the average of the pure-tone responses to each of the frequency-specific ILDs occurring in that spectrum. The details of this procedure are given in the methods section. The sum of pure-tone responses yields the *ILD-alone receptive field* because both ITD and ABL were fixed for all pure-tone measurements. Hence, the sum of their responses must also be independent of these two variables. It should be emphasized that this method of transforming pure-tone responses into ILD-alone receptive fields is purely linear.

The pure-tone predicted ILD-alone receptive field was compared against the ILD-alone receptive field measured with broadband sounds. As detailed in the methods section, broadband ILD-alone stimuli were created by maintaining the normally occurring ILD spectrum at each location but setting ITD and ABL to the same value at every location. We have provided a description of the results of this test in a previous paper (see Chapter II of this dissertation). The results are presented here solely for the purposes of comparison with the pure-tone responses. Broadband ILD-alone receptive fields were obtained for only 34 of the 46 cells in our complete sample. For all cells, we also measured the "true" spatial receptive field, defined as the receptive field measured with all cues--ITD, ABL, and ILD--varying in the same way they do under free field conditions. In

Figure 4. ILD-frequency response surfaces, pure-tone predicted ILD-alone receptive fields, and broadband ILD-alone receptive fields. Each row shows the data from a single cell. The first and third columns show directly measured cellular responses: the ILD-frequency response surface and the ILD-alone receptive field, respectively. The white line traversing each ILD-frequency surface indicates those ILDs occurring at the cell's preferred spatial location. The diamonds in the second and third columns represent all locations in the frontal hemifield, from the owl's perspective. Coordinates are double-polar (Knudsen, 1982). The white loop shows the half-height contour line surrounding each cell's true receptive field (true receptive field not shown). The second column shows the results of summing pure-tone responses according to the HRTF-based ILD values. This generates a predicted ILD-alone receptive field. The scale bars for columns 1 and 3 indicate firing rate, in spikes per stimulus, less the spontaneous rate. The scale bars for column 2 indicate the averaged sum of pure-tone responses, as described in the text.

MEASURED ILD-FREQ RESPONSE

SUM OF PURE TONE RESTPONSES

MEASURED ILD-ALONE RECEPTIVE FIELD
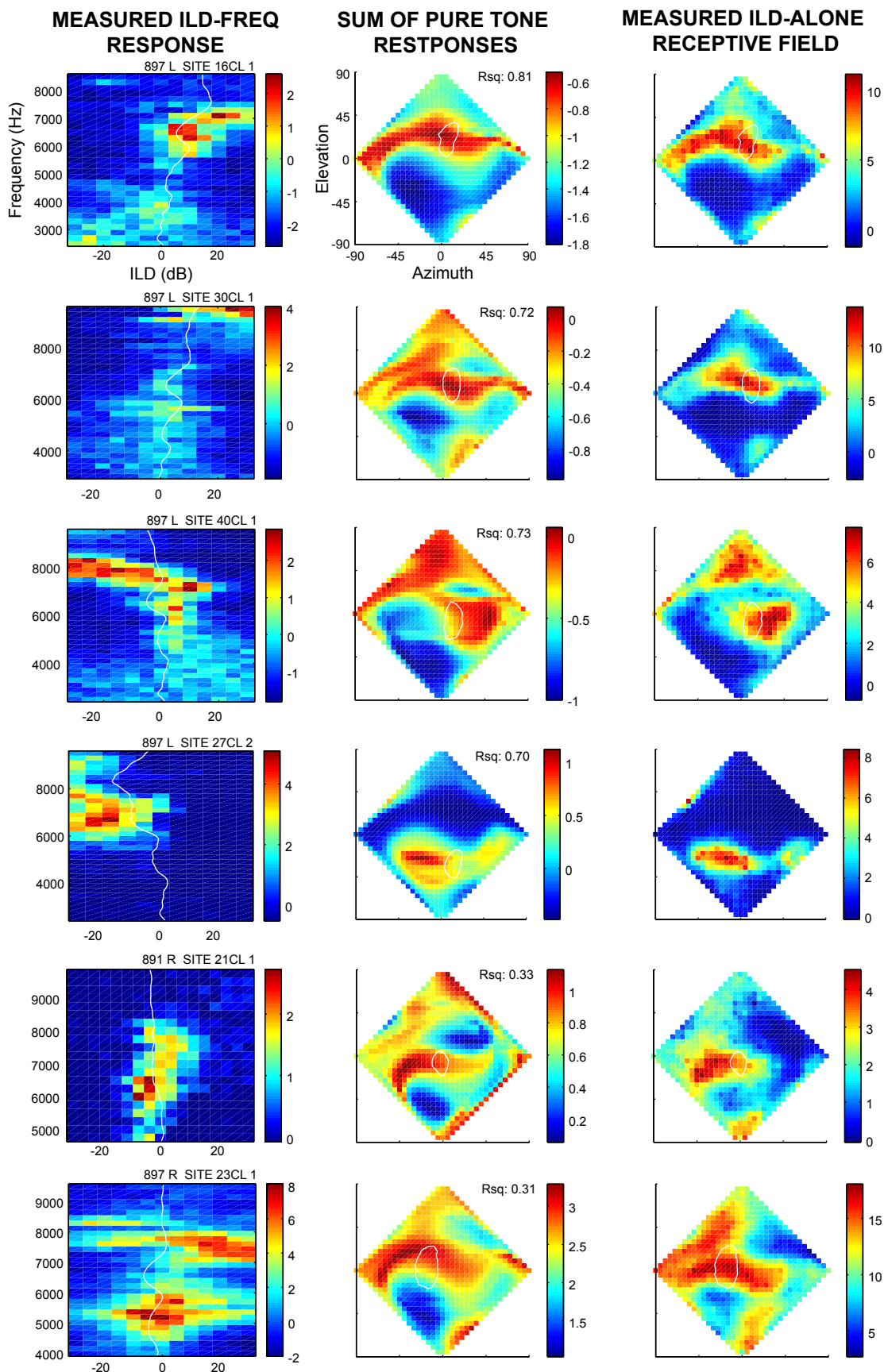
other words, the true receptive field is the same as the classical free-field

receptive field, though in our case we measured it using virtual sound sources.

For clarity, the various predicted and measured spatial receptive fields discussed

in this section and the next are summarized in Table 1.

Table 1. The varieties of spatial receptive fields and how they were obtained.

		Source of Measured Data	
		Pure Tones	*Broadband*
Type of Spatial Receptive Field	*ILD-alone*	Pure Tone Predicted ILD-alone Receptive Field: Pure tone responses to ILDs and frequencies are summed using the HRTFs	Broadband ILD-alone Receptive Field: Cellular responses are measured to broadband stimuli filtered with HRTFs that have been altered so that ITD and ABL are constant for all locations
	True Space	Pure Tone Predicted True Receptive Field: Pure-tone ILD-alone receptive fields (from above) are combined with ITD-alone receptive field	Broadband True Receptive Field: Cellular responses are measured to *normal* spatial stimuli in which ITD, ILD, and ABL all vary

Figure 4 shows pure-tone predicted ILD-alone receptive fields along with

the corresponding broadband ILD-alone receptive fields for comparison. Pure-

tone predicted ILD-alone receptive fields were similar in overall shape to those

obtained with broadband noises. In general, both pure-tone and broadband ILD-

alone receptive fields were amorphous, lacking easily describable topologic

features; however, we usually observed a horizontally oriented band of activity.

For broadband ILD-alone receptive fields, this excitatory band almost always passed through the center of the true receptive field. For the pure-tone predicted ILD-alone receptive fields, slight misalignments between the excitatory band and the true receptive field were common, as shown in the bottom row of Figure 4. For both broadband and pure-tone ILD-alone receptive fields, the excitatory band was flanked above and/or below by zones of minimal activity. Responses in these zones where demonstrably inhibited in cases where spontaneous activity was high enough to allow such an assessment.

Compared with *true* receptive fields, ILD-alone receptive fields, both pure-tone and broadband, showed much greater firing at peripheral locations. This effect may have been due to ABL equalization. Under free-field conditions, ABL falls off by as much as 40 dB as one moves away from the region of space directly in front of the bird. This contributes to the lack of firing seen at peripheral locations in true spatial receptive fields. In ILD-alone tests, however, ABL is set everywhere equal, so peripheral locations have their amplitude increased relative to those in central space. This increases firing rates in the periphery.

Curiously, in some cases with strong spontaneous activity, the pure-tone predicted ILD-alone receptive field was dominated by negative values. This occurred because many of the pure-tone responses fell below spontaneous activity (see Figure 4, rows 1 and 2). Thus, with pure tones, the net strength of inhibition is sometimes stronger that the net excitation. With broadband sounds, on the other hand, positive responses always dominated the ILD-alone receptive

field. This suggests that, relative to pure tones, some mechanisms must emphasize the excitatory inputs to a cell in the context of broadband sounds. To facilitate comparison between pure-tone predicted and broadband ILD-alone receptive fields, both receptive fields were usually scaled so that the minimum response was zero and the maximum response was one.

Though the pure-tone predicted and measured ILD-alone receptive fields are similar in many respects, there are differences. In some cases, pure-tone ILD-alone receptive fields were noticeably misaligned relative to the broadband ILD-alone receptive field (e.g., Figure 4, row 6). However, even in the worst cases, such as the one shown in Figure 4, row 6, the same general shape was usually recognizable. In many cases, pure-tone predicted receptive fields captured idiosyncratic auxiliary zones seen in the broadband receptive field. In the third row of Figure 4, for example, the pure-tone and broadband receptive fields share a zone of excitation at higher elevations. However, in other cases, pure-tone receptive fields were much more extended (e.g., Figure 4, row 5). In general, broadband ILD-alone receptive fields were more restricted than pure-tone ILD-alone receptive fields.

To quantify the fit between pure-tone predicted and broadband measured ILD-alone receptive fields, we matched the two receptive fields on a location-by-location basis and took the Pearson's product moment correlation (i.e., "R-squared"). This value corresponded well with our visual assessment of the similarity between two receptive fields. Figure 5 shows the activity in the
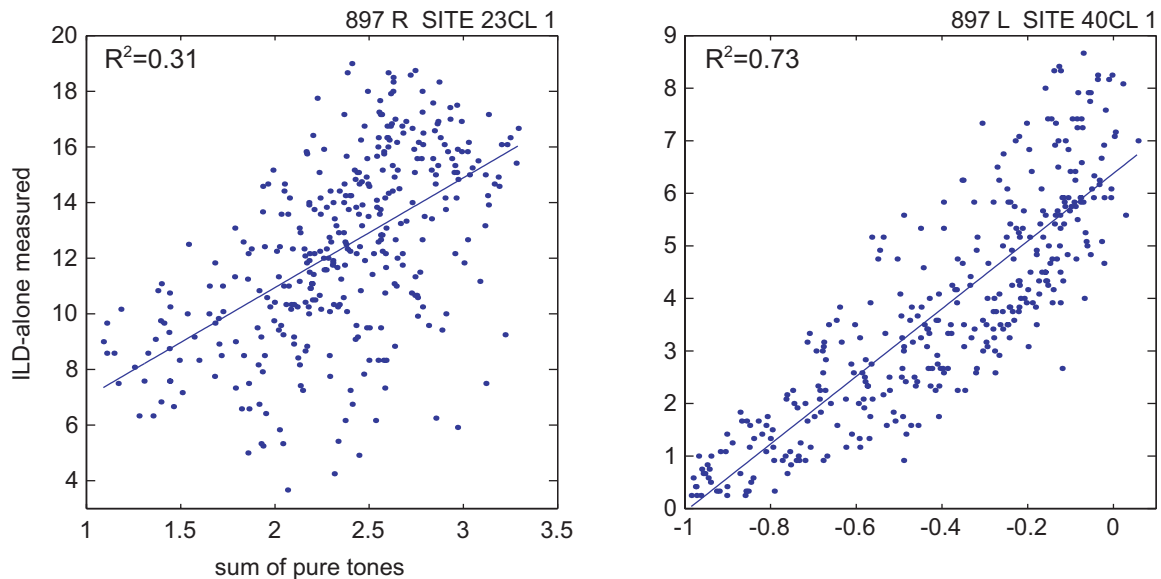
Figure 5. Example broadband versus sum of pure-tone ILD-alone receptive fields plotted on a location-by-location basis. The R-squared value for each plot is show in the upper right. The plot on the left shows a cell in which the ability of pure tones to predict the broadband response was poor while for the plot on the right the prediction is quite good. Axes values have not been scaled.

broadband ILD-alone receptive field against the corresponding activity in the

pure-tone ILD-alone receptive field along with the best-fitting regression lines. In

all cases, the slope of the regression line differed significantly from zero (p<0.01).

As shown in Figure 6A, R-squared values ranged from 0.20 to 0.83 with many

cells in the 0.7 to 0.8 range. The mean R-squared was 0.56; i.e., the linear sum

of pure-tone responses accounted for roughly 56 percent of the variance in the

broadband ILD-alone response.

Obviously, some of the variance in the broadband response is due to

random noise introduced during the measurement of the cell's response.

Similarly, errors in measurement of a cell's response to pure tones will propagate
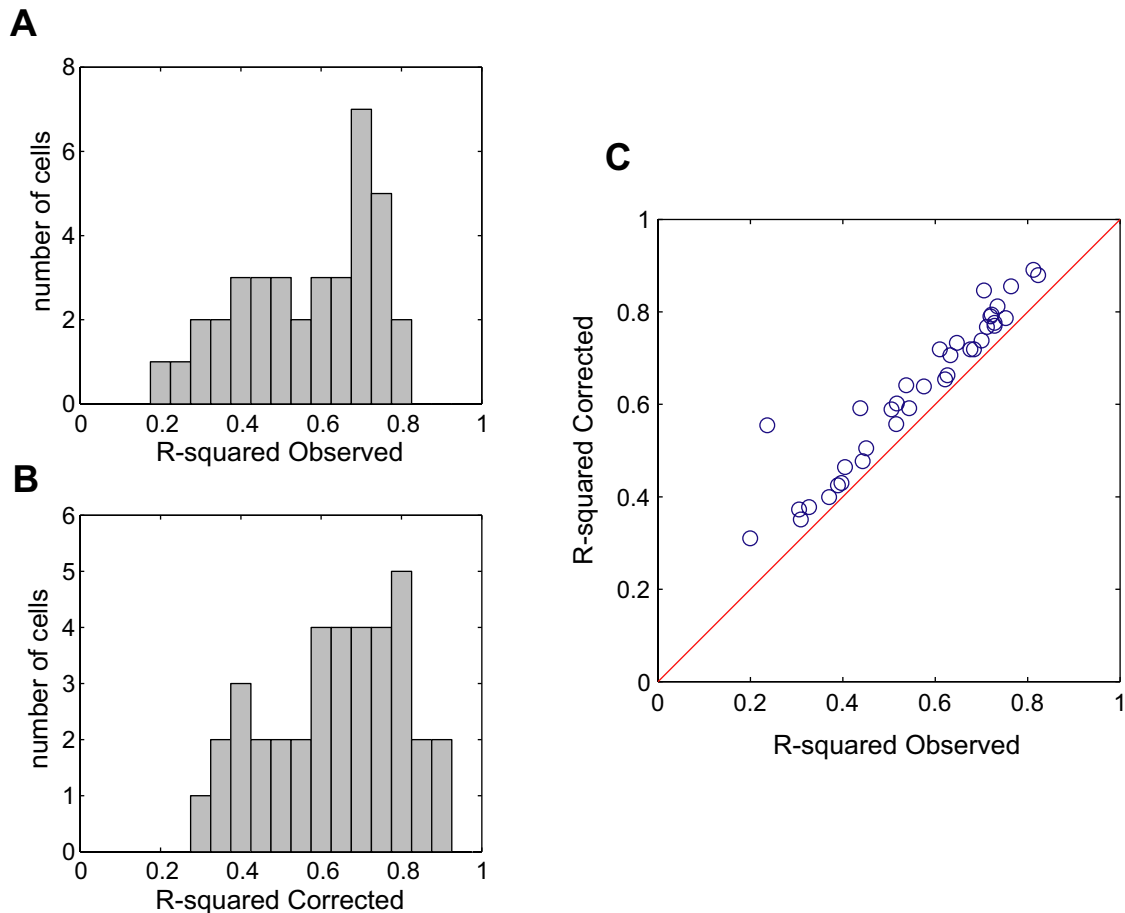
Figure 6. R-squared values for predicting broadband ILD-alone receptive field values from a linear sum of pure-tone responses. A, Distribution of all R-squared values based on a simple sum or pure-tone responses. B, Same as A, except that R-squared has been adjusted to compensate for the effects of random noise in the neural data (see text). C, Estimated improvement in quality of pure-tone prediction, on a cell-by-cell basis, after compensating for neural measurement error.

to the predicted ILD-alone receptive field. This error variance lowers our

estimates of the R-squared between pure-tone and broadband receptive fields.

In appendix A, we describe the technique we used to adjust for the effects of this

random measurement error on the observed R-squared values. After

compensating for measurement error, the mean R-squared increased to 0.63.

The distribution of corrected R-squared values is shown in Figure 6B. Figure 6C shows the effect of this compensation for each cell. It is clear from this plot that the two cells with the lowest R-squared values might have had much higher R-squared values had measurement error not been a factor.

The prediction errors have many sources, many of whose effects are apparently random. However, in some cells we did observe a systematic tendency for the sum of pure-tone responses to overestimate firing rates at locations with intermediate response magnitudes. In other words, measured ILD-alone receptive fields were more restricted than the pure-tone predicted ones. As shown in Figure 7, this effect manifests itself as a downward bowing when pure-tone predicted and broadband ILD-alone receptive fields are scaled and plotted against one another. To quantify the degree of bowing, we fit a line of the form $y = x^n$ to each cell's pure-tone vs. broadband data plot. In some cases, the data were highly variable, as shown in the upper left plot of Figure 7A. We quantified this random error[1] by taking the variance of the data about the mean value, measured in 10 discrete intervals between zero and one and then averaged. Figure 7B shows the distribution of exponents as a function of the random variance. Obviously, when the random variance is large, it makes it impossible to observe systematic deviations in the data. Hence, we excluded all cells in which the random variance was greater than an arbitrarily chosen value

---

[1] We call the error "random" to contrast it with systematic variations in the cell's response.
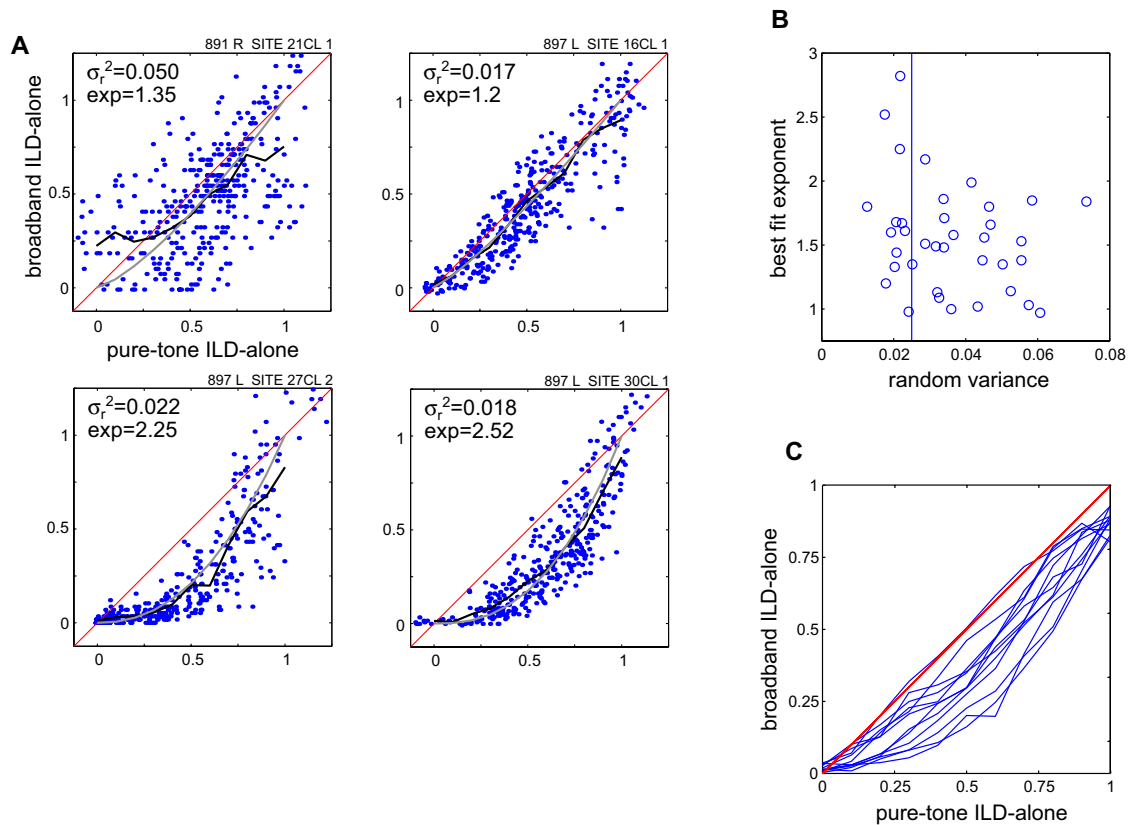
Figure 7. Analysis of a systematic non-linearity in the prediction of ILD-alone receptive fields based on a sum of pure-tone responses. A, Each plot shows the normalized broadband ILD-alone firing rate as a function of the response predicted from a sum of pure-tone responses. Data are plotted on a location-by-location basis. The jagged black line shows the running average of the distribution while the gray line shows the best fitting curve of the form $y=x^n$. The variance due to non-systematic effects ("random variance" or σ_r^2) was estimated as described in the text and is shown in the upper left corner of each plot. The exponent ("exp") of the best fitting curve is also shown. B, The exponent of the best fitting curve is plotted as a function of the estimated random variance. The solid line through 0.025 on the x-axis indicates the arbitrary cut-off used to define low-variance cells. C, For each of the low-variance cells in B, we plot the running average line on a single axis for comparison. All curves have a systematic downward bow.

of 0.025. Figure 7C shows the mean response for the 12 cells that met this

criterion. A downward bow is apparent in the majority of these low-variance

cells. The average exponent for these 12 cells was 1.74. This suggests that the

broadband response might be better approximated by the square of the summed

pure-tone responses.

We have previously suggested that, during development, a cell becomes

tuned in such a way that ILD inhibits sounds arising from locations above and

below the preferred location but along the vertical strip defined by the cell's best

ITD (Chapter II). The broadband ILD-alone receptive fields are consistent with

this hypothesis.However, the broadband ILD-alone receptive field reflects the

influence of both excitatory and inhibitory inputs at each point in space. In order

to assess the contribution of inhibitory inputs alone, we took a subset of our cells

that had significant spontaneous activity and converted only the inhibitory regions

Figure 8. Spatial correlates of inhibitory pure-tone responses. Spontaneous rates were subtracted from pure-tone responses to yield negative firing rates wherever inhibition was present. We then took the inhibitory weights and converted them to space, using the same linear sum of pure-tones used to generate full pure-tone predicted ILD-alone receptive fields. The white asterisk indicates the location of the cell's true spatial receptive field.

of the ILD-frequency responses surface into spatial receptive fields. The results

from three representative cells are shown in Figure 8. The inhibitory ILD-alone

receptive fields show clearly how inhibition serves to limit responses to locations

above and below the receptive field. In cases where true receptive fields were

located at extremely low elevations, inhibition was observed only above the best

location. Similarly, if the true receptive field elevation was high, inhibition was

only seen below.

Relationship Between Pure-Tone ILDs and
True Spatial Receptive Field

In this analysis, we addressed whether a cell's *true* receptive field could be

adequately predicted from its response to pure tones. The pure tone responses

were combined to yield an ILD-alone receptive field, which constitutes the ILD

contribution to spatial tuning. This had to be combined with the cell's ITD tuning

in order to predict the true spatial receptive field. In addition, because ABL is

constant in the ILD-alone test but not in a true space test, we had to compensate

for ABL. This analysis addresses how ILD-alone receptive fields relate to true

spatial receptive fields but it also sheds light on how ILD and ITD cues are

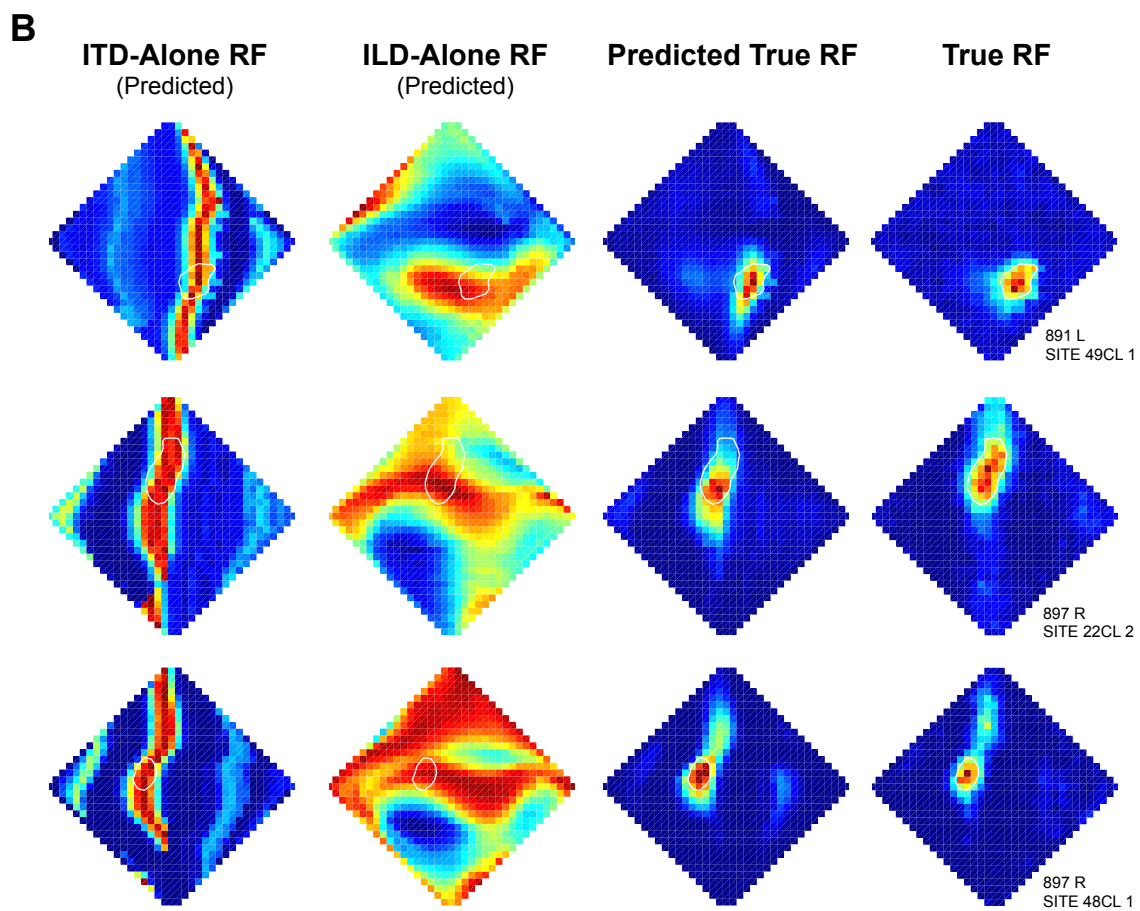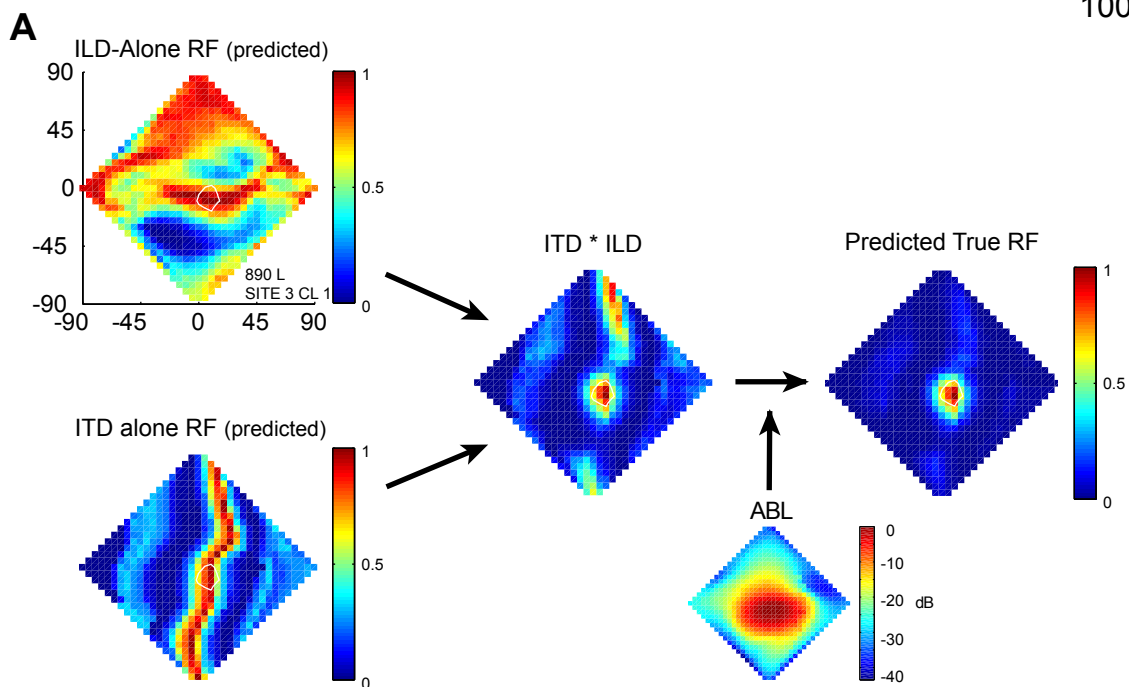combined by space-tuned cells.

Based on the ITD tuning curve, we generated an "ITD-alone receptive field,"

defined as the receptive field that would result were a cell sensitive solely to ITD.

One of the prominent features of our ITD-alone receptive fields is the occurrence

of elevated firing in one or two vertical bands on either side of the main excitatory peak. These "side-bands" occur because space-tuned cells are susceptible to a phenomenon known as "phase-ambiguity" which arises because ITD is initially computed using a cross-correlation-like mechanisms in neurons narrowly tuned to frequency. Because these cells compute the time differences between two signals that are essentially sine waves, they respond equally well when one of the sine waves is shifted by a full period. This corresponds to the ITD at the side-peak. Phase ambiguity is partially resolved by cross-frequency convergence in the LS to ICx projection, but side-peaks still persist even in the most tightly space-tuned cells (Takahashi and Konishi, 1986).

Previous reports have suggested that space-tuned cells respond strongly only when both ITD and ILD cues are near optimal (i.e., any deviation from optimal values in either cue causes the cell to stop firing) (Moiseff and Konishi, 1983; Olsen et al., 1989). We captured this behavior using a simple multiplication. As illustrated in Figure 9A, both ILD-alone and ITD-alone receptive fields were scaled between zero and one and the results multiplied. As noted previously, this is not directly comparable to the true receptive because both ITD-alone and ILD-alone receptive fields were generated under the assumption that ABL values were everywhere the same. In fact, as indicated above, ABL values decrease by up to 40 dB at certain peripheral locations (see Figure 9A). Knowing the starting firing rate from the produce of the ILD-alone and ITD-alone receptive fields and the ABL-based attenuation at each location, it

Figure 9. Predicting a true receptive field based on a cell's ILD and ITD tuning curves. A, The first column shows the ILD-alone and ITD-alone receptive fields generated from the ILD-frequency response surface and ITD tuning curve, respectively (see text). These two single-cue receptive fields were then multiplied, resulting in the ABL-equalized spatial receptive field (middle plot). The ABL values (shown in small inset plot) were then used to adjust the firing at each location, resulting in a predicted true receptive field (on the right). With the exception of the ABL plot, the color scale throughout indicates firing rate scaled between zero and one. The ABL scale bar shows how attenuated each location in the true space test is relative to the location with the loudest ABL value. B, Analyses based on three cells showing how ITD-alone and ILD-alone receptive fields can be combined as described in A to yield predicted true receptive fields. Each row corresponds to a single cell. White loops are the half-height contours for each cell's true spatial receptive field.

A

ILD-Alone RF (predicted)

ITD alone RF (predicted)

ITD * ILD

ABL

Predicted True RF

B

ITD-Alone RF (Predicted)	ILD-Alone RF (Predicted)	Predicted True RF	True RF

was possible to estimate the reduction in firing at each location due to ABL. The

result was a prediction of the cell's true spatial receptive field.

Figure 9B shows the results of our analysis for three representative cells. The

predicted true spatial receptive field often captures both the location and overall

shape of the measured receptive field. Slight misalignments between the two

receptive fields, like the ones shown in the second row, were not uncommon. In

cases where true receptive fields had some internal structure, such as the extra

response at higher elevations in the bottom row, the model often captured this

structure. We assessed the ability of a product of ITD-alone and ILD-alone

receptive fields to predict the position of the true receptive field for all cells in our

sample, as shown in Figure 10. As is apparent, prediction of a cell's azimuthal

position, which relies primarily on the cell's ITD tuning, was quite accurate. The

slope of the regression line, 0.87, differed significantly from one (t=4.43, df=44,

p<0.0001), probably owing to two outliers at extreme azimuths. The intercept did

not differ significantly from zero (intercept = .61, t=1.14, df=44, p=0.26). The

prediction of elevation was much noisier, but a linear trend was still readily

apparent. The slope of the regression line, 0.89, differed significantly from one

(t=1.42, df=44, p=0.16), but the intercept did not differ from zero (intercept =

0.94, t=0.89, df = 44, p=0.38). While, statistically speaking, the predicted slope

for both azimuth and elevation did differ significantly from one, the important

point for the present analysis is that in both cases the slope was *near* one.
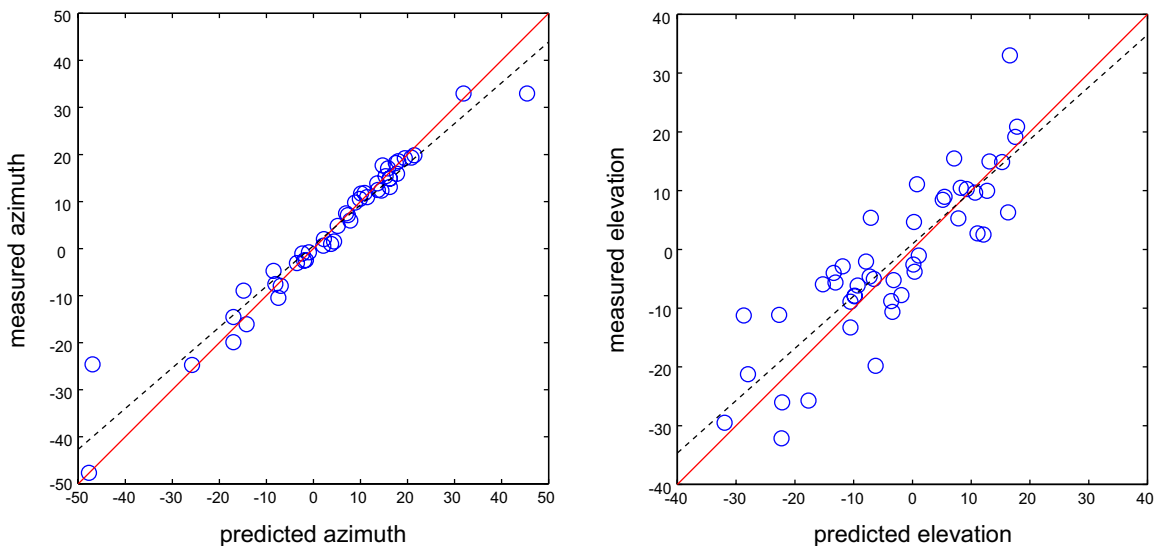
Figure 10. Prediction of a cell's receptive field position based on ILD-frequency and ITD tuning curves. In the left plot, the x-axis value indicates the azimuth of the true receptive field predicted by the model while the y-axis shows the azimuth of the cell's true receptive field. The plot on the right is similar but for elevation. Each circle represents the data from one cell. The solid line is indicates y=x, while the dotted line shows the best-fitting regression line.

Correspondence Between Pure-Tone ILD Tuning and
## Best Location Acoustic ILD Values

We wished to test the hypothesis that a cell's preferred ILD at each

frequency would match the frequency-specific ILD values that occurred at the

cell's preferred location. This venture is not as straightforward as it might initially

seem. We can determine the cell's preferred ILD at each frequency, thus

defining a ridge along the ILD-frequency response surface. However, not all

points along this ridge are equally valid or important to the cell. In some

instances, the cell's response at a particular frequency was very low, presumably

reflecting the fact that this frequency is relatively unimportant to the cell. In other

instances, the response was robust but too noisy to allow for an accurate determination of the best ILD.   ILD comparisons were thus made only at frequencies that met two criteria. First, the maximum firing rate at the given frequency had to be at least 20 percent of the maximum firing rate. Second, the standard deviation in the estimate of the peak (i.e., preferred ILD) had to be less than three dB.

Figure 11A shows the comparison between ILD tuning and best-location ILD values for six representative cells. In some cells, the ILD-frequency ridge corresponded well with the acoustic ILDs from the cell's best location (top row, column 1 and 2). This close correspondence was usually seen only at frequencies below 7000 Hz. In other cells, the preferred ILD ridge and the best-location ILDs had parallel slopes on the ILD-frequency surface, but the two lines were displaced in ILD over certain frequency ranges (top row, column 3). In many cases, the preferred ILD ridge failed to correspond exactly with the best-location ILD values, but the ILD ridge followed the same leftward or rightward trend. For example, if the best location ILDs were mainly left-louder, the cell was tuned to left-louder ILD values (bottom row, column 1). In other cases, there was no obvious correspondence between a cell's preferred ILDs and the ILDs from its best location (bottom row, columns 2 and 3).

When the data were collapsed across cells, an interesting pattern emerged. Figure 11B plots preferred ILD against the best-location ILD value for all cells in our sample. The data are grouped according to frequency range. We included

Figure 11. Correspondence between pure-tone ILD tuning curves and ILD values at a cell's best location. A, ILD-frequency response surfaces from six cells. Preferred ILD values and standard deviations were computed as described in the text. Black circles show preferred ILDs that were included in further analyses and open squares indicate values that were excluded based on excessive variance or lack of response. The horizontal bars indicate the standard deviation in the estimate of the best ILD. The black line traces those ILDs that occurred at the cell's preferred location, as determined from the HRTFs. Scale bars indicate firing after spontaneous rate had been subtracted. B, Preferred ILD plotted against best location ILD for all cells. Data have been broken down by frequency regions as indicated by the title of each plot. The black line indicates y=x while the gray line shows the best fitting regression line. Regression coefficients are given in Table 2

A
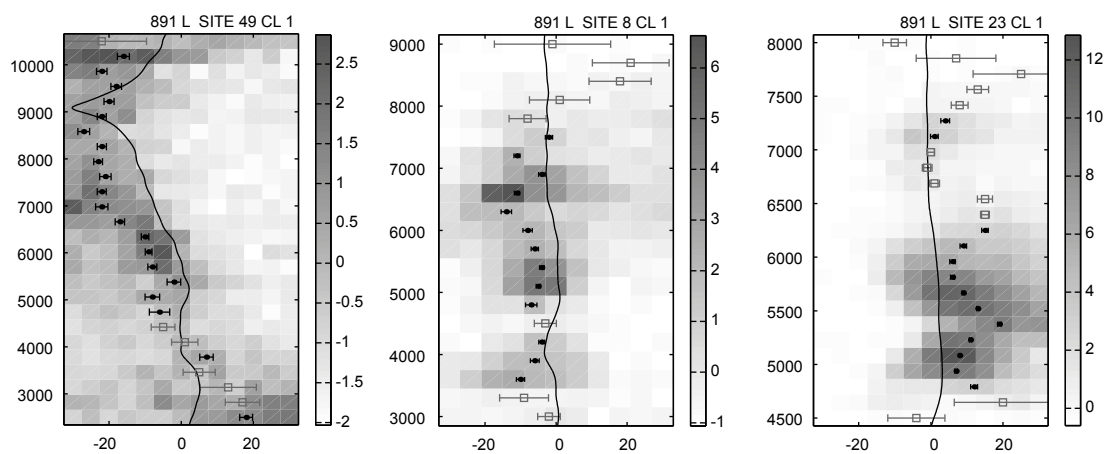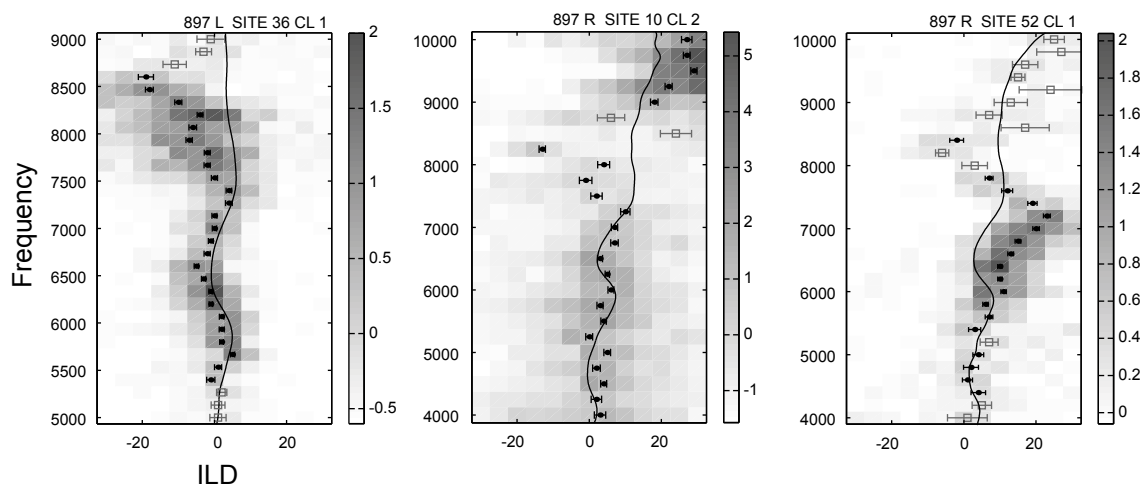
B
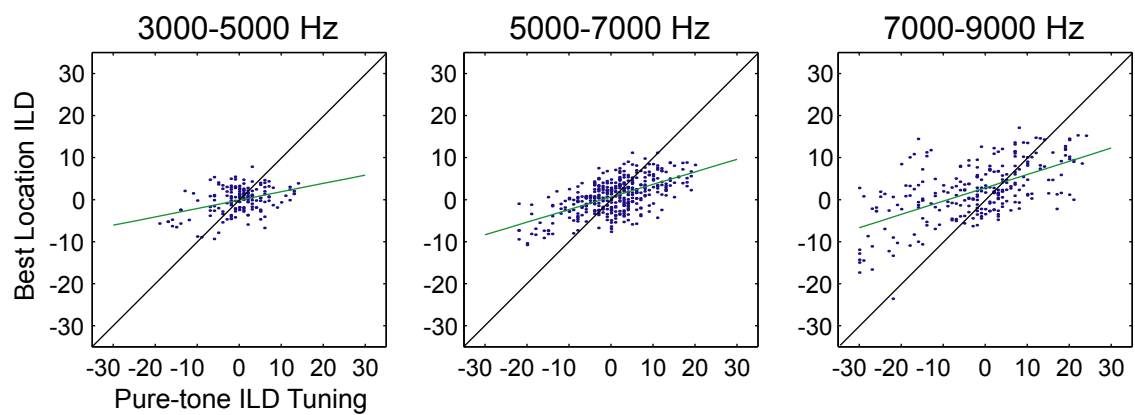
only those ILD peaks that met the selection criteria of robust firing and low

variance, as discussed above. Visual inspection of these results reveals that

preferred ILD values were consistently more extreme than best-location ILDs.

For example, in the middle plot, if the preferred ILD was +20 dB, the best-location

ILD was, on average, closer to +10 dB. This pattern is confirmed by a regression

analysis, the results of which are presented in Table 2. While all slopes were

significantly different from zero, they are much less than one (which would have

indicated perfect correspondence). The intercepts, however, are close to zero,

showing that preferred ILDs tended to match best-location ILDs near zero.

Table 2. Results of a regression of pure-tone preferred ILDs against acoustic
ILDs occurring at a cell's best location. Results are broken down by frequency
range.

frequency range	slope	intercept	t	df	p
3000-5000 Hz	0.20	-0.12	5.4	161	<.0001
5000-7000 Hz	0.30	0.62	14.6	380	<.0001
7000-9000 Hz	0.32	2.81	11.7	249	<.0001

Performance of an Optimized Linear Model

In predicting the broadband ILD-alone receptive fields from the sum of pure

tone responses, the sizeable portion of variance left unexplained lead us to

question whether a linear system was sufficient to account for the measured ILD-

alone receptive fields. As we will argue later, it is possible that the system is

fundamentally linear when tested with broadband sounds, but that certain non-

linear effects, such as thresholding, limit our ability to fully see this linearity when

probing with pure tones. To address this question we developed a simple model

of an ICx cell, trained via backpropagation (Rumelhart and McClelland, 1986) to

reproduce ILD-alone receptive fields. We also sought to uncover the pattern of

pure tone responses we might expect from the fully trained cell (i.e., from a linear

neuron). We hoped that a comparison of these predictions with the actual

measured pure-tone responses would shed light on the sources of error in our

pure tone ILD-alone receptive fields.

The model had input units narrowly tuned to ILD and frequency, analogous

to LS cells. These cells were driven by ILD values taken from the ILD-alone

spatial stimuli. The activity in the single output unit was determined via a

weighted sum of all input unit activities. Weights were trained so that the output

mimicked as closely as possible the ILD-alone receptive field for a given cell.

The ability of this model to capture the shape of the ILD-alone receptive fields

was quite good, as shown in Figure 12 (compare row 1 with row 2). Unlike the

sum of pure tone responses, the output of the model was only slightly less

selective than the real cell. That is, the downward bowing seen when comparing

predicted and measured ILD-alone responses on a location-by-location basis

was not as prominent in the output of the backpropagation model. Thus, the

model somehow compensated for this bowing effect using only linear

mechanisms. An assessment of how well the model accounted for the data from

all cells is provided in Figure 13. R-squared values ranged from 0.75 to 0.94 with

a mean of 0.88. This accounts for much more of the variance than the sum of

pure tone responses (mean=0.56).

The model's response to tonal ILD-frequency stimuli is directly interpretable from the weights. The stronger the weight between an input unit with a particular ILD and frequency tuning, the stronger the output cell's response to that ILD-frequency combination (see Figure 12). Examined in this way, the weight matrices reveal that the model is often tuned to ILD values near the best location ILDs; however, like the neurons themselves, in many cases ILD tuning curve peaks don't match exactly with the best-location ILD values (bottom row of Figure 12). These differences are of theoretical importance, as will be discussed later. The model also developed inhibitory responses to ILD-frequency combinations that flanked the ridge defined by the preferred ILD (dark blue areas in bottom row of Figure 12).

The model and true cell shared only a loose similarity in their ILD-frequency responses (compare rows 3 and 4 of Figure 12).   Inhibitory regions were much better defined in the model's response. This is not surprising given that the ability to measure inhibitory responses in real cells is limited. The frequencies to which the model and cell responded are similar in some cells, as shown in rows 1 and 2 of Figure 12; however, in row 3 and many other cells the relationship is not apparent. The model often responded over a much wider range of frequencies than did the cell; it was not uncommon to see robust responses at frequencies to which the true cell responded only minimally. The frequencies to which the

Figure 12. ILD-alone receptive fields and ILD-frequency response surfaces predicted by a backpropagation model compared with those measured from real cells. Each column contains corresponding data from a single cell. In the first and second rows, the white circle defines the half-height contour line surrounding the cell's true receptive field. The scale bar indicates scaled firing rate and is the same for all space plots. The fit of the model to the cell's ILD-alone receptive field is given by the R-squared value in the upper right corner of the plots in row 2. In the bottom two rows, the white line traces the ILD values present at the cell's preferred location. In both of these rows, the ridge of the ILD-frequency response surface is indicated by black dots, using the same method of determining preferred ILDs as was used in Figure 11. Missing values in the third row indicate frequencies where data was not collected. (An initial screening suggested the cell would not respond to these frequencies.) Scale bars in the third row indicate average firing per stimulus less the spontaneous rate. Scale bars in the fourth row are the raw weight strength values.
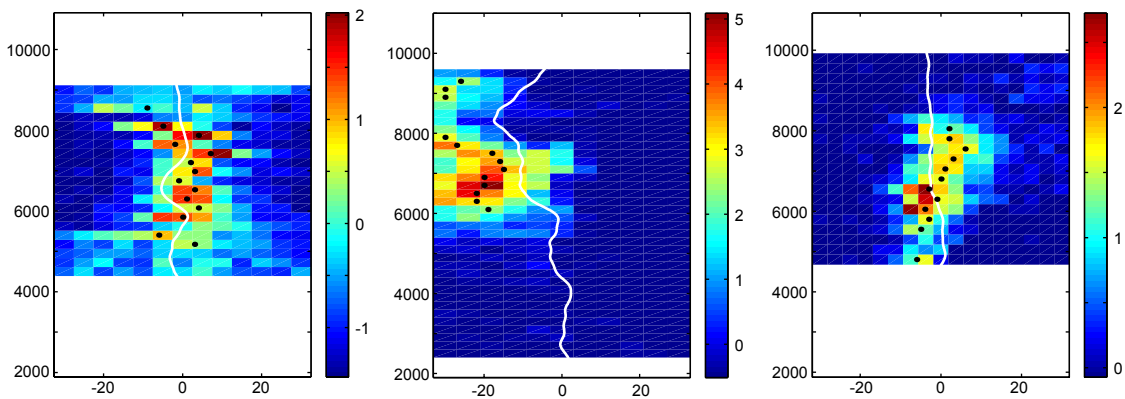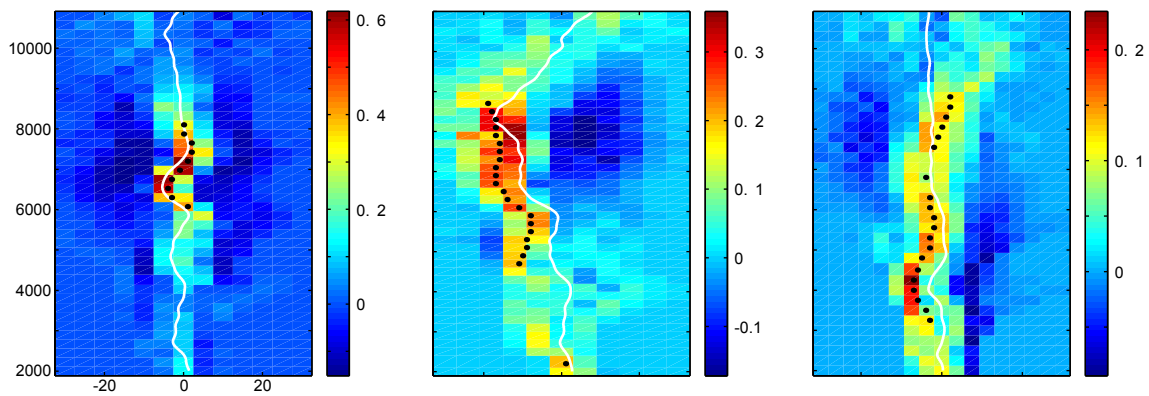
MEASURED ILD-ALONE RF

897 R SITE 7 CL 1   897 L SITE 27 CL 2   891 R SITE 21 CL 1
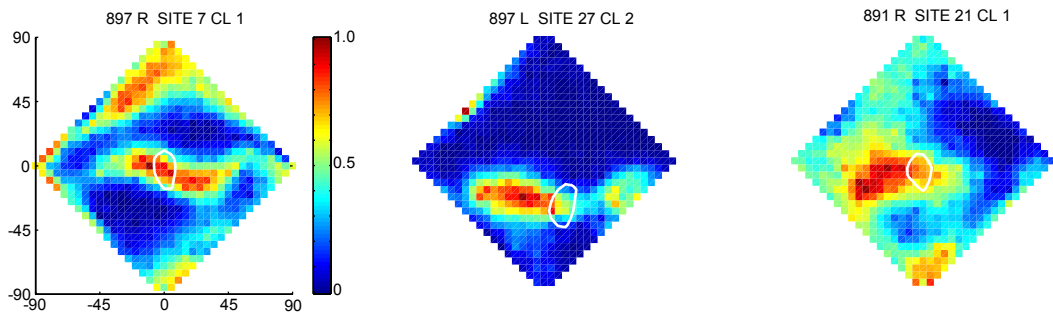
BP MODEL ILD-ALONE RF

Rsq: 0.93   Rsq: 0.91   Rsq: 0.87
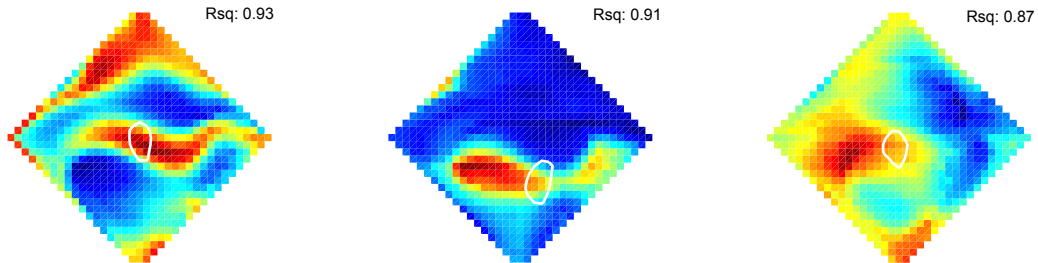
MEASURED ILD-FREQ RESPONSE

BP MODEL ILD-FREQ RESPONSE

model responded more readily than the cell were usually below 4000 Hz. We

also observed a tendency for the model and cell to deviate from the best-location

ILD line in the same direction. For example, in column 3 both the cell and the

model prefer more negative ILD values than were present at the best location.

This suggests that some of the observed lack of correspondence between pure-

tone preferred ILDs and best-location ILDs may be due to the fact that cells are

not tuned exactly to the best location ILD values.
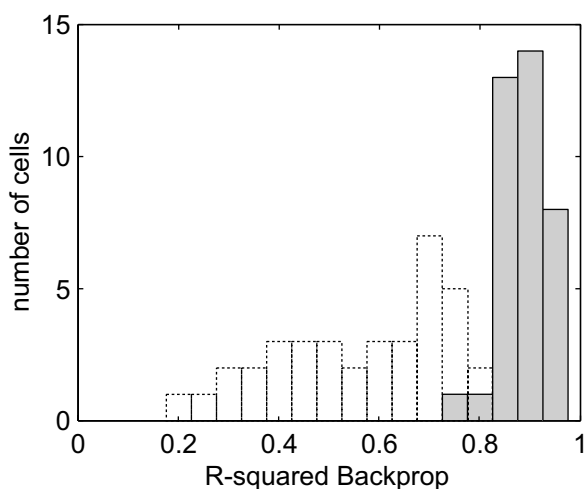
Figure 13. Distribution of R-squared values for the backpropagation model. The R-squared values from the model are shaded while the R-squared values obtained by a simple sum of pure tone responses are shown in white (copied from Figure 6).

Characteristics of Binaural Intensity Tuning
at High Frequencies

One of the most striking features of our ILD-frequency plots was the

occurrence of strongly lateralized (i.e., left-louder or right-louder) ILD tuning at

frequencies above 7000 Hz. Of the 46 cells in our sample, 17 showed this pattern of response (though this may underestimate the frequency of occurrence because not all tests were conducted at high frequencies; see methods). This excitatory response was usually restricted to a narrow frequency band less than 1000 Hz wide. The ILD tuning curves at these frequencies were unusual not only because of their preference for extreme left or right ILD values but also for the magnitude of their response. The maximum firing rate at these high frequencies was sometimes two to three times as great as the response at any other frequency.

The peculiar nature of these high-frequency ILD tuning curves lead us to conduct an additional test on some cells, designed to uncover the binaural excitatory and inhibitory forces that shape the ILD tuning. In this test, referred to as a binaural interaction plot (BIP), we measured the cell's response to every combination of left and right intensity within a subset of intensity values. We plot left intensity along the y-axis and right intensity along the x-axis. In such a plot, ILD changes most rapidly as one moves from the upper left (left ear much louder than the right) to the lower right (right ear much louder). Similarly, the ABL increases along the diagonal from the lower left (both ears very quiet) to the upper right (both ears very loud). All BIPs were conducted at a fixed frequency.

Figure 14 shows ILD-frequency plots and BIPs for four representative cells. The top pair of plots, included by way of contrast, demonstrates how a cell would be expected to respond when tested at a frequency where it is ILD tuned. The

strong, diagonally-oriented response shows that this cell prefers a fixed ILD of approximately 15 dB. The cell also shows clear sensitivity to ABL, going from minimal response at the lower left to maximum in the upper right. Below this (second row) is a BIP from a cell with a high-frequency extreme ILD preference. This cell clearly prefers sounds louder in the left ear. As with the preceding cell, its response is also influenced by ABL. ILD tuning curves for this cell are clearly open to the left but it is significant that the crossover point remains fairly constant over a range of ABL values. In other words, the line separating the minimum and maximum responses follows the upward-going diagonal. This shows that the cell is selective for the same ILD over a range of ABLs, though its ILD tuning is sigmoidal.

The bottom two plots, taken at very high frequencies, show a very different response profile. In the third row, for example, the cell's response increases dramatically as the sound in the right ear increases above 50 dB. This increase is insensitive to the sound pressure level in the left ear over a wide range; however, when the left ear intensity reaches a certain point it suppresses the cell. This left-inhibitory response is the mirror image of the right excitatory response in that it is insensitive to all but the most extreme intensity values in the right ear. This cell shows little evidence of increases its response to increasing ABL. Instead, the monaural drive seems to completely determine its excitation. While the cell is clearly sensitive to ILD, especially at high ABL values, the ILD tuning curves change with ABL. In fact, at many lower ABL values, the cell has a region

of null response for all but the most extreme ILD values. For these reasons, the response of these two cells is best conceptualized not in terms of ILD, a binaural parameter, but in terms of the monaural excitatory and inhibitory responses that drive it.
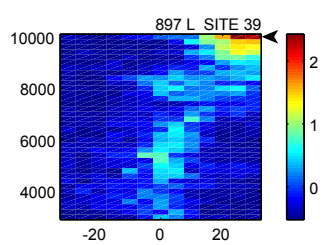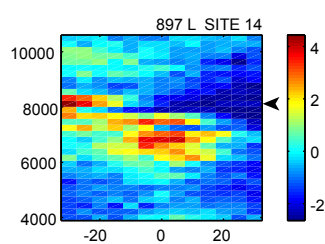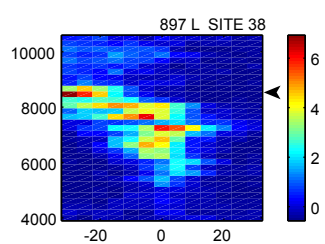
BIPs were measured in 10 out of the 17 cells with high-frequency extreme-ILD responses. Whether a cell was driven by separate monaural inputs or by a binaural input seemed to depend on frequency. All cells whose ILD tuning to extreme ILDs occurred at frequencies over 9000 Hz were strongly monaurally driven. Below this frequency there was a mix of responses, with some cells appearing to be monaural (e.g., Figure 14, row 4) while others were ILD selective but with a sigmoidal ILD tuning curve (e.g., Figure 14, row 2). In fact, there appears to be a continuum of response characteristics, with some cells, such as the one in row 3 of Figure 14, appearing to be partly binaurally driven and partly monaurally driven. Patterns of monaural excitatory and inhibitory inputs did not appear to be contingent upon the side of the brain we recorded from. We found examples of cells driven by the ipsilateral ear and inhibited by the contralateral ear as well as cells showing the reverse pattern. However, our sample size is too small to make any estimates of the frequency of occurrence of these different patterns of response.

The monaural excitatory drive explains in part why certain cells responded more strongly to a high-frequency extreme ILD than to any other frequency and ILD combination. In order to generate these extreme ILD values and keep the

Figure 14. ILD-frequency surfaces and binaural interaction plots for four cells.
Each row contains data from the same cell. The arrowhead on the right of each
ILD-frequency response surface indicates the frequency at which the binaural
interaction plot was run. Left and right amplitude values are in decibels, but zero
decibels was assigned arbitrarily to the lowest intensity value included in a test.
In all plots, scale bars indicate spikes per stimulus less the spontaneous rate of
the cell.

ILD-FREQ RESPONSE

BINAURAL INTERACTION PLOT

897 L SITE 21

Freq: 6440 Hz

897 L SITE 38

Freq: 8468 Hz

897 L SITE 14

Freq: 8100 Hz

897 L SITE 39

Freq: 10200 Hz
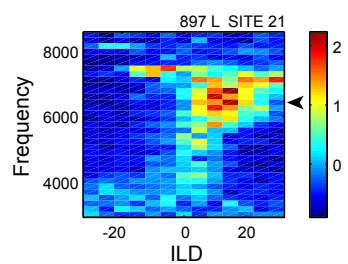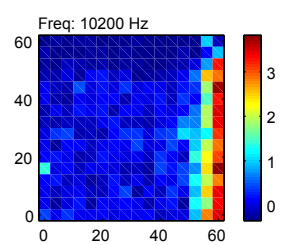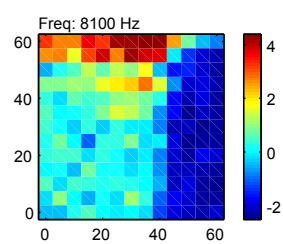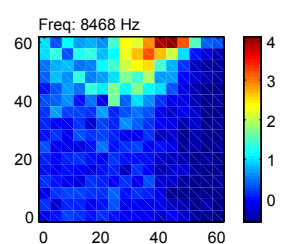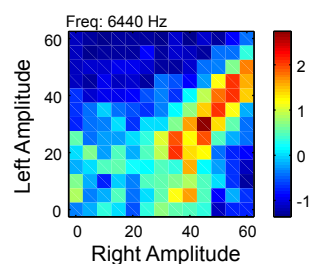
ABL constant, the intensity in one ear had to be increased to very high levels.

These levels were strong enough to trigger the cell's excitatory monaural drive

quite strongly. Had we conducted our ILD tuning curves at lower ABLs, we might

never have seen these influences.

<p style="text-align: center;">Discussion</p>

<p style="text-align: center;">Frequency-Integration by Space-Tuned Cells</p>

In this study, we assessed whether a space-tuned cell's spatial receptive

field, measured with broadband noises, could be predicted based on its

responses to pure tones. We have shown that pure-tone ILD tuning curves can

be combined, using purely linear mechanisms, to yield good qualitative estimates

of both the ILD contribution to spatial tuning (i.e., the ILD-alone receptive field)

and, in combination with the ITD tuning curve, the true receptive field. This

demonstrates that the responses of space-tuned cells can be analyzed by

separately measuring the frequency-specific components that contribute to their

broadband, free-field response.

One of the key innovations of our approach is the use of ILD-alone test

stimuli, in which ITD and ABL are held fixed for all locations in space. This

approach has two benefits. First, the ILD-alone receptive field provides a directly

measurable response surface against which to validate our sum-of-pure-tone

spatial receptive fields. A cell's pure-tone ILD-alone receptive field can be

combined with the ITD-alone receptive field to predict the true receptive field, but

this approach entails added assumptions about the nature of the ILD-ITD interaction and the effects of ABL on a cell's response. Second, the ILD-alone test produces graded responses over a wide range of locations. This contrasts with normal spatial stimuli, which produce strong responses in a focal region and almost no response at all other locations. The continuum of response values allowed an examination of the spectral tuning of space-tuned cells in finer detail than was previously possible.

One of our central concerns was the linearity of the frequency-integration process leading to spatial tuning in the IC. If this process is linear, then a simple summation of pure-tone ILD-frequency responses should yield identical results to those obtained using the same set of frequency-specific ILDs presented together as a broadband noise. Our data show that a linear sum of pure-tone responses can account for, on average, 56 percent of the variance in the broadband ILD-alone receptive field. In a fair number of cells, the variance explained was greater than 70 percent. These results show clearly that there is a strong linear component to the frequency-integration process, but leave open the possibility that some aspects of the process are non-linear.

Of the roughly 44 percent unexplained variance, the amount accounted for by random error is probably small. Some of the mismatches between the sum of pure tones and broadband responses may be due to the intrinsic variability of neural responses. As detailed in the results section, we estimate that roughly six percent of our error variance is due to neural noise. While this noise is

significant, it leaves a sizeable amount of variance unaccounted for.

Other errors may have arisen from the virtual sound source technique; however, we believe these errors to be small. Keller et al. (1998) have documented the efficacy of our virtual space technique in detail. Using microphones inserted in the ear canals, they showed that the acoustic characteristics of sounds delivered over headphones were nearly identical to those induced by a free-field sound source. Further, spatial receptive fields measured with virtual sound sources were nearly identical to those measured with free field sources. In our analysis, errors in the measurement of the HRTFs would tend to be cancelled because the same filters are used to synthesize stimuli for the broadband ILD-alone receptive fields and in the generation of ILD-alone receptive fields from pure tone responses.

A possibly significant error related to the use of virtual sound sources arises from differences in the position of the earphones from one recording session to the next. We digitally compensate for the filtering characteristics of the ear canal and earphone. However, the acoustic recordings used to generate the inverse filters that canceled the effects of earphones and ear canal were recorded only once, under the assumption that, from one neural recording session to the next, there would be little change in characteristics of this system. To assess the amount of error that earphone placement might have accounted for, we recorded the earphone-ear canal transfer function for multiple insertions of the earphones. At any given frequency, the maximum deviation of ILD from the mean ILD was

always less than five dB. The standard deviation, averaged across all

frequencies, was 1.2 dB. This error is small in comparison to the range of ILD

values of approximately 60 dB. Errors in the measurement and use of HRTFs

are therefore unlikely to account for the lack of correspondence we observe

between ILD-alone receptive fields predicted from pure tones and those

measured with broadband noise.

   A more significant source of differences between the sum of pure-tone

responses and broadband responses likely arises from differences in the way

that cells respond to tones. First, thresholds are higher for pure tones than for

broadband noises. Even under the assumption of linearity, if a cell has the

equivalent of 20 discriminable frequency channels converging to give it its spatial

response, then the driving force behind one of them alone should provide $1/20^{th}$

the excitation. This may not be enough to raise the cell's firing above

spontaneous rate. Hence, the spectral density of a tone must be much greater

than the spectral density in the equivalent region of a broadband spectrum in

order to elicit a response from a broadband cell. In our case, both tones and

noises were presented at roughly 15 dB above the broadband noise or pure-tone

thresholds, respectively. This meant that the peak to peak amplitude of both

tones and noises were about equal. Under these conditions, the total spectral

energy received by a cell with a 1000 Hz bandwidth is approximately 30 dB

greater with the pure tone than with the broadband noise. Consequently, earlier

processing stages, which maintain narrowly-tuned frequency channels, may

saturate. The higher amplitude may cause other changes in the ILD processing pathway, as discussed below. The limited dynamic range of the auditory system thus puts limits on our ability to test linearity under realistic stimulus conditions.

Beyond these practical limitations, there also appear to be some fundamental differences in the way that space-tuned cells respond to pure tones as opposed to broadband noises. Typically, a space-tuned cell responds robustly to broadband sounds with favorable temporal (i.e., ITD) and spectral components. However, when given a pure tone, even one at the cell's best ILD and ITD, a cell typically responds with an onset burst of 1-2 spikes followed by silence (Knudsen and Konishi, 1978c). The firing rate during the silent period often falls below spontaneous rate, suggesting an active inhibitory process whose function is to inhibit responses from one frequency channel when it occurs alone, but to allow excitation when a broadband sound is presented.   This probably accounts for the finding that, in cells with inhibitory responses to pure tones, the predicted ILD-alone receptive fields are sometimes dominated by inhibition.   Measurements with pure tones may underestimate the true driving force of a particular frequency-specific input. If inhibitory responses were not likewise reduced, this would account for the observed pattern of responses.

These limitations related to the use of pure tones are difficult to overcome. The amplitude issue can be partly resolved by using narrow-band noises instead of pure tones. However, increasing the bandwidth of the stimulus to the point where it can elicit a response from the cell will ultimately result in a stimulus

whose bandwidth is so wide that it obscures the frequency-specific ILD tuning of the cell. In other words, the measured ILD tuning will be the average of the ILD tuning at each of the frequency sub-bands contained within the narrowband stimulus. An alternative to using narrow-band sounds would be to record intracellularly. This would allow one to see the sub-threshold inputs elicited by low-intensity pure tones. Inhibition might also be studied this way because the inhibitory post-synaptic potentials could also be seen. Though powerful, this technique is technically challenging when applied to in vivo recording situations such as ours. Inhibition might also be studied by artificially elevating the cells spontaneous activity via iontophoresis of some neural stimulant such as glutamate. The higher rate of activity would allow for measurement of the full range of inhibitory effects.

The only *systematic* non-linearity we observed was the tendency of the sum of pure tones to overestimate broadband responses at locations with intermediate firing rates, as demonstrated by the downward bow observed when pure-tone predicted activity is plotted against broadband activity on a location-by-location basis. This effect was seen, to a greater or lesser extent, in most cells studied. Several non-linear processes might account for this effect. The first arises from the aforementioned inability to fully measured the extent of inhibition when using pure tones. At those locations that elicit intermediate responses, broadband responses probably reflect both excitatory and inhibitory influences. The sum of pure tones, however, will only reflect excitatory inputs at these

locations, the inhibitory information being truncated by a floor effect. As a consequence, the sum of pure tone responses would be expected to be stronger than the broadband response. At locations where firing is near the minimum value, the broadband inhibitory response will also be truncated. Hence, where ILD-alone receptive fields have minimum response, the sum of pure tones and the broadband responses may match. A match at the best location and at the worst location along with a tendency for the pure-tones to overestimate the firing at intermediate values essentially captures the behavior we observe from real cells. Another possible cause of the bow-like relationship between pure-tone sum and broadband responses is that ILD tuning is sharper in the context of broadband sounds than when probed with pure tones. The broadening of ILD tuning curves would lead to less restriction in space, which is exactly the pattern we observe. A final possibility is that space-tuned cells may behave like a logical AND gate with respect to frequency integration. In other words, they may not fire unless all frequency-specific inputs are strongly active. The observation, noted above, that pure tones fail to elicit more than one or two spikes suggests that some such AND-like integration mechanism is at play. Because locations whose spectra elicit intermediate responses are optimally activating only a portion of the cell's input channels, they may not be capable of driving the cell as strongly as those locations with optimal ILD values at each frequency. Although these last two possibilities result in similar predicted responses, they can be discriminated based on the physical locus of the effect. A tightening of ILD tuning curves might

occur via cross-frequency interactions in one of the nuclei in the intensity pathway leading up to the IC. An AND-like mechanism, on the other hand, might be instantiated by non-linear integration processes in the dendrites of a space-tuned cell. At this point, the data are insufficient to discriminate these various possibilities.

It is perhaps worth reiterating that, in spite of the limitations of the pure-tone approach, a simple linear sum of pure-tone responses still captures more than half the variance of the broadband response. To see whether a linear mechanism might be *sufficient* to account for the observed ILD-alone receptive fields, we employed a modeling approach. Our model ICx cell received inputs from an array of ILD- and frequency-tuned LS cells. The model's output was based purely on a linear sum of its inputs. Under these conditions, our model could be trained to reproduce very closely the ILD-alone receptive fields measured with broadband noises. The variance explained averaged 88 percent even without accounting for measurement error. This strong fit to the data, consistent across cells, shows clearly that a linear mechanism is capable of accounting for the main effect of the frequency integration process.

To summarize, the success of the linear model in reproducing ILD-alone receptive fields suggests that, in the context of a broadband noise, a cell's response is determined via a near-linear summation of the contributions of individual frequency channels. However, when a cell is tested with pure tones, non-linear mechanisms come into play. The nonlinearities observed with pure

tones may be due to practical limitations, such as saturation effects due to high stimulus intensities; however, it is also possible that cells have mechanisms that effectively block narrow-band inputs.

Because of the importance of the backpropagation model to our conclusions, it is important to consider a possible objection to the model at this point. A close examination of the details of the model will reveal that the number of patterns used in training the model is comparable to the number of weights (i.e., degrees of freedom). Under normal circumstances, this would invalidate the model. In the context of a backpropagation model, this overabundance of weights leads to the phenomenon of "overtraining," where the model has essentially built a specific template for each input pattern. We overcame this problem by adding random noise to the input patterns during training and by using a limited number of training cycles. The variance of the added noise was set so that input cells with similar tuning characteristics had similar weights in the final solution. The redundancy of the weights shows that the model has effectively solved the mapping problem using far fewer degrees of freedom that it was allowed; however, a rigorous quantification of the degrees of freedom employed by the model was not attempted. Conclusions based upon the model must therefore be treated as tentative.

Correspondence Between ILD Tuning and Spatial Tuning

While it is often tacitly assumed that a space-tuned cell derives its receptive

field via a selectivity, on a frequency-by-frequency basis, for the cue values occurring at its best location, there is relatively little evidence to support or refute this supposition. One of the few studies to address the issue was performed by Brainard et al. (1992), who used pure tones to assess the spatial receptive fields of cells in the owl's optic tectum. The resultant receptive fields were amorphous and spatially ambiguous; however, the overlap of pure-tone receptive fields corresponded well with the broadband true receptive field. From the fact that a cell's receptive field measured with a single pure tone includes the cell's broadband receptive field, it necessarily follows that the cell must be tuned to the ILD and ITD values that occur in the vicinity of the cell's best location *at that single frequency*. That the pure-tone receptive fields all overlap at the cell's best location implies that the cell's frequency-specific ILD tuning matches the HRTF-derived best-location ILD values at all frequencies. While these findings show that pure-tone ILD and ITD tuning are close to the acoustic ILD and ITD cues that occur at the cell's best location, they are not specific enough to determine whether the *peak* of the ILD or ITD tuning curves matches exactly the cue values at the center of the receptive field.

The specific correspondence between preferred ILD and best-location ILD values was examined in more detail by Gold and Knudsen (2000). They measured ILD tuning curves at several frequencies using narrow-band noises and compared the best ILD with the frequency-specific ILD values that occurred at the center of the visually-determined receptive field. (Cells in the optic tectum

have overlapping visual and auditory receptive fields). They claim to have found a correspondence between ILD tuning and best-location ILD values. However, the range of deviations between ILD tuning and ILD cue values (roughly -8 to +13 dB) is barely larger than the range of best ILDs (roughly -6 to + 20). Hence, whether their results support their claim is difficult to assess.

Our experiment is nearly identical to Gold and Knudsen's experiment except that we used pure tones instead of narrowband noises and that we measured responses in the IC not the optic tectum; however, our own results show clearly that a cell's frequency-specific best ILDs, measured with pure tones, do not always match the ILD values evoked by a sound at the cell's best location. In addition to the apparently random deviations of preferred ILDs from the best-location ILDs, we also observed a systematic trend whereby pure-tone tuning tended to be more extreme than ILD values contained in the HRTFs (e.g., if the best-location ILD value was positive five dB at a given frequency, the peak of the measured ILD tuning curve might be closer to positive ten dB).

We have also shown that a model ICx cell, whose response is based on a linear sum of LS inputs, can be tuned using backpropagation to duplicate the ILD-alone receptive fields of space-tuned IC cells. If we suppose, for the moment, that IC cells really are linear, then the model can be used to infer the pattern of frequency-specific ILD tuning that would have been necessary to create an observed ILD-alone receptive field. The model shows clearly that in many cases ILD tuning curve peaks do not match exactly with the best-location

ILD values.

We are inclined to accept the results of this analysis. In an earlier paper, we have argued, based on the structure of ILD-alone receptive fields and a developmental model, that ICx cells develop their spatial tuning to satisfy two constraints (Chapter II). First and most obviously, a cell must be tuned to so that its inputs provide maximum excitation at the center of its receptive field. We argued that a cell must also develop inhibitory weights to suppress responses to non-preferred locations along the strip corresponding to the cell's preferred ITD. Because of these dual constraints, the cell would be expected to generate ILD tuning that was close to the ILD values at the best location, but not matching exactly, just as the backpropagation model shows.

It is thus possible that some of the mismatch between pure-tone ILD tuning and best-location ILDs reflects the cell's true preference for ILDs other than those at its best location. The location for which ILD tuning and best-location ILD values should match best would be the location that evokes maximum response under ILD-alone test conditions. As we have pointed out in a previous paper (Chapter II), this ILD-alone best location is not always at the center of the true spatial receptive field. Although we have not presented the data, it is true that we get better fits between ILD tuning and ILD cue values when we determine the best location from the ILD-alone receptive field rather than from the true receptive field.

The largest puzzle is why the ILD tuning of a cell is consistently more

extreme than the ILD cue values at the best location. This mismatch cannot be

explained based on the preceding argument. Instead, the backpropagation

model, as well as Brainard et al.'s (1992) data, suggests that a cell should have

ILD tuning *near* the ILDs at its best location. When preferred ILD is regressed

against best-location ILD, the intercept is close to zero (Table 2). This shows

that, on average, the ILD tuning of a cell is zero when the ILD cue value is zero;

however, this correspondence breaks down for more extreme ILD values. When

ILD cue values are significantly different from zero, we see ILD tuning

overestimating HRTF-based ILD values by roughly a factor of two. There are two

possible explanations for this phenomenon. One possibility is that cells really are

tuned to the observed extreme ILD values, even in the context of broadband

sounds, and that the broadband ILD-alone receptive fields reflect radical

nonlinearities in a cell's response. The other possibility is that cells are in fact

linear, except that idiosyncrasies associated with the use of tonal stimuli caused

us to measure ILD values that were more extreme than they might have been in

the context of a broadband sound.

　　We are inclined to believe the second of these two possibilities. It is

plausible that the louder sound pressure levels used with pure tones affected

earlier auditory processing stages, causing a shift in the ILD tuning of LS cells.

In the nucleus ventralis lemnisci lateralis, pars posterior (VLVp), the nucleus in

which ILD is initially computed, cells are sigmoidally tuned to ILD. Manley et al.

(1988) showed that the slope of the crossover point of the ILD tuning curve shifts

towards more extreme values with increasing sound pressure level. Based on the idea that ILD tuning in the LS is derived via bilateral inhibitory inputs from the VLVp, as suggested by Adolphs (1993), this shift in ILD tuning in the VLVp is in the correct direction to account for amplitude-sensitive shifts of preferred ILD in the LS. Olsen et al. (1989) have reported that broadband ILD tuning curves in the optic tectum also shift with increasing amplitude towards more extreme ILD values, but only for cells whose initial ILD tuning is greater than 5 dB. This exact same pattern of results would account for our own observations; the deviations between expected and measured best ILD are greatest for cells whose best ILDs are more extreme. Note that the use of louder stimulus levels with pure tones is unavoidable. Were the spectral density of the tone adjusted to be comparable with spectral densities in broadband sounds, cells would not have responded to the tones at all.

<div align="center">Role of Inhibition in Shaping a Receptive Field</div>

Theoretical considerations discussed in a previous paper (Chapter II) suggest that a cell will be ILD-tuned to meet the dual constraints of being maximally excited at the center of its receptive field and maximally inhibited for locations above and below but along the best-ITD strip. The finding that cell's preferred ILD peaks don't match perfectly with best-location ILDs is consistent with this scenario. The necessity of being inhibited to certain locations compromises the cell's ability to become optimally tuned to the spectrum from its

preferred location. The ILD-alone receptive fields also show clearly that a cell is often inhibited above and below the receptive field. However, the ILD-alone receptive field represents the influences of both excitatory and inhibitory inputs at all locations in space. To verify that inhibitory responses alone were tuned so as to inhibit locations above and below the receptive field, we converted the inhibitory regions of ILD-frequency response surfaces into an ILD-alone receptive field. The resulting receptive fields, shown in Figure 8, demonstrate clearly that a cell is tuned to inhibit locations above and below the receptive field. The points of maximum inhibition don't lie directly along the best ITD strip, but do cut through it in locations that would allow for the appropriate elevational restriction. Presumably, cells do not become tuned to inhibit locations more closely aligned with the best-ITD strip because doing so would cause unacceptable attenuation of responses at each cell's best location.

It is worth noting that, for cells whose best location was either extremely high or low (absolute value greater than ~30 degrees), the inhibition due to ILD only served to push the receptive field away from the center but not to restrict it from the top or bottom. As we discussed in a previous paper (Chapter II), the reasons for this asymmetric inhibition may be developmental in origin, resulting from the fact that sounds at extreme elevations, either high or low, are greatly attenuated relative to sounds at locations directly ahead. For a single cell tuned to extreme elevation, symmetric inhibition may not be necessary to insure a tightly restricted receptive field. Consider a cell tuned to an elevation well above

the horizontal plane. For sounds located at even higher elevations the sound
intensity will be so quiet that it will not drive the cell. Thus, inhibition at extremely
high elevations is not necessary. A similar argument pertains for cells tuned to
elevations well below the horizontal plane.

Intensity Tuning at High Frequencies

We were surprised to find that some of our cells were tuned to extreme ILD
values (i.e., greater than +20 dB or less than –20 dB) at frequencies above 7000
Hz. Our results show that in some cases these cells are not ILD tuned but
instead are responding as if driven separately by monaural inputs. To clarify, in
most cases, IC cells are ILD tuned. ILD tuning arises via the interaction, within
the VLVp, of the two processing streams arising from the left and right ears. The
nucleus essentially performs a subtraction of the left and right inputs via a
commissural projection between left and right portions of the nucleus (Takahashi
and Keller, 1992a). The signal from that point on is binaural in the sense that it
depends on both left and right channels simultaneously. In other words, you
cannot change the intensity in one ear without affecting the response. For cells
in our sample with high-frequency extreme ILD tuning, however, there are many
combinations of left and right intensity at which changes in one ear have no
impact on the cell's firing while changes in the other ear do. These cells are, in
conventional terms, "EI" or "IE" cells, where the first letter refers the contralateral
ear's contribution, excitatory (E) or inhibitory (I), and the second letter refers to

the ipsilateral ear's contribution. As such, they would normally be referred to as binaural cells. However, they differ from normal "binaural" IC cells in that the inputs that drive them at high frequencies are monaural.

These high-frequency responses suggest an alternate input pathway to the IC in addition to the established time and intensity pathways, which arrive via the IC Core and VLVp, respectively. Anatomical studies have show clearly that, besides VLVp and IC Core, several brainstem and midbrain nuclei send direct projections to the IC. Candidate input pathways include the contralateral nucleus angularis, the contralateral superior olive, and the ipsilateral nucleus lemnisci lateralis, pars ventralis (Takahashi and Konishi, 1988a).

The functional significance of these high-frequency lateralized responses is unknown; however, it is perhaps not insignificant that this is the exact same frequency range where steep notches appear in the HRTFs. This lead us to wonder whether the monaural drive seen at high frequencies might be related to a cell's spatial receptive field. To address this issue, we mapped the cell's high-frequency ILD tuning onto a spatial response using the HRTFs and the same technique used to transform ILD-frequency surfaces into ILD-alone receptive fields. In roughly half the cases, the extreme ILD tuning corresponded to a notch in the ILD spectrum that cut directly through the cell's true receptive field. In the other cases, there was no clear relationship between the two. The notches are known to be highly frequency-dependent and they are in a region where HRTF measurement accuracy starts to decline. The short wavelength of the sound

means that small changes in the microphone or headphone placement can have large impacts on the results. It is thus possible that these highly lateralized responses are contributing to spatial localization and that some of our measurements were in error. Clarification of the role of these high-frequency responses will hopefully be provided by further studies.

If the high frequency responses were part of an IC cell's machinery for computing spatial location, then it would probably be most important for sounds that are quite loud. Intensity levels in the excitatory ear must typically be 20 dB greater than the ABL levels that drove the cell at lower frequencies where preferred ILD values were closer to zero. However, once intensity reaches this higher threshold, the cell's response increases rapidly with increasing intensity, having a much steeper rate-intensity function than that seen at lower frequencies. If owls do use monaural cues for louder sound levels, it would be contrary to the situation in mammals where monaural cues are most important for sound pressure levels just above the animals perceptual threshold while binaural level differences dominate for louder sounds (King et al, 1994; Palmer and King, 1985).

ILD Tuning of Space-Tuned Cells

The conversion of ILD into a spatial receptive field is a multi-step process starting with the formation of sigmoidal ILD tuning curves in the VLVp (Manley et al., 1988). The VLVp projects to the LS, where some cells have sigmoidal ILD

tuning curves while other cells have peaked curves (Adolphs, 1993; Mazer, 1995). The LS, in turn, projects to the ICx where cells are commonly reported as being exclusively peaked (Moiseff and Konishi, 1983; Adolphs, 1993; Mazer, 1995). Peaked tuning curves are also reported for cells in the optic tectum Olsen et al, 1989). ILD is likely converted into space via a multi-step processing cascade within the LS (Mazer, 1995). It is commonly assumed that peaked ILD tuning is necessary for generating a restricted receptive field; however, our own observations suggest that this may not always be true.

The aforementioned studies of ILD tuning were based entirely on measurements with broadband noises whose ILD was the same at each frequency. The ILD tuning curves measured were thus an average ILD tuning across frequency. The finding that frequency-averaged ILD tuning curves are peaked is completely congruent with our own results, because the majority of a cell's frequency-specific ILD tuning curves are peaked. However, when viewed on a frequency-by-frequency basis, some space-tuned IC cells have sigmoidal ILD tuning curves at some frequencies. Other curves appear to be "open peaked," meaning that the curve is peaked but one flank stays high even at extreme ILDs. Further, the degree of "open-ness" seems to be determined by the preferred ILD of the cell. Cells tuned to left ILDs tend to be open to the left and vice versa for cells tuned to the right. Of course, we cannot rule out the possibility that ILD tuning curves would have been peaked had we extended our measurements to more extreme ILD values. However, the tendency of the slope

of the curve to get shallower at extreme ILD values suggests that this is not the case. Further, in the few cells where we measured ILD tuning out to +/-50 dB, ILD curves often maintained an open-peaked ILD profile. It should be noted that the most extreme ILDs experienced by the owl under normal circumstances are roughly +/- 40 dB, and most HRTF-based ILDs are less than 20 dB. So perhaps it is more accurate to say that ILD tuning curves of space-tuned cells are often open-peaked within the normal range of naturally occurring ILD values.

Ultimately, whether an ILD tuning curve is peaked or open may have little relevance to a space-tuned cell. Its task is to fire when a sound is in a restricted region of space. An open-peaked or sigmoid cell still carries spatial information in that its "closed" leg, where responses are inhibited, effectively limits the response over wide regions of space. By combining different restriction patterns at different frequencies, a cell may build a receptive field even though the ILD tuning at a particular frequency may not be peaked. A single-frequency sigmoidal ILD tuning curve may also be useful for picking out focal regions. At some frequencies, the spatial distribution of ILDs has a local minimum or maximum, forming a "pit" or "peak" in the ILD surface. A cell whose ILD tuning curve was sigmoidal at the correct frequency might select for an ILD pit or peak, thus acquiring a focal spatial receptive field.

CHAPTER IV

SUMMARY AND CONCLUSION

This dissertation consists of two studies focussed on the single question of how space-tuned cells in the owl's IC transform interaural level difference (ILD) cues into spatial receptive fields. In the first study (Chapter II), I used virtual sound sources to dissociate ILD from interaural time difference (ITD), allowing me to visualize the receptive field a cell would have were it tuned solely to ILD (i.e., the ILD-alone receptive field). This study yielded the following findings:

- ILD-alone receptive fields showed a broad horizontal band of activity that included the true (i.e., free-field) receptive field center.

- ILD-alone receptive fields were not restricted in azimuth. Therefore, low frequency ILD cues that could have restricted a receptive field in azimuth are not used by space-tuned cells.

- Responses were often inhibited above and below the true receptive field center.

- The ILD spectrum that elicited maximum response was often different than the one associated with the center of the true receptive field.

The results, when combined with previous findings from others, suggest the following functional analysis of how a restricted receptive field is formed. ITD

limits a cell's activity to a narrow vertical band (Moiseff and Konishi, 1983). ILD

further limits activity along this band using active inhibition within the IC. The

result is a tightly restricted receptive field.

In Chapter II, I also present a developmental model of a space-tuned IC cell,

based on a simple sum of inputs that are narrowly tuned to ILD, ITD, and

frequency. There were three key findings:

- The model effectively replicates the true receptive fields of real cells.

- When trained only on a cell's true receptive field, the model is capable of

  predicting a cell's ILD-alone receptive field. This finding is crucial

  because it provides an independent validation of the model.

- The model performs best when allowed to use both excitatory and

  inhibitory inputs.

The model provides a plausible account of how developmental forces shape

the ILD selectivity of cells in the mature owl. The model develops connection

strengths subject to two constraints. First, the cell must respond as strongly as

possible to the ILD spectra from the cell's preferred location. Second, the cell

must be maximally inhibited by ILD spectra from locations above and below the

preferred location but along the vertical strip defined by the cell's best ITD.

The premises upon which this model is built have been proposed by other

authors; the basic mechanisms for creating receptive fields based on visually-

guided learning and Hebbian-style plasticity have are discussed by Knudsen

(1994, 1999) and others (King, 1999; Gold and Knudsen, 2000). However, by

instantiating my model computationally I have provided insights into the way that

ILD, ITD and ABL interact during development to yield the patterns of selectivity

for ILD spectra we observe in adult owls. The significance of these findings is

perhaps best appreciated by contrasting it with a simpler model, tacit in many

treatments of the subject, in which only excitatory weights are trained and the

effects of ITD are ignored. According to this model, a cell should be tuned

maximally to the spectrum from the location of its true receptive field. In addition,

ILD cues by themselves should support restriction of a receptive field in both

elevation and azimuth. Both of these predictions are contrary to the evidence

obtained from the measured ILD-alone receptive fields. My model, on the other

hand, matches the ILD-alone receptive fields closely.

In the second study (Chapter III) I used pure tones to measure responses to

combinations of ILD and frequency with the aim of uncovering the mechanisms

whereby independent frequency channels are combined by a space-tuned cell to

yield selectivity to ILD spectra. The primary focus of this study was to determine

whether the relationship between a cell's response to pure tones and its

response to broadband spatial stimuli could be described by a linear model. I

found that:

- A linear sum of pure-tone responses could predict, on average 56 percent of the variance in the measured broadband ILD-alone receptive fields.

- ILD-alone receptive fields predicted from pure tone responses were consistently less restricted than the ILD-alone receptive fields measured with broadband noise.

- Pure tones responses and the cell's ITD tuning curve could be used effectively to predict the location of a cell's receptive field.

- A cell's preferred ILD at each frequency was related to the HRTF-derived ILD at the cell's best location, but the relationship was not one-to-one. Instead, the pure-tone preferred ILDs corresponded with the HRTF-based ILDs at zero but were consistently more extreme than HRTF-based ILDs for preferred ILDs away from zero.

The results of this second study show that there is a strong linear component to the frequency-integration process performed by IC cells. Other processes that operate in the context of broadband sounds seem to better restrict the receptive field and improve accuracy.

APPENDIX A

LIST OF ABBREVIATIONS

ABL	average binaural level
BIP	binaural interaction plot
HRTF	head related transfer function
IC	inferior colliculus
ICx	external nucleus of the inferior colliculus
ILD	interaural level difference
ITD	interaural time difference
LS	lateral shell of the central nucleus of the inferior colliculus
VLVp	nucleus ventralis lemnisci lateralis, pars posterior

APPENDIX B

ESTIMATING THE EFFECT OF RANDOM ERROR ON THE CORRELATION

BETWEEN TWO VARIABLES

The question addressed here is: Given two variables how does the measurement error in each affect their correlation? Assume we have two random variables, X and Y, each with normally distributed and independent errors. For the ith measurement:

$$X_i = X_i' + \varepsilon_{X_i} \text{ and} \tag{1}$$

$$Y_i = Y_i' + \varepsilon_{Y_i}.$$

Here, X_i' and Y_i' are the true values for the ith measurement while X_i and Y_i are the actual measured values. The error in the ith measurements are given by ε_{X_i} and ε_{Y_i}.

For variables with independently distributed errors, such as X, it can be shown that the variance in the actual measurement, σ_X^2, is the sum of the error variance, $\sigma_{X_{err}}^2$, plus the variance in the true value of the variable, $\sigma_{X'}^2$ (Myers and Well, 1991, p. 112):

$$\sigma_X^2 = \sigma_{X'}^2 + \sigma_{X_{err}}^2.\tag{2}$$

The identical argument holds for Y.

The square of the pearson product-moment correlation, R^2, for two measured variables X and Y is given by:

$$R^2_{meas} = \frac{\sigma^2_{XY}}{\sigma^2_X \sigma^2_Y},$$ (3)

where σ^2_{XY} is the square of the covariance between variables X and Y with individual variances given by σ^2_X and σ^2_Y, respectively. Given the measured R^2, what we would like to estimate is the R^2 without the noise:

$$R^2_{true} = \frac{\sigma^2_{X'Y'}}{\sigma^2_{X'} \sigma^2_{Y'}}.$$ (4)

where $\sigma^2_{X'Y'}$ is the square of the covariance between the true values of X and Y. The true values of X and Y have variances $\sigma^2_{X'}$ and $\sigma^2_{Y'}$, respectively. The effect of random noise is the reduce the correlation between two variables. Hence, the value of R^2_{true} will be greater than R^2_{meas}.

Our goal is thus to solve for R^2_{true} in terms of R^2_{meas}. We start by showing that $\sigma_{XY} = \sigma_{X'Y'}$. The covariance between the measured values of X and Y is given by:

$$\sigma_{XY} = \frac{1}{N-1} \sum_{i=1}^{N} (X_i - \overline{X})(Y_i - \overline{Y}),$$ (5)

where N is the total number of measurements and bars are used to indicate the mean. In the following derivations, *we make the assumption that N is infinitely large*, but the results will still be approximately true for reasonably large N.

Using Equation (1) we can express X and Y in terms of a true value plus a measurement error. Equation (5) becomes:

$$\sigma_{XY} = \frac{1}{N-1}\sum_{i=1}^{N}\left(X_i' + \varepsilon_{X_i} - \overline{(X' + \varepsilon_X)}\right)\left(Y_i' + \varepsilon_{Y_i} - \overline{(Y' + \varepsilon_Y)}\right).$$

We now assume that N is large. Since the errors in both variables are, by supposition, normally distributed, they will not effect the mean. Hence:

$$\sigma_{XY} = \frac{1}{N-1}\sum_{i=1}^{N}\left(X_i' + \varepsilon_{X_i} - \overline{X'}\right)\left(Y_i' + \varepsilon_{Y_i} - \overline{Y'}\right).$$

Because the errors are also independent, the sum of their product with any other variable is zero (e.g., $\sum_{i=1}^{N}\varepsilon_{X_i}Y_i' = 0$). Hence the cross terms in this sum of products will vanish, leaving:

$$\sigma_{XY} = \frac{1}{N-1}\sum_{i=1}^{N}\left(X_i' - \overline{X'}\right)\left(Y_i' - \overline{Y'}\right).$$

Comparing with Equation (4), we see the right hand side of this equation is simply the covariance between the true values of X and Y. We have thus shown that

$$\sigma_{XY} = \sigma_{X'Y'}. \tag{6}$$

We use Equation (6) to eliminate $\sigma^2_{X'Y'}$ from Equation (4) and then use Equation (2) to substitute for the variances:

$$R^2_{true} = \frac{\sigma^2_{XY}}{\left(\sigma^2_X - \sigma^2_{X_{err}}\right)\left(\sigma^2_Y - \sigma^2_{Y_{err}}\right)}.$$

Combining with Equation (3) yields the desired solution:

$$R_{true}^2 = R_{meas}^2 \frac{\sigma_X^2 \sigma_Y^2}{\left(\sigma_X^2 - \sigma_{X_{err}}^2\right)\left(\sigma_Y^2 - \sigma_{Y_{err}}^2\right)}.$$

Thus, the true correlation between two variables measured with errors can be estimated from the measured correlation provided that some estimate can be made of the variance of each of the error terms.

BIBLIOGRAPHY

Adolphs R (1993) Bilateral inhibition generates neuronal responses tuned to interaural level differences in the auditory brainstem of the barn owl. J Neurosci 13:3647-3668.

Batteau DW (1967) The role of the pinna in human localization. Proc R Soc Lond B Biol Sci 168:158-180.

Blauert J (1969/70) Sound localization in the median plane. Acustica 22:205-213.

Bloom J (1977) Creating source elevation illusions by spectral manipulation. J of the Audio Engineering Society 25:560-565.

Brainard MS, Knudsen EI (1993) Experience-dependent plasticity in the inferior colliculus: a site for visual calibration of the neural representation of auditory space in the barn owl. J Neurosci 13:4589-4608.

Brainard MS, Knudsen EI, Esterly SD (1992) Neural derivation of sound source location: resolution of spatial ambiguities in binaural cues. J Acoust Soc Am 91:1015-1027.

Bregman AS (1990) Auditory Scene Analysis. Cambridge, MA: MIT Press.

Brugge JF, Reale RA, Hind JE, Chan JC, Musicant AD, Poon PW (1994) Simulation of free-field sound sources and its application to studies of cortical mechanisms of sound localization in the cat. Hear Res 73:67-84.

Calford MB, Pettigrew JD (1984) Frequency dependence of directional amplification at the cat's pinna. Hear Res 14:13-19.

Carlile S (1990a) The auditory periphery of the ferret. I: Directional response properties and the pattern of interaural level differences. J Acoust Soc Am 88:2180-2195.

Carlile S (1990b) The auditory periphery of the ferret. II: The spectral transformations of the external ear and their implications for sound localization. J Acoust Soc Am 88:2196-2204.

Carlile S, King AJ (1994) Monaural and binaural spectrum level cues in the ferret: acoustics and the neural representation of auditory space. J Neurophysiol 71:785-801.

Carlile S, Pettigrew AG (1987) Directional properties of the auditory periphery in the guinea pig. Hear Res 31:111-122.

Carr CE, Konishi M (1990) A circuit for detection of interaural time differences in the brain stem of the barn owl. J Neurosci 10:3227-3246.

Delgutte B, Joris PX, Litovsky RY, Yin TC (1995) Relative importance of different acoustic cues to the directional sensitivity of inferior-colliculus neurons. In: Advances in Hearing Research (Manley GA, Klump GM, Koppl C, Fastl H, Oeckinghaus H, eds), pp 288-299. Singapore: World Scientific.

Delgutte B, Joris PX, Litovsky RY, Yin TC (1999) Receptive fields and binaural interactions for virtual-space stimuli in the cat inferior colliculus. J Neurophysiol 81:2833-2851.

Egnor SER (2000) The role of spectral cues in sound localization by the barn owl. Doctoral dissertation, California Institute of Technology.

Esterly SD, Knudsen EI (1989) Frequency-dependent tuning for interaural difference cues in space-specific neurons in the owl's optic tectum. In: Annual Meeting of the Society for Neuroscience Abstracts, p 115. Phoenix, AZ: Society for Neuroscience.

Feldman DE, Brainard MS, Knudsen EI (1996) Newly learned auditory responses mediated by NMDA receptors in the owl inferior colliculus. Science 271:525-528.

Feldman DE, Knudsen EI (1997) An anatomical basis for visual calibration of the auditory space map in the barn owl's midbrain. J Neurosci 17:6820-6837.

Feldman DE, Knudsen EI (1998) Experience-dependent plasticity and the maturation of glutamatergic synapses. Neuron 20:1067-1071.

Fujita I, Konishi M (1991) The role of GABAergic inhibition in processing of interaural time difference in the owl's auditory system. J Neurosci 11:722-739.

Gold JI, Knudsen EI (2000) Abnormal auditory experience induces frequency-specific adjustments in unit tuning for binaural localization cues in the optic tectum of juvenile owls. J Neurosci 20:862-877.

Hartmann WM, Wittenberg A (1996) On the externalization of sound images. J Acoust Soc Am 99:3678-3688.

Hartung K, Sterbing SJ (1997) Generation of virtual sound sources for the electrophysiological characterization of auditory spatial tuning in the guinea pig. In: Acoustical Signal Processing in the Central Auditory System (Syka J, ed), pp 407-412. New York, NY: Plenum Press.

Hebrank J, Wright D (1974) Are two ears necessary for localization of sound sources on the median plane? J Acoust Soc Am 56:935-938.

Keller CH, Hartung K, Takahashi TT (1998) Head-related transfer functions of the barn owl: measurement and neural responses. Hear Res 118:13-34.

King AJ, Moore DR, Hutchings ME (1994) Topographic representation of auditory space in the superior colliculus of adult ferrets after monaural deafening in infancy. J Neurophysiol 71:182-194.

Knudsen EI (1982) Auditory and visual maps of space in the optic tectum of the owl. J Neurosci 2:1177-1194.

Knudsen EI (1999) Mechanisms of experience-dependent plasticity in the auditory localization pathway of the barn owl. J Comp Physiol [A] 185:305-321.

Knudsen EI, Brainard MS (1991) Visual instruction of the neural map of auditory space in the developing optic tectum. Science 253:85-87.

Knudsen EI, Esterly SD, Olsen JF (1994) Adaptive plasticity of the auditory space map in the optic tectum of adult and baby barn owls in response to external ear modification. J Neurophysiol 71:79-94.

Knudsen EI, Knudsen PF (1989) Vision calibrates sound localization in developing barn owls. J Neurosci 9:3306-3313.

Knudsen EI, Konishi M (1978a) A neural map of auditory space in the owl. Science 200:795-797.

Knudsen EI, Konishi M (1978b) Center-surround organization of auditory receptive fields in the owl. Science 202:778-780.

Knudsen EI, Konishi M (1978c) Space and frequency are represented separately in auditory midbrain of the owl. J Neurophysiol 41:870-884.

Knudsen EI, Konishi M (1979) Mechanisms of sound localization in the barn owl (Tyto alba). J Comp Physiol [A] 133:13-21.

Knudsen EI, Konishi M (1980) Monaural occlusion shifts receptive-field locations of auditory midbrain units in the owl. J Neurophysiol 44:687-695.

Knudsen EI, Konishi M, Pettigrew JD (1977) Receptive fields of auditory neurons in the owl. Science 198:1278-1280.

Kohonen T (1997) Self-Organizing Maps, 2nd Edition. Berlin: Springer.

Konishi M, Sullivan WE, Takahashi T (1985) The owl's cochlear nuclei process different sound localization cues. J Acoust Soc Am 78:360-364.

Kulkarni A, Colburn HS (1998) Role of spectral detail in sound-source localization. Nature 396:747-749.

Manley GA, Koppl C, Konishi M (1988) A neural map of interaural intensity differences in the brain stem of the barn owl. J Neurosci 8:2665-2676.

Mazer J (1995) Integration of parallel processing streams in the inferior colliculus of the owl. Doctoral dissertation, California Institute of Technology. Dissertation Abstracts International 56 (06B):3062.

Mazer JA (1998) How the owl resolves auditory coding ambiguity. Proc Natl Acad Sci U S A 95:10932-10937.

Mehrgardt S, Mellert V (1977) Transformation characteristics of the external human ear. J Acoust Soc Am 61:1567-1576.

Middlebrooks JC (1997) Spectral shape cues for sound localization. In: Binaural and spatial hearing in real and virtual environments. (Gilkey RH, Anderson TR, et al., eds), pp 77-97. Mahwah, NJ, USA: Lawrence Erlbaum Associates, Inc.

Middlebrooks JC, Green DM (1991) Sound localization by human listeners. Ann Rev Psychol 42:135-159.

Middlebrooks JC, Makous JC, Green DM (1989) Directional sensitivity of sound-pressure levels in the human ear canal. J Acoust Soc Am 86:89-108.

Mogdans J, Knudsen EI (1992) Adaptive adjustment of unit tuning to sound localization cues in response to monaural occlusion in developing owl optic tectum. J Neurosci 12:3473-3484.

Moiseff A (1989) Bi-coordinate sound localization by the barn owl. J Comp Physiol [A] 164:637-644.

Moiseff A, Konishi M (1981) Neuronal and behavioral sensitivity to binaural time differences in the owl. J Neurosci 1:40-48.

Moiseff A, Konishi M (1983) Binaural characteristics of units in the owl's brainstem auditory pathway: precursors of restricted spatial receptive fields. J Neurosci 3:2553-2562.

Mori K (1997) Across-frequency nonlinear inhibition by GABA in processing of interaural time difference. Hear Res 111:22-30.

Musicant AD, Chan JC, Hind JE (1990) Direction-dependent spectral properties of cat external ear: new data and cross-species comparisons. J Acoust Soc Am 87:757-781.

Myers JL, Well D (1991) Research Design and Statistical Analysis. New York, NY: HarperCollins Publishers, Inc.

Nelken I, Bar Yosef O, Young ED (1997) Response of Field AES neurons to virtual-space stimuli. In: Psychophysics and Physiological Advances in Hearing (Palmer AR, Rees A, Summerfield AQ, Meddis R, eds), pp 504-512. London: Whurr.

Oldfield SR, Parker SP (1986) Acuity of sound localisation: a topography of auditory space. III. Monaural hearing conditions. Perception 15:67-81.

Olsen JF, Knudsen EI, Esterly SD (1989) Neural maps of interaural time and intensity differences in the optic tectum of the barn owl. J Neurosci 9:2591-2605.

Palmer AR, King AJ (1985) A monaural space map in the guinea-pig superior colliculus. Hear Res 17:267-280.

Payne RS (1971) Acoustic location of prey by barn owls. J Exp Bio 54:535-573.

Poon PW, Brugge JF (1993) Virtual-space receptive fields of single auditory nerve fibers. J Neurophysiol 70:667-676.

Rayleigh L (1907) On our perception of sound direction. Philosophy Magazine 13:214-232.

Reale RA, Brugge JF (2000) Directional sensitivity of neurons in the primary auditory (AI) cortex of the cat to successive sounds ordered in time and space. J Neurophysiol 84:435-450.

Rice JJ, May BJ, Spirou GA, Young ED (1992) Pinna-based spectral cues for sound localization in cat. Hear Res 58:132-152.

Rice JJ, Young ED, Spirou GA (1995) Auditory-nerve encoding of pinna-based spectral cues: rate representation of high-frequency stimuli. J Acoust Soc Am 97:1764-1776.

Rumelhart DE, Hinton GE, Williams RJ (1986) Learning internal representations by backpropagation. In: Parallel distributed processing: Explorations in the microstructure of cognition (D. Rumelhart JM, and the PDP Research Group, ed), pp 318-362. Cambridge, MA: MIT Press.

Shaw EA (1974) Transformation of sound pressure level from the free field to the eardrum in the horizontal plane. J Acoust Soc Am 56:1848-1861.

Spezio ML, Keller CH, Marrocco RT, Takahashi TT (2000) Head-related transfer functions of the rhesus monkey. Hear Res 144:73-88.

Sullivan WE, Konishi M (1984) Segregation of stimulus phase and intensity in the cochlear nucleus of the barn owl. J Neurosci 4:1787-1799.

Takahashi T, Konishi M (1986) Selectivity for interaural time difference in the owl's midbrain. J Neurosci 6:3413-3422.

Takahashi T, Moiseff A, Konishi M (1984) Time and intensity cues are processed independently in the auditory system of the owl. J Neurosci 4:1781-1786.

Takahashi TT, Barberini CL, Keller CH (1995) An anatomical substrate for the inhibitory gradient in the VLVp of the owl. J Comp Neurol 358:294-304.

Takahashi TT, Keller CH (1992a) Commissural connections mediate inhibition for the computation of interaural level difference in the barn owl. J Comp Physiol [A] 170:161-169.

Takahashi TT, Keller CH (1992b) Simulated motion enhances neuronal selectivity for a sound localization cue in background noise. J Neurosci 12:4381-4390.

Takahashi TT, Konishi M (1988a) Projections of the cochlear nuclei and nucleus laminaris to the inferior colliculus of the barn owl. J Comp Neurol 274:190-211.

Takahashi TT, Konishi M (1988b) Projections of nucleus angularis and nucleus laminaris to the lateral lemniscal nuclear complex of the barn owl. J Comp Neurol 274:212-238.

Wagner H, Takahashi T, Konishi M (1987) Representation of interaural time difference in the central nucleus of the barn owl's inferior colliculus. J Neurosci 7:3105-3116.

Wightman FL, Kistler DJ (1989a) Headphone simulation of free-field listening. I: Stimulus synthesis. J Acoust Soc Am 85:858-867.

Wightman FL, Kistler DJ (1989b) Headphone simulation of free-field listening. II: Psychophysical validation. J Acoust Soc Am 85:868-878.

Zheng W, Knudsen EI (1999) Functional selection of adaptive auditory space map by GABAA-mediated inhibition. Science 284:962-965.